Optical Deconvolution of Multiple Co-eluting Proteins in Chromatography

By Deniz Ucan

A thesis presented for the degree of Engineering Doctorate in Biochemical Engineering and Bioprocess Leadership

University College London

Department of Biochemical Engineering

Bernard Katz

University College London

Gower Street

London

WC1E 6BT

Declaration

I, Deniz Ucan confirm that the work presented in my thesis is my own. Where information has been derived from other sources, I confirm that this has been indicated in the thesis.

Abstract

The in-line time-resolved fluorescence spectroscopy-based approach explored in this thesis for protein quantification in monoclonal antibody biomanufacture eliminates the need for a size exclusion chromatography (SEC) column and the application of formulation constraints to downstream chromatography feeds unlike other analytical techniques. This reduces the time, labour and associated costs for critical quality attribute (CQA) validation and offers superior analytical flexibility in the quantifiable protein species when compared to the current industrial standards of high-pressure liquid chromatography – size exclusion chromatography (HPLC-SEC). Linear correlations of 0.999 and 0.69 have been respectively achieved for monomer and aggregate-fragment quantity analysis between TRF spectroscopy and HPLC-SEC for concentrations below 2.8 mg/mL. The proof of concept for in-line host cell protein (HCP) quantification using TRF spectroscopy demonstrates intrinsic fluorescence decay intensity contributions that are reflective of monoclonal antibody (mAb) and the overall HCP content of separate and co-eluting species, as well as the capability for implementation between multiple bioprocess stages. This project has demonstrated that TRF spectroscopy can resolve independent species-quantity describing decay associated chromatogram (DAC) signal intensities for mAb and HCP-rich Protein A flow-through formulations, when run on their own and mixed together. The lower limit of measurement for HCP in a formulation with mAb was found to be equivalent to the HCP content in industrial Protein A flow-through (1E5-1E6 ng/mL). TRF spectroscopy was found to offer a far greater dynamic range, with measurable total protein concentrations over 10-fold of the concentrations that could be tested on industry-standard HPLC-SEC without UV absorbance peak truncation. Quantitation measurements could be performed on samples with total protein concentrations over 10000 times above those that were required to fall within the standard range for enzyme-linked immunosorbent assays (ELISAs). Thus setting the precedent for future strides in evaluating this technology in an industrial setting and expanding testing to include more protein products.

Acknowledgments

I express my deepest gratitude to my UCL project supervisor Prof Paul Dalby and my industrial supervisor Nathan Todd whose perspectives, time and expertise throughout have been central to project progression. Their vast knowledge and experience have been extremely valuable in the interpretation of results, disseminating research, identifying optimal data processing strategies and ensuring more people understand the business and healthcare benefits our analytical method can bring.

This work would not have been possible without the patience and unwavering perseverance of Dr John Hales whose work I build upon and whose academic input has been instrumental to results generation. I am deeply grateful for the time you have invested in this project and the valuable academic guidance you have provided me with, from its underpinning physics and how best to present highly technical subjects, through to the nature of questions to expect from journal reviewers.

I am also very grateful to Dr Samir Aoujdane who also helped develop the technology I tested. Thank you Sam for always being ready and available to help, come rain, shine or apocalypse! I have lost count of the number of instrument fixes you did, but I know I would not have half as much results if it weren't for them. Cycling into central London at the height of a pandemic lockdown to keep plants and equipment alive – the department was lucky to have you.

Dr John Welsh, I thank you greatly for your time and valuable perspectives, Dr Nigel Jackson, I thank you for your generosity in the bioprocessing samples you had delivered to me, likewise, Dr Steven Harris, Dr Keith Gillette, and Dr Terése Joseph, the samples and useful information you provided have been paramount to this work.

Dr Thomas Johnson, you were in my present position the first time we introduced ourselves, I am very grateful for the wisdom you have shared over the last couple of years. You have been the bridge between UCL and Pall Biotech and have supported the new EngDs greatly – whether it be giving us presentation training or insights into how to navigate academic processes, you were there.

Dr Cheng Zhang I extend my gratitude to you for helping smooth my transition into the laboratories with training on key procedures. You helped train us researchers and provided me with the Fab samples, Protein G flow-through, *E. Coli* host cell cultures, as well as, copious amounts of centrifugal concentrators that were crucial for my experiments.

Dr Peter Levison and Dr Dan Bracewell, I thank you for your input during our quarterly, annual review meetings and throughout this project – your perspectives have been instrumental in shaping my research focus.

Dr Naveraj Gill, you were the heart of the UCL-Pall Biotech Centre of Excellence team, together with Dr Edita Sehic-Botonjic, Dr Marianna Sofman, Marios Liarommatis and Rebecca Kale I thank you for the time and guidance you have shown me on this journey.

Mark Adam-Kellerman, thank you for training me on how to run gel electrophoresis, your warm greetings, positive and can-do attitude were a ray of sunshine for the Level 6 labs.

And finally, mum, dad, I thank you from my heart for your support and encouragement throughout my life. You helped me keep rowing when land was far. You deserve this doctorate more than me.

Preface

Whilst the fundamentals of fluorescence spectroscopic techniques have remained largely the same since the publishing of Grinvald and Steinberg (1974) the same cannot be said for the vastly evolved computing platforms on which to collect and perform decay measurements. Measurement systems have since simplified, become more sensitive and have a greater ease of handling.

Now with the advent of quantum computing and increasing industrial enthusiasm for efficiency-driven artificial intelligence (AI) programs, the prospect of analysing the concentrations and conformational states of protein species in mixtures, in-line and within a mere matter of seconds is within reaching distance. This project was set out with the aim of demonstrating the capabilities of time-resolved fluorescence (TRF) spectroscopy in quantifying key species in bioprocess samples and establishing its potential in multi-stage process analytical technology (PAT).

During this project we have seen that in-line measurements to the unaltered sample stream can be performed to detect the presence of product and process-related impurities. As original unaltered samples are tested in flow, results are ready in a matter of minutes, compared to the hours required for the current industrial standards in analysing the bioprocess feed.

This project has been a true example of multidisciplinary and has drawn extensive expertise from biochemistry and physics. It has explored the frontier in spectroscopic-quantification techniques and identified novel technology with the potential to be added to the developing industrial arsenal of in-line analytical methods. The underlying rationale has been that in-line time-resolved fluorescence spectroscopy can save industry the time, money and waste associated with current industrial standards in assessing key product indicators of quality and that long term cost reductions will eventually be translated to reductions in product costs. The efforts expended in my studies have been for the chance of bringing this closer to reality – a reality where product cost does not become the barrier to cancer treatments with superior target specificity.

Table of Contents

Table of Acronyms and Abbreviations:

AEX	Anion exchange (chromatography)
CEX	Cation exchange (chromatography)
cGMP	Current good manufacturing practise
CHO	Chinese hamster ovary
CMM	Cation mixed mode (chromatography)
CPP	Critical process parameter
CQA	Critical quality attribute
DAC	Decay associated chromatogram
DC	Decay chromatogram
DF	Diafiltration
ELISA	Enzyme-linked immunosorbent assay
EM	Electromagnetic
Fab	Fragment antigen-binding
FAD	Flavin adenine dinucleotide
Fc	Crystallisable fragment
FPLC	Fast performance liquid chromatography
HCP	Host cell protein
HGPRT	Hypoxanthine guanine phosphoribosyltransferase
HPLC	High-pressure liquid chromatograph
IR	Infra-red
LC-MS	Liquid chromatography mass spectrometry
mAb	Monoclonal antibody
NADH	Nicotinamide adenine dinucleotide hydrogen
PAGE	Polyacrylamide gel electrophoresis
PA	Protein A (chromatography)
pI	Isoelectric point
PPH	Post pH hold
PTM	Post translational modification
SDS-PAGE	Sodium dodecyl sulphate-polyacrylamide gel electrophoresis
SEC	Size exclusion chromatography
SOP	Standard operating procedure
TFF	Tangential flow filtration
TPP	Target product profile
TRF	Time-resolved fluorescence
Tris	Tris (hydroxymethyl)aminomethane
UF	Ultrafiltration
UV	Ultraviolet

Table of Units:

a.u.	Arbitrary units
AUs	Absorbance unit second
˚C	Degrees Celsius
kDa	Kilodalton
mg	Milligram
µJ	Microjoule
µL	Microlitre
mL	Milliitre
MΩcm	Resistivity
mV	Millivolt
ng	Nanogram
ns	Nanosecond
V	Volt
Vs	Volt-second
VsmL	Volt-second millilitre

1. Introduction

With their high specificity and broad extracellular target range, therapeutic monoclonal antibodies (mAbs) have successfully been used in the treatment of cancers, viruses, autoimmune disorders and other genetic conditions (Carvalho et al., 2017; Chartrain and Chu, 2008; Ecker et al., 2015; Reichert, 2010). The biopharmaceutical industry has witnessed a steep increase in the production and approval of therapeutic mAb products, with demand projected to increase in the coming decade (Ecker et al., 2015; Orellana et al., 2015).

High product costs severely impede the accessibility of mAbs to the general population, with prices ranging from $60,000 per patient for a year's supply of breast cancer drug Herceptin®, through to $400,000 per patient for Soliris® used to treat the rarer neuromyelitis optica spectrum disorder (Hersher, 2012; Orellana et al., 2015; Waltz, 2005). The high cost of mAb production can largely be attributed to the methods and technologies used to ensure products meet regulatory standards. Given the possibility of evoking an undesirable immune response, they must be manufactured to be free from process and product related impurities, such as host cell protein (HCP) and mAb aggregates, respectively (Nicoud et al., 2016; Shire et al., 2004; Vázquez-Rey and Lang, 2011). The proportion of content of these impurities at each stage of the bioprocess, and within the final product, form some of the critical quality attributes (CQAs), reported to regulatory agencies, that must be met for every batch produced.

Current industrial standard methods for analysing CQAs in drug manufacture often require significant sample preparation, including buffer exchange or reformulation, and modification of the protein concentration to fit the analytical constraints of the method, resulting in potential perturbations to the sample profile, and an inaccurate picture of relative species quantities at each bioprocess stage. Enzyme-linked immunosorbent assays (ELISAs) and high pressure liquid chromatography – size exclusion chromatography (HPLC-SEC) are prepared manually, with measurements performed off-line on batches of samples over the course of several hours. A bench-top, in-line fluorescence spectrometer has already been established at UCL and can resolve decay associated signals pertaining to multiple protein species to generate quantities in original bioprocess samples in a matter of minutes. Our method opens the potential for limitless, automated in-line multistage bioprocess analytics, a more accurate insight of protein species in the bioprocess, and reduced analytical times, risks of product contamination, and operational costs.

Time-resolved fluorescence (TRF) spectroscopy has recently been used to characterise the decay profiles of different protein species, in turn, allowing them to be quantified when co-eluting as part of a mixture without a requirement for buffer modification (Hales et al., 2021). Inherently in-line, the candidacy of TRF spectroscopy for replacing expensive, time-consuming and off-line ELISAs for quantifying process related impurities such as HCPs during therapeutic mAb manufacture has been investigated using mAb samples from a variety of bioprocessing stages. The aim has been to achieve an analysis of species concentrations that are more representative of the bioprocessing stage.

As will be explored later, the fluorescence decay parameters for key process and product impurity species, together with, the product itself have generated species proportions that are representative of the bioprocess stages samples were sourced from. Benchmarking studies have demonstrated the capability of time-resolved fluorescence spectroscopy for generating strongly correlating protein species quantities in relation to HPLC-SEC and ELISA. Preliminary tests have established upper and lower concentration limits of operation.

Future work revolves around scaling down the current fluorescence spectrometer into a portable format to allow easier implementation of in-line time-resolved fluorescence spectroscopy by industry. The automated generation of mean decay parameters and decay associated peak areas for species found in the biomanufacturing line can reduce data processing times even further, readily allowing a library of protein species to be quantified.

In-line TRF spectroscopy is proposed as a solution to time-consuming and costly disadvantages of off-line analytical standards to calculating product and process-related impurities. A market gap exists in fluorescence-spectroscopy-based in-line analytical methods for measuring the concentrations of multiple co-eluting protein species. TRF spectroscopy is used here to generate fluorescence decay parameters for the species in a formulation, these are then used to fit decay contributions to total fluorescence intensity signals for unknown samples. These decay contributions are represented by the areas underneath decay associated chromatogram (DACs) signal traces. It is these areas that are proportional to the quantity of a species in a mixture (John et al., 2021).

Having an in-line real-time system of quantifying the protein constituents of bioprocess feeds such as the method proposed here, can potentially substitute off-line HPLC-SEC and ELISA in the characterisation of species and their quantities. In doing so, all of the costs, time, labour and sample and mobile phase constraints associated with using an SEC column would be eliminated. Repeat measurements can be conducted in a fraction of the time frame required for HPLC-SEC – in the order of seconds for each sample, rather than the 20-60 minutes for a typical HPLC-SEC run time for one injection or 7 hours for ELISA. Equilibrating the SEC columns with mobile phase can take several hours, together with cleaning validation and larger column sizes, column preparation and maintenance can run into days. The high SEC pressures used can also lead to non-bioprocess stage-representative aggregate and fragment percentages being generated. The serial dilutions that need to be applied to ELISA samples to assess unknown HCP content increase the error in final HCP concentrations.

As the analytes remain within the bioprocess, none of these disadvantages would apply to TRF spectroscopy. Instead, the results presented here demonstrate its candidacy as an in-line process analytical technology for multistage species analysis – which forms the overarching aim of this study. The objectives have therefore been to explore the mechanisms of decay parameter generation and their use in the fitting of decay intensities that are proportional to species concentrations. This allowed the head-to-head analysis of the quantification capabilities of in-line TRF spectroscopy against the current industrial standard for product-related impurity analysis, HPLC-SEC, and for process-related impurity analysis, ELISA. For industry, these results shine light on its capability in providing a more detailed insight into the biophysical interactions of the protein species present in their biomanufacturing lines, more efficiently than can presently be achieved.

2. Literature Review

2.1. Monoclonal Antibody Therapeutics

MAb therapies have been used successfully in the treatment of a wide range of diseases from cancer (Zahavi and Weiner, 2020), to autoimmune disorders (Reichert et al., 2005; Steinman, 1990; Weiner, 2007) and even viral infections such as covid-19 (Aleem and Slenker, 2022). MAb product approval and clinical deployment has been increasing each decade since the FDA approved the use of orthoclone OKT3 to reduce acute kidney transplant rejection in 1986 (Smith, 1996; Buss et al., 2012). As mAbs form an integral part of the immune response, they have effectively been used in its training to neutralise viral and tumorigenic pathologies (Rosenberg, 2006). With respect to the debilitating side effects associated with the widely used cancer treatments of chemotherapy and radiotherapy, any side effect arising from the use of therapeutic mAbs are immunogenic and short-lived (Baldo, 2013).

The clinical success of mAbs and biologics has transformed the pharmaceutical industry. By 2010 near US$100 billion was spent on biologic products, and by 2025 it is projected that over 70% of new drug approvals will be formed by biologics (Erickson, 2010; Berkowitz et al., 2012). As a number of drugs reach patent protection expiry, an opportunity emerges for industry to develop generic versions with abbreviated approval processes (Busse and Lüftner, 2019). In the early 2000s, the European Union established regulatory provisions for biosimilar approval (Walsh, 2010). These generally involve the demonstration that the drug contains active ingredients at the same purity and dosage forms, or pharmaceutically equivalent, and that the drug is metabolised by the body at similar rates, that is, bioequivalent, when compared to the original drug. With lower cost, faster approval times, generic versions of drugs have reduced the costs incurred by health-care systems (Agostini et al., 2015).

The regulatory pathway for patent protection-expired biologics is more tortuous. Small peptides that are quality assessed via established analytical methods, such as recombinant insulin and growth hormone, follow a shorter and simpler path towards regulatory approval under an abbreviated pathway. However, for larger therapeutic proteins such as mAbs, current analytical technologies provide a limited field of view into the clinical comparability of a generic follow-on version and its original (Woodcock et al., 2007; Berkowitz et al., 2012).

2.1.1. Monoclonal Antibody Physiology

The exterior surfaces of pathogenic organisms are embellished with signature arrangements of protein, polysaccharide, lipid or nucleic acid. The immune system responds by recognising these signatures as foreign and proceeds to neutralise the organism. This response can be innate where toll-like receptors bind to certain molecules and initiate defence pathways, or adaptive, where pathogen-specific antibodies are deployed by B lymphocytes to bind to unique microbial proteins they have familiarised with (Rosenberg, 2006).

MAbs have a high antigen specificity to not only microbial proteins, but proteins innate to the human body itself. Early mAbs targeted CD4 and CD3 lymphocytes to reduce immunological rejection of organ transplants (NIDDKD, 2012). In 1890, Behring and Kitasato took a landmark stride in our understanding of mAbs to treat disease, in their paper they demonstrated that the administration of serum from animals immunised against diphtheria could cure animals that were infected with the disease (Behring and Kitasato, 1890). Later Ehrlich (1897) put forward the theory that the immune system is mediated by cell side-chain receptors binding to pathogens. That, a side-chain could have a molecular structure that was complementary to a toxin or microorganism was in agreement with the 'lock-and-key' enzyme-substrate model formulated by Fischer in 1894. The side-chains were suggested to be detachable from the cell surface, whereupon release into the bloodstream they could act as we presently understand antibodies to act – that is they would bind to pathogens and prevent them from binding to host cells (Yamada, 2011; Bosch and Rosich, 2008). This concept then evolved into his 'Zauberkugel' or 'magic bullet' which were drugs that target specific cell structures; harming pathogens yet remaining harmless to healthy tissues (Strebhardt and Ullrich, 2008).

Work on characterising lymphocytes by Maximow (1902) and Kolouch Jr. (1938) eventually led to the breakthrough by Fagraeus (1947) which concluded that cells in the blood plasma produce antibodies. Pauling (1940) had previously developed the theory that an antigen formed a template for an antibody. Later Burnet (1957) and Talmage (1957) stated that antibodies are secreted by lymphocytes before their encounter with pathogenic antigens. The next breakthroughs came two years later with the amino acid and molecular weight analysis of antibodies by Porter (1959) and four years later with Edelman et al. (1961) who published the gel electrophoresis results of antibodies with different specificities and descriptions of the structures they correlate to. Inbar et al. (1972) presented direct evidence for the locations of the variable regions and their compositions. Each of these research teams, and the teams of whose work they consolidated upon, laid a paving stone towards our modern-day understanding of mAb structure and biochemical behaviour. Eventually leading to the instrumental work of Köhler and Milstein (1975) who demonstrated the production of monoclonal antibodies from the

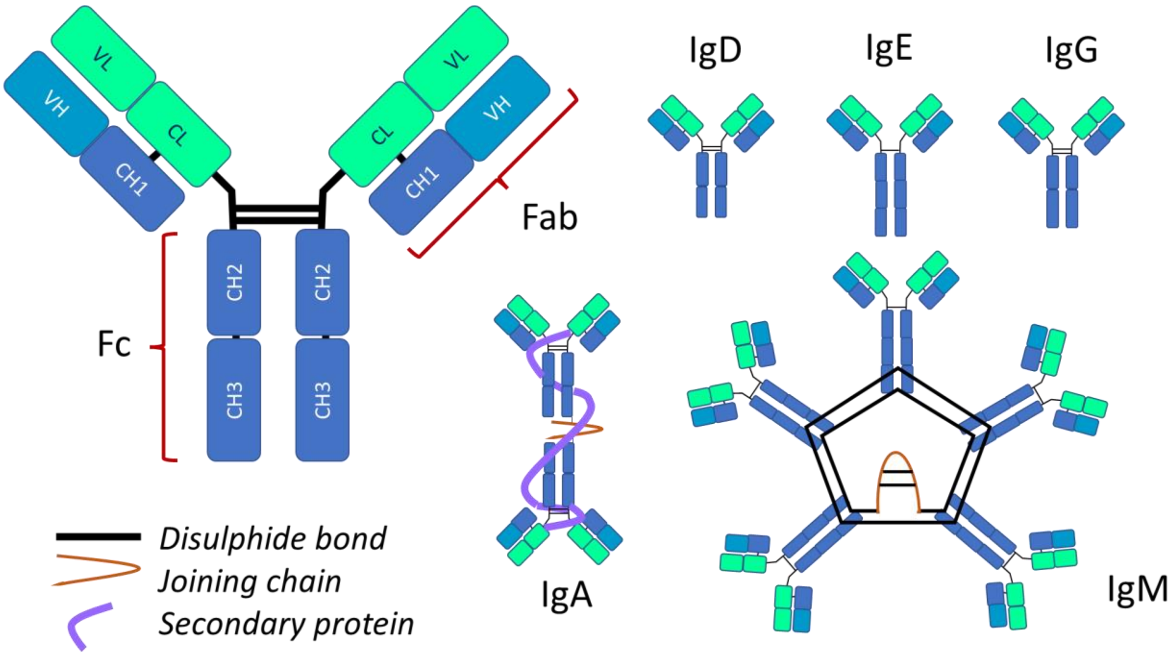

Figure 1: Schematic of the structure of an IgG antibody. Nomenclature: XYZ, where X: variable (V) or constant (C) domain, Y: heavy (H) or light (L) chain, and Z: number for repeating regions. General structure of main antibody classes on the right.

fusion of a murine myeloma and the spleen cells of an immunised donor, which laid the foundations for the modern era of mAb production.

Antibodies form a roughly Y-shaped immunoglobin class of protein molecule. Their structure is divided into the variable region at the top which binds to a specific antigen and the constant region, at the stem which interacts with effector cells. Based on the length of their constant regions immunoglobins can be classified into the following classes: IgG, IgA, IgE, and IgM. IgA form dimers and IgM are pentamers, whilst IgG and IgE antibodies are mainly monomeric. As the most abundant type in the human body, IgG antibodies were used in the proof-of-concept studies throughout this project and will be the focus of this thesis. IgGs are composed of two heavy (50kDa) and two light (25kDa) chains of amino acids as shown in fig. 1, making their total molecular weight total approximately 150 kDa. Connecting the heavy and light chains, as well as the two heavy chains are several di-sulphide bonds. The hinge region offers a degree of flexibility in bivalent antigen binding and the activation of Fc in effector functions. By order of abundance in human plasma and due to the differences in their heavy chains, IgG antibodies can be further divided into subclasses: IgG1, IgG2, IgG3 and IgG4. Hinge length and interchain disulphide bond locations differ between these subclasses (Wang et al., 2007; Chan et al., 2004).

Through a simpler process of host immunisation with an antigen and antiserum collection, polyclonal antibodies are relatively cheap and simple to produce compared to monoclonal antibodies. However, each host produces a limited titre of antibodies and variation can be observed between serum batches. The continuous culturing of B cell hybridomas generates more reproducible batches and a potentially infinite supply of specific antibody. Outside of their notable therapeutic applications, mAbs are paramount to the manufacture of standardised immunoassay systems such as enzyme-linked immunosorbent assays (ELISAs) which are discussed in greater detail later (Nelson et al., 2000; Tomita and Tsumoto, 2011).

2.1.2. Impurity Kinetics

2.1.2.1. Aggregation

Aggregation begins with two or more protein molecules assembling into stable complexes, often held together with strong non-covalent interactions (see Figure 2). Aggregation in conjunction with conformational distortion can be irreversible, i.e. changes to pH or reformulation will not dissociate aggregates (Roberts, 2014). In mAbs, aggregation can begin with dimerisation then progress towards larger multimers with thermodynamically favourable conditions. Protein degradation can lead to unfolded or partially unfolded regions that may be hydrophobic and can promote the formation of intermolecular bonds that lead to aggregation (Vázquez-Rey et al., 2011; Córdoba-Rodríguez, 2008; Kiese et al., 2008).

MAbs display instability through denaturation and aggregation, which can be interlinked. They are relatively resistant to thermal stress and have been found not to melt until the temperature exceeds 70 ℃ (Chen et al., 2003; Welfle et al., 1999; Li et al., 2005). However, incubation at temperatures above 20 ℃ for 6 weeks and over, has led to the observation of aggregate formation and deamidation (Wang et al., 2007; Chen et al., 2003; Cleland et al., 2001; Kroon et al., 1992; Zheng and Janis, 2005). MAbs have been found to be generally resistant to the denaturing shear stresses in bioprocessing. Bee et al. (2009) studied the effects of shear far in excess of those expected during normal bioprocessing operations (20,000 s-1, <0.06 pN). They found shear alone was not the cause of aggregation as prolonged shear in a stainless-steel rheometer generated minor reversible aggregation (<0.3%). When formulations containing heat-induced aggregates (17%) were subjected to further shear, aggregate populations did not change significantly. When Pabari et al. (2011) stressed trastuzumab with freeze-thaw, sonication, lyophilisation, spray-drying and encapsulation they found no loss of structural integrity, conformation nor a significant alteration to biological activity. They instead observed low levels of aggregation (<9%) at the lowest concentration (0.4 mg/mL) that was tested. Lyophilisation, whilst commonly used to improve antibody shelf-life, has also been found to alter antibody structures. Zhang an et al. (2001) showed that when the antibody MMA 383 was formulated with NaCl, phosphate, saccharose and mannitol it lost 10-20% of its normal immunogenic response rate suggesting a reduction in binding affinity with the target antigen. They also found that the fluorescence lifetime for lyophilised antibodies were smaller and non-lyophilised antibodies had a greater variety of angles between Fab moieties, therefore a greater flexibility. In this case study, evidence for increased denaturation was not found for lyophilised antibodies, but the loss of their *in vivo* immunogenic properties were attributed to conformational change.

MAb aggregation poses a significant problem to industry as it can occur at any stage of the bioprocess and has the potential to affect purification strategies, target product profile, pharmaceutical efficacy and product safety (Obrezanova et al., 2015). Some *in vivo* activity can be maintained through reversible dissociation of self-associated antibodies; however, the aggregation of larger sized molecules can contribute to increases in solution viscosity, presenting challenges to bioprocessing and administration (Wang and Roberts, 2018). Aggregates can form through physical association where primary structures remain unchanged, by chemical bonding or localised protein-protein attractions which increase with concentration (Pindrus et al., 2015). The latter interactions between proteins have been found to be responsible for viscosity increases (Woldeyes et al., 2019), with mAbs being found to display anomalous increases in solution viscosity with protein concentrations in comparison to other globular proteins (Zhang and Liu, 2017). Each route may generate aggregates that are soluble or insoluble (Singla et al., 2016).

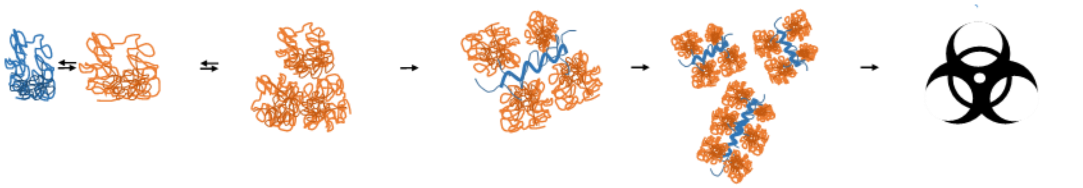

Figure 2: A schematic overview of the protein aggregation process.

Rather than using the low pH values commonly used in viral inactivation, solvent and detergent treatment of proteins has been suggested as a method of reducing aggregate levels (Vázquez-Rey et al., 2011; Horowitz et al., 1998). Pumping high concentration mAb solutions from one bioprocess stage to the next is a very common practise but exposes them to aggregate-inducing shear stress. Gomme et al. (2006a, b) investigated the use of lobular pumps on large-scale protein purification, they found that the shear stress forces on protein solutions dissipated through pump lobes. Reducing pump head distance reduced shear stress further and associated aggregate formation.

Nicoud et al. (2016) investigated heat-induced aggregation for a model mAb at different buffer pH and formulated to low-moderate concentrations. They found that for dilute conditions, aggregation is dependent upon the aggregate fractal dimension or aggregate compactness and the Fuchs stability ratio, which describes the energy barrier preventing the aggregation of colliding molecules. They also found decreasing the formulation pH below protein isoelectric point (pI) leads to an improvement in colloidal stability (increase in Fuchs ratio) and a decrease in conformational stability (increase in unfolding rate constant) (Nicoud et al, 2016).

With greater advantages in efficient administration and pharmaceutical preference for the treatment of some conditions, achieving high mAb concentrations (~ 100 g/L) is industrially sought after. However, such concentrations raise the risk of aggregate formation, thereby increasing solution viscosity and reducing solubility, which may all reduce drug efficacy and trigger adverse immunological responses (Nicoud et al., 2016; Vázquez and Lang, 2011; Shire et al., 2004). Highly concentrated mAb formulations also pose analytical challenges as dilutions are required for accurate results, even though, the dilutions themselves can impact quantities generated and aggregate equilibrium positions. Improving current understandings of the effect of protein concentration on the kinetics of aggregation is important to optimising final drug formulation concentrations. The complex biochemical nuances in behaviour make this challenging – in dilute environments the intramolecular interactions between product and protein surface nonuniformity are fewer, but lower product dosages can have negative implications for pharmaceutical efficacy. Concentration-dependent aggregation has been considered to be one of the greatest challenges in the production of high-titre, high concentration mAb formulations (Shire et al., 2004). Aggregates also have the potential to be immune enhancing due to the multiplicity of epitopes (Hermeling et al., 2004; Wang et al., 2007). The immunogenicity of therapeutic mAbs can be reduced by site-specific mutagenesis, PEGylation, exon shuffling and humanising mAbs. The use of animal models has been suggested as a means of predicting therapeutic protein immunogenicity (Schellekens, 2002).

2.1.2.2. Fragmentation

Fragmentation, together with aggregation forms a CQA that requires regular assessment as a characteristic of protein integrity and bioprocess control parameters. Fragmentation, in the general sense, is the disruption of covalent bonds in proteins due to spontaneous or enzyme-mediated reactions. Despite the intrinsic chemical stability of the peptide bond, the flexibility of the mAb backbone and side chain can increase the rate of fragmentation. As can the presence of certain residues which are involved in specific degradation mechanisms (Vlasak and Ionescu, 2011). Studies have reported that the majority of mAb fragmentation events are facilitated by the following protein residues: Asn, Asp, Cysteine, Glycine, Serine, or Thr. Direct hydrolysis, free-radical hydrolysis and specific cleavage reactions can lead to fragmentation (Liu et al., 2008; Vlasak and Ionescu, 2011).

Smith et al. (1998) measured the effect of pH on peptide bond fragmentation, they concluded that at a neutral pH the reaction rate is minimal but accelerated in acidic or basic conditions. Around a neutral pH, half-lives over several hundreds of years have been reported (Smith et al., 1998; Radzicka and Wolfenden, 1996; Vlasak and Ionescu, 2011).

The pH dependence of peptide bond hydrolysis for a specific acid (k_{H3O+}) and base (k_{OH-}) can be described by rate constant k, in Eq. 1 (Smith and Hansen, 1998; Vlasak and Ionescu, 2011):

$$k = k_{H_2O} + k_{H_3O^+}[H_3O^+] + k_{OH^-}[OH^-] \qquad (1)$$

When Liu et al. (2008) investigated fragmentation of recombinant mAbs incubated at various pH values, they found that the peptide bonds near domain-domain interfaces, near loop structures were susceptible to hydrolysis as was the hinge region. They also found a pH of 6 to be optimal in reducing the rate of fragmentation (Liu et al., 2008).

2.1.3. Risks Posed by mAb Aggregate and Fragment Species

Small proportions of developed drugs ever become commercialised. Aside from increasing manufacturing costs, several of the reasons for this revolve around ensuring safety and efficacy. High-throughput de-risking measures have been suggested to support the early assessment of potential issues and reduce product failure later on (Obrezanova et al., 2015; Zurdo, 2013). Protein aggregates have been found to be an immune response enhancer to monomeric protein forms. Molecular weight has been identified as a key factor in determining immunogenicity – with larger aggregates (>100kDa) found to be the most efficient immune response inducers. Other factors include the presence of neoepitopes, glycosylation, immunomodulatory product contaminants and mAb origin (Rosenberg, 2006).

The main risk of aggregates and fragments in the final product is the product becoming the target of the immune response rather than the source of disease. Clinical concerns surround the adverse effects associated with the immune response and the inhibition of product efficacy through non-specific anti-complimentary activity. More seriously, an endogenous protein counterpart can become neutralised after cross-reaction, leading to a critical hypersensitivity response and anaphylaxis (Rosenberg, 2006; Ring et al., 1979; Gomme et al., 2006a). Upon storage, proteins can aggregate, whether they consist of whole mAb or the fragments, and in doing so, they can form insoluble particles (Volkin et al., 1989). The diagram in fig. 2 charts one aggregate pathway towards insolubility. When these particles are intravenously administered, they can lead to vessel blockages and pulmonary granulomas (Backhouse et al., 1987; Puntis et al., 1992; Dorris et al., 1977). Aggregation post-storage reduces the shelf life of products. This poses an issue for industries maintaining supply chains to the public (Gomme et al., 2006a).

2.1.4. Current Analytical Systems

Analytical validation involves two levels: a pre-study assessment that demonstrates objective fulfilment by a method and in-study evaluation of a method over time using quality control samples (Boulanger et al., 2009; Oliva et al., 2016). Validation can occur after an establishment of the analytical target profile, product acceptance criteria and performance level characteristics, for example the accuracy, precision dynamic range and sensitivity. Moving range or X-bar control charts have been suggested as a suitable method control strategy (Schweitzer et al., 2010; Montgomery, 2008; Oliva et al., 2016).

The successful clinical application of mAbs requires diligent monitoring for degradation – the main characteristics of which are aggregate and fragment formation. Due to drug complexity, a range of different analytical methods need to be used in assessing purity and thus, product safety and efficacy. As a standard, the techniques used are required to detect and quantify the active ingredients in formulations and the products of their degradation. Their potential immunogenicity renders aggregates and fragments as key CQAs in mAb manufacture. They are generally characterised by techniques that assess molecular weight such as sodium dodecyl sulphate, polyacrylamide gel electrophoresis (SDS-PAGE), field flow fractionation, mass spectrometry and light scattering methods (Wang, 1999; Fraunhofer and Winter, 2004; Kükrer et al., 2010; Fekete et al., 2014).

A commonly used industrial standard in the analysis of aggregate and fragment species is HPLC-SEC. Advantages of the method are the generation of reproducible and robust results, and the use of mild mobile phase conditions to minimise impact on protein conformational structure (Fekete et al., 2004; Oliva et al., 2016).

The stationary phase of SEC is composed of pore-size controlled spherical particles through which analytes diffuse. Their hydrodynamic radius determines the length of time they spend in the column or their retention time, before they elute out for UV absorbance measurements. Aqueous buffers are usually predetermined for each column regardless of the protein, which can lead to aggregate and fragment percentages that are not truly representative of the bioprocess conditions the sample was sourced from.

The SEC separation process is entropically controlled, without chemical adsorption. This can be represented by the Gibs free-energy equation:

$$InK_D = -\frac{\Delta S_0}{R} \quad (2)$$

The negative ratio of the change in system entropy ΔS_0 and the gas constant R, gives rise to the inverse logarithm of the thermodynamic retention factor, K_D. Temperature effects retention times by altering protein conformations, solute diffusivity and the viscosity of the mobile phase. K_D can also be described as the proportion of intraparticle pore volume that can be accessed by the analyte (Barth and Saunders, 2012; Hong et al., 2012; Fekete et al., 2013).

Engelhardt and Ahr (1983) suggested that the ratio of the probability of a sample remaining in the pores or moving in the mobile phase within the interstitial volume, could be encapsulated as a retention factor, k^*. For SEC, the upper limit of k^* , k_{MAX}, is the ratio of column pore volume, V_P, and interstitial volume, V_Z, or equally, column pore porosity, ε_P, and interstitial porosity, ε_Z:

$$k^*_{MAX} = \frac{V_P}{V_Z} = \frac{\varepsilon_P}{\varepsilon_Z} \quad (3)$$

For a given separation case, k^*_{MAX} therefore provides the range of analyte retention and this is dependent on pore porosity: interstitial porosity. Separation selectivity can therefore be modified through packed column particle density, particle pore volume, and particle size.

The largest protein molecules elute first as they cannot pass through the pores that would lengthen their distance to the column outlet, subsequent proteins then elute in descending order of size. Nevertheless, it should be noted that protein morphology could also have an impact on retention times as can the presence of rod, globular or flexible chain structures and undesirable adsorptive behaviour. Also, the fact that the Stokes radii of a protein does not correlate with its molecular weight, can all lead to errors in the SEC calibration curves for known analytes. The calibration curves are generated by plotting the logarithm of the molecular weight, M, against the retention volume, this typically forms a third order polynomial relationship, from which the highest molecular weight accuracy can be obtained by the linear region. The equation of this linear portion is (Kopaciewicz and Regnier, 1982; Fekete et al., 2013; Arakawa et al., 2010; Golovchenko et al., 1992):

$$\log M = mK_D + b \quad (4)$$

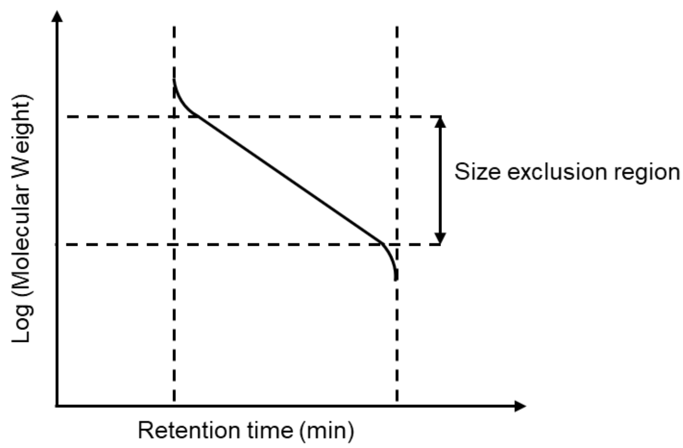

Figure 3: A typical SEC calibration curve with a linear region described by eq. 4.

Where b is the y-intercept and m is the gradient of the line. As can be seen the thermodynamic retention factor directly impacts the gradient, m – as pore size distribution decreases, the gradient increases, and column selectivity increases which allows the discrimination of similar-sized analytes.

Intrinsic fluorescence measurements have been coupled with SEC methods to evaluate the degradation profiles of drug products related to interferon alpha-2 (Diress et al., 2010). Debaene et al. (2013) used on-line TRF techniques with native MS to monitor the formation of immune complexes during Fab-arm exchange, where heavy chains of antibodies with different specificities undergo dissociation and recombine in bispecific antibodies.

SEC combined with light scattering (LS) has been brought forward as a reliable and accurate technique to assess macromolecule behaviour (Oliva et al., 2001; Wyatt, 1993; Oliva et al., 2016) and protein conformation through SEC column retention times and LS-derived molecular masses (Oliva et al., 2016; Wen et al., 2016).

Recent developments to HPLC-SEC through the packing of <2 µm particles have given rise to 2-5 times lower plate heights than conventionally packed columns with 5 µm particles, and analysis time reduction by up to 4 times. However, the high pressures, frictional heating and shear forces at these column packing configurations generate additional aggregates and artifacts when quantifying them (Fekete et al. 2013). In addition, polymeric resins can undergo compression under the high pressures, which limits the chromatographic resolution and particle size reduction that can be achieved (Hong et al., 2012).

Achieving high throughputs and short analysis times are a great interest for modern era HPLC-SEC techniques. Some strides have been made in reducing the column void volume: flow rate ratio, thus reducing separation times. Opting for a smaller column is a straightforward step and backpressures have been maintained at acceptable levels with high flow rates (Khoo and Leow, 2021), but this also reduces the theoretical plate number. Larger solutes undergo a slower mass transfer between pore and interstitial volumes, so with high speed and shorter columns, a steep reduction in resolution can be observed (Hong et al., 2012; Fekete et al., 2013).

2.2. Monoclonal Antibody Biomanufacture

The efficacy of mAbs to treat cancers, autoimmune disorders and recent viruses such as Ebola and COVID-19 has been established over the last three decades since the FDA first approved Muromonab-CD3 to treat acute kidney transplant rejection in 1986 (Aleem and Slenker, 2022; Leavy, 2010; Adams and Weiner, 2005; Tshiani Mbaya et al., 2021). MAb therapeutics have since been approved by the Food and Drug Administration (FDA) for over 30 diseases (Shepard et al., 2017). The dominant mode of mAb production remains recombinant expression through host cell systems, particularly, through Chinese hamster ovary (CHO) cells due to their ability to generate modified proteins with similar physiologies to those in humans (Kunert and Reinhart, 2016; Jones et al., 2021).

Host cell protein (HCP) species constitute a major process-related impurity in the biomanufacture of mAbs, requiring close monitoring to ensure regulatory standards are met (Bracewell et al., 2021). As a derivative of harvested cell culture components, traces of HCP can remain in eluates even after subsequent chromatography purification steps, increasing the risk posed by the product to the safety of patients (Molden et al., 2021; Jawa et al., 2016). Process and product-related impurities are sequentially removed in downstream processing by Protein A affinity purification, followed by a combination of viral inactivation, ionic exchange chromatography and filtration (Nakazawa et al., 2010). Unspecific HCP co-elution, formation of aggregates post purification, higher regulatory product quality demands and batch off-line monitoring methods have presented challenges scaling up production. Higher upstream titres have been found to create complex profiles of process-related impurities, making not only higher chromatography selectivity and separation capacity essential, but also more targeted critical quality attribute (CQA) analysis of HCPs (Kornecki et al., 2017; Mazzer et al., 2015). Enzyme linked immune-sorbent assays (ELISAs) remain to be the current industrial standard in HCP analysis, however, they do not provide a complete picture of the individual proteins present in HCP populations and different kits provide different immunoreactivities against the HCPs of each bioprocess. This makes it difficult to compare HCP measurements across different biomanufacturing lines (Molden et al., 2021; Jones et al., 2021).

A proof of concept for in-line HCP quantification using TRF spectroscopy is presented in this thesis which demonstrates sample peak areas reflective of mAb and the overall HCP content of HCP-rich Protein A flow-through-spiked mAb samples. Our approach opens the potential for increased quantification accuracies and reduced analysis times required for validating HCP content in mAb bioprocess stages from the several hours required for ELISAs to a few minutes per sample with TRF spectroscopy.

2.2.1. Host Cell Systems

Manufacturing complex recombinant proteins such as mAbs requires the use of cellular systems that are capable of facilitating protein folding and assembly and post-translational modifications (Hogwood et al., 2014). Common hosts for the synthesis of recombinant DNA proteins are *E. coli*, CHO, and yeast, with growing interest in transgenic animals as host cell models. With its inexpensive fermentation media, rapid growth (population doubling every ~ 20 minutes) and high levels of expression (typically up to 20% of cellular protein total), the lowest cost option is *E. coli.* It is used in recombinant protein production without glycosylation, phosphorylation or post-translational modification requirements. The inclusion bodies and the protein product they contain can easily be separated by centrifugation. The product may be found in a misfolded state. The proteases released during inclusion body disruption can further compound the problem with the creation of truncated molecules amongst the complete product. The refolding and purification processes are product-specific and will add to the cost of manufacturing. As can the presence of endotoxin – observed at higher levels for proteins expressed in the periplasm. Its removal is a key validation requirement, together with misfolded proteins, nucleic acids, molecules with unwanted methionine arrangements, HCP and product that has undergone proteolytic digestion. Human growth hormone, insulin, interleukin 2 and α- and γ- interferons are just some of the commercialised products synthesised by *E. coli.* Antibody fragments with the same binding capacity as whole mAb, such as the Fab and Fc regions can also be produced in *E. coli* and have been approved for therapeutic use. Humanised antibodies have been recovered for the *E. coli* periplasm. However, the occurrence of translational errors in therapeutic proteins can have an adverse immunogenic response in humans. These are caused by a number of rare codons present in the heterologous genes which can induce tertiary structure changes and affect biological activity (Baeshen et al., 2015; Sofer and Hagel, 1997).

A significant risk of in vitro antibody production is antibody cross-reactivity with undesired human tissue antigens. MAbs produced using murine cells can induce an antibody response against them, or an anti-murine antibody (HAMA) response. The human immune system is known to reject mouse-derived antibodies, leading to allergies and a reduced effectiveness of the mAb (Sofer and Hagel, 1997; National Research Council, 1999). Unlike *E. coli* systems, post-translational modifications can be made to proteins produced through CHO cell systems. CHO cell systems are used in the production of 60% of all mAbs, the remainder are produced by myeloma cells (Maruthamuthu et al., 2020; Grilo and Mantalaris, 2019).

In addition to their widespread use in mAb manufacture, CHO cells are also used in erythropoietin, plasminogen activator and recombinant human DNase. The costs of their culture and subsequent product purification are much greater, but receptor-specific mAbs can be properly programmed and synthesised (Sofer and Hagel, 1997; Orellana et al., 2015). The majority of mAbs are developed as humanised recombinant proteins in CHO cells (Wurm, 2004). The risk of bovine spongiform encephalopathy contamination has greatly reduced with the adoption of serum-fee culture media and the avoidance of animal components during cell growth (Sofer and Hagel, 1997; Kim et al., 2012). High costs are derived from exhaustive screening for each production line, which can vary in cell growth and productivity. Current methods for CQA analysis themselves require expensive components and time-consuming processes. The last two decades have seen bioprocess optimisation boost mAb yields over 100-fold, with 5-10g/L being a common production concentration today. Much of the optimisation has been in the application of cell culture conditions, media, and feeding strategies (Wuest et al., 2012). Host cell enhancement through genetic engineering can induce changes to cell metabolism, growth cycle, apoptosis and product synthesis (Lim et al., 2010; Fussenegger et al., 1998; Fogolín et al., 2004; Chiang and Sisk, 2005; Mohan et al., 2007).

The CHO cell genomic sequence was completed in 2011 and marked a greater understanding on how gene-editing tools, such as clustered regularly interspaced short palindromic repeats (CRISPR) and the enzyme Cas9, could be used to improve the cell lines used in mAb manufacture (Grav et al., 2017). Transgene integration into such cell lines can improve productivity for a target protein (Maruthamuthu et al., 2020). However, few enhanced cell lines are used by industry and the majority of advancements to increase product titres have been bioprocess optimisation (Wuest et al., 2012; Orellana et al., 2015).

2.2.2. Hybridisation and Culture

Following the traditional murine-derived-mAb production process, the first stage begins with the selection of an appropriate mouse, extraction of B cells from its spleen that respond to a specific antigen and the hybridisation of these. *In vivo* or in vitro immunisation can be performed with synthetic antigenic peptides, in some cases, with an immune-enhancing adjuvant. Hybrisation involves the fusion of the murine B cells with myeloma cells. It is noted that the selected myeloma cells are deficient in the hypoxanthine guanine phosphoribosyltransferase (HGPRT) enzyme. This can be achieved by culturing the myeloma cell lines in 8-azaguanine. The reason for this is to prevent the myeloma cells from employing a salvage pathway for purine biosynthesis, using the de novo pathway instead. The spleen cells and HGPRT negative myeloma cells are mixed together with polyethylene glycol as the fusing agent, followed by centrifugation. The desired outcome from these steps are splenic B cell hybridomas which can be cultured. It is necessary to remove unfused cells as they will compete for nutrients in culture and potentially outgrow the hybridomas. A selective medium consisting of hypoxanthine, aminopterin, and thymidine is used. The aminopterin, of which, can block cells from using the de novo pathway, the only pathway unfused myeloma cells can use to start with, so they will eventually die (Nelson et al., 2000). A similar method is followed with CHO cells instead of splenic mice cells. The cells are hybridysed with lymphocytes that produce the antibody of choice, then cultured (Chen et al., 2003).

Eventually, the newly established hybridomas to grow into colonies and begin producing antibodies. The meticulous screening process involves the isolation and selection of hybridomas that generate antibodies with the desired specificities – this is performed by testing the antibodies in the supernatant of the hybridoma culture, for example through an ELISA. Removal of unwanted hybridomas is important to reduce the incurrence of time and costs associated with culturing cells that will not be used. Hybridomas are initially cultured in multiwell plates before progressing onto flasks and bioreactors. Cell culture expansion not only generates sufficient mAb for processing and later formulation as a commercial product, but also allows some to be stored through cryopreservation for future investigation. Future investigations can include mAb isotype characterisation – for example mAb class or subclass, or the presence of either. These help with the subsequent selection of column-based purification techniques and mobile phases (Nelson et al., 2000).

Recombinant product recovery then begins with the harvesting of the cell culture, where the cell culture fluid undergoes lysis followed by the downstream processing purification steps summarised below (Hogwood et al., 2014).

2.2.3. Upstream Processing

The CHO cells first undergo process of perfusion in a bioreactor for up to 40 days, during which time, the product is removed and the media is replenished at specific intervals, resulting in cell densities by the order of 10^8/m. When a fed batch reactor is run for a shorter 10-21 days, a 10-fold lower cell density can be observed. First patented in 1989, the main advantage of operating a perfusion reactor is that the spent media and waste products are removed intermittently. Conversely, a fed-batch reactor is limited in cell culture volume and nutrient concentration for optimal cell growth (Petrossian and DeGiovanni, 1989). Amino acid compositions can be analysed by PAT to assess culture growth stages and optimise parameters accordingly (Claßen et al., 2017). As cells are grown in medium with air pumped into it, PAT sensors will need to be able to operate in solid, liquid and air phases (Bluma et al., 2010). These can measure partial pressures of respiratory gases, temperature, metabolite levels, bioburden, shear force, pH, leachables, secondary metabolites, in addition to cell density, viability, and productivity (Li et al., 2010). The in-line measurement of protein structure can allow aggregates, host cell protein and other impurities to be identified, quantified and addressed during product validation (Grav et al., 2017). Currently, the determination of viral loads takes several days and has not been amenable to in-line or on-line monitoring. Viral inactivation traditionally involves the bioprocess feed be held in large tanks, maintained at a low pH for up to an hour. Gillespie et al. (2019) had recently built a prototype viral inactivation system to support narrow residence time distributions and continuous flow. Many traditionally batch processing methods are being replaced by continuous processes – this streamlines the production line, increases manufacturing efficiency, and reduces carbon footprints.

2.2.4. Downstream Processing

Time constants in downstream processing span hours rather than the days in upstream. Protein A affinity chromatography capture of the mAb product soon follows on from viral inactivation, together with the removal of HCP.

The structure of the Protein A ligand is composed of five homologous domains which bind to the Fc moieties of the manufactured IgG molecules and is immobilised to agarose or polymeric column-packing media, with particle sizes between 45 to 125 µm (Ramos-de-la-Peña et al., 2019). Product loading, buffer wash and desorption are all performed co-currently. Protein A resins can account for over half of the cost of mAb separation and therefore undergo regular cleaning and reusing, up to 200 cycles. Gauging separation efficiency and binding affinity with the product by the in-line analysis of the eluate profile would help with decisions on when to replace column resins (Ladisch, 2001; Maruthamuthu et al., 2020). Successive chromatographic purification steps typically involve ion exchange chromatography and are further used in the removal of HCP and other impurities such as nucleic acids (Maruthamuthu et al., 2020; Gillespie et al., 2019).

A form of UF/DF, tangential flow filtration (TFF) can be used in the removal of salts and soluble from the mobile phases of the previous chromatography steps and increase its concentration. In a continuous configuration, a TFF systems needs to have the capability to handle diminishing volumes with multiple incoming units of fluid. Current analytical systems of process assessment involve mainly batch off-line protein characterisation and CQA validation studies such as ELISA for HCP and mass spectrometry (MS) for structures.

Continuous monitoring of chromatography eluates is the ultimate goal – refractive index, conductivity, UV fluorescence and absorbance detection-based techniques have all been proposed to achieve it (Harrison, 2020; Ladisch, 2001). In-line measurement capability, in particular, are of particular importance for generating real-time, accurate representations of analytes and reducing measurement times, contamination risks, and costs (Maruthamuthu et al., 2020).

Major strides have been taken in the implementation of continuous bioreactor operations upstream (Ahn et al., 2008; Konstantinov et al., 2006), downstream (Grabski and Mierendorf, 2009; Bisschops et al., 2009; Jagschies and Lacki, 2010) and integrated together (Warikoo et al., 2012). The integration of continuous upstream and downstream bioprocesses would streamline and simplify the process train, reducing value-redundant hold steps, residence and cycle times. In addition to cost savings, this can help reduce equipment size and the size of the overall facility. Recent successes in pharmaceuticals have attracted the attention of the FDA, who published guidelines on the continuous manufacture of synthetic drugs (FDA, 2011; Warikoo et al., 2012).

2.2.5. Current Analytical Methods

Bioindustries are responsible for ensuring the adherence to current good manufacturing practices (CGMP). This involves the following of standard operating procedures (SOPs) for equipment from equipment preparation such as chromatography column packing to running, the formal qualification of equipment (calibration, construction materials, validation), security, and adequate record keeping (Sofer and Hagel, 1997; Brannon-Pepas, 1993; FDA 1991).

Residual HCP from the CHO host cell systems are process-related impurities that require removal from the product and close monitoring from a regulatory standpoint due to clinical safety risks (Hogwood et al., 2014; Wang et al., 2009). Viable cell counts, media component changes, metabolite levels, and mAb production can be measured by liquid chromatography (LC)-mass spectrometry (MS), rheometers, osmometers, and Coulter counters all with timeframes spanning from half to several hours. For chemical analyses, chemometrics combined with data analytics have been used (Maruthamuthu et al., 2020).

First developed in 1970, enzyme-linked immunosorbent assays (ELISAs) have grown to become a standard technique in the quantitation of HCP concentrations (Engvall, 2010; Krawitz et al., 2006; Champion et al., 2001). A variety of types exist, for example, direct, indirect, competitive and sandwich. Sandwich ELISAs are commonly used in HCP quantification where the HCP antigen molecule becomes ‘sandwiched’ between a capture antibody bound to the surface of a 96-well plate and a biotin-labelled reporting antibody. Enzyme-linked antibodies are then added which bind to the primary reporting antibody, followed (Engvall and Perlmann, 1971; Gan and Patel, 2013).

Whilst sensitivity can be high with several nanograms of HCP detected, the process is labour-intensive and can take around 7 hours for each sample batch. Faster ELISA-related methods have been proposed such as those using glass nanoreactors and microfluidics, however, these still remain to be off-line and bioprocess samples would still require several serial dilutions to give accurate results. ELISAs are currently impossible to prepare directly with a bioprocess feed stream sample (Wang et al., 2009; Van Manen-Brush et al., 2020). The limited surface area and number of capture antibodies means that the abundant analyte needs to be reduced to a target concentration range for a particular ELISA kit. For bioprocess lines where HCP content is unknown, several dilutions usually need to be carried out to generate HCP concentrations within the standard range. After that, the ELISA derived HCP concentrations are scaled up according to the dilutions that were applied. This can introduce errors to the calculated final HCP concentrations which increases with each addition of a serial dilution step. Meaning that ELISA HCP tests are mainly limited to downstream processing steps where levels and risk weightings are much lower than pre-capture stages (Wang et al., 2009).

The ultimate goal of ELISA usage in bioprocessing is the development of anti-HCP antibodies that target a broad range of species with sensitivity up to parts per million in the drug substance. As such, the development of target analyte-specific antibodies for ELISA can be more expensive than generic kits that target a limited range of species present in a particular bioprocess.

2.2.6. Industrial Advantages of TRF Spectroscopy

The downsides to current methods of CQA assessment stem from their off-line nature which ultimately leads to long sample preparation analysis times, time and material-associated costs and limited manufacturing efficiency due to bottlenecks in the volumes that can be analysed. Limited information is generated on the effectiveness of bioprocess parameters due to formulation constraints which forms a barrier to implementing targeted manufacturing improvements.

In-line analysis is what this research has been aiming to validate – as outlined in the example in fig. 4. Here the main product feed is analysed in real-time, continuously, without any product loss or risk of contamination, therefore eliminating batch processing bottlenecks and speeding up total analysis times to under 20 minutes per in-line measurement. Raw fluorescence decay measurements of the feedstream together with subsequent decay fitting of

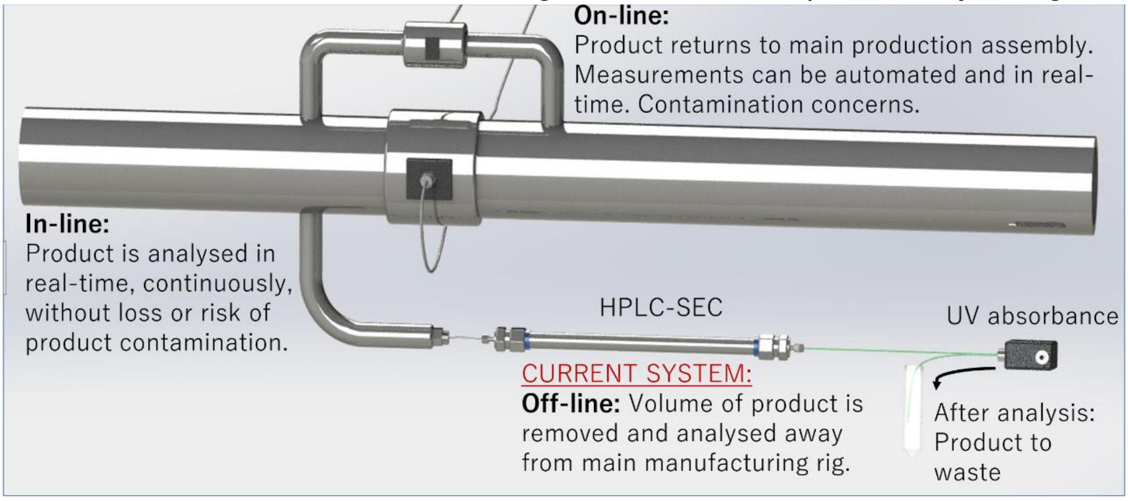

Figure 4: A comparison of the different possible analytical arrangements in the bioprocess. Quantification through inline TRF spectroscopy does not require a preceding off-line chromatography step or supplementary sample assays.

species using pre-selected decay parameter settings, every 20 minutes, can provide a snapshot of bioprocess performance. Species quantities can be logged with each sampling to outline performance over time and with the application of different CPPs.

One solution to the analytical bottlenecks of current off-line methods is to use the in-line time-resolved fluorescence spectroscopy instrument introduced in the previous chapter. TRF spectroscopy meets the above measurement criteria. Evaluating this method for the quantification of process-related impurities such as HCP has been another major focus of my EngD project. This study aimed to evaluate the prospect of its use in industrial bioprocessing from an investigation into its dynamic range, proof-of-concept tests and head-to-head measurements of HCP against ELISA. As samples can be run without an off-line device as they are, modifications to their buffer or concentration do not need to be applied, therefore sample preparation and analysis times are a fraction of standard techniques. This allows it a greater flexibility of positioning between multiple bioprocess stages and offers information that is more bioprocess representative than methods that require significant dilutions and buffer exchanges, thereby supporting the FDA's QbD framework.

2.3. Quantum Mechanics

Light can be considered as electromagnetic energy, packed into photon particles travelling on a linear path at a speed, c, of 3×10^{10} cm/s. An oscillating electrical field is perpendicular to the direction of the travelling light wave and perpendicular to the plane of oscillation for this electrical field, there is an oscillating magnetic field. The frequency, v, of the light wave can be described as the frequency of oscillation of these field vectors. One wavelength of light, λ, is the distance travelled by a photon during one complete oscillation. The speed of light is related to its wavelength and frequency through the following equation:

$$c = \lambda v \tag{5}$$

Due to the electric field possessed by light, if an electrically charged particle, such as an electron was to be placed in the light path, it would be possible for it to absorb energy from that electric field. An electron in a molecule in its ground state would be raised to an unoccupied electron orbital upon the absorption of energy from the electric field of light. It can then be transported to another site in the molecule, and the molecule is said to be electronically excited. The frequencies of light that are absorbed by a molecule are dependent upon the combination of elements, chemical bonding, local chemical environment and the fluorophores present.

The "packet" or quanta of energy, E, that is carried by one photon along one wavelength of light with frequency v, can be summarised by the following equation:

$$E = hv = \frac{hc}{\lambda} \tag{6}$$

Where h is Planck's constant at 6.626068 x 10^{-34} m^2 kg s^{-1}. The energy difference between the excited E_e and the ground state E_g of a molecule must be equal to the energy of the photon for it to be absorbed, that is:

$$E_e - E_g = hv \tag{7}$$

Due to the changes in the molecular distribution of electric charge when light is absorbed, the absorbing molecule is said to undergo electronic dipole transition. Different molecular electronic states result in different dipole moments, with the direction of polarisation being the line on which the dipole moment changes after going from the ground state to the excited state. The range of any given absorption bands in a spectrum are associated with the energy of electronic transition, whereas the intensity of absorption is formed by the magnitude of the electronic transition dipole moment. The electronic absorption spectrum represents the quantum response (Sharma and Schulman, 1999). The simplified Jablonski diagram in fig. 5 illustrates the energy level changes that occur when a fluorophore absorbs energy hv_A and emits a photon in the form of fluorescence at energy hv_F. Γ, the rate of emission for a fluorophore, and k_{nr}, the rate of non-radiative decay to ground state S_0, can be used to calculate the quantum yield, Q:

$$Q = \frac{\Gamma}{\Gamma + k_{nr}} \tag{8}$$

Eq. 8 describes the ratio of photons emitted to photons absorbed or the proportion of fluorophores that undergo fluorescence decay. Q can reach close to 1, if $k_{nr} < \Gamma$ or the radiationless decay rate is less than the rate of radiative decay (Lakowicz, 2006).

For a given fluorophore, the decay lifetime, τ, is defined as the average time spent by a molecule in the excited state before it returns to ground state. In equation form this is:

$$\tau = \frac{1}{\Gamma + k_{nr}} \tag{9}$$

The intrinsic or natural decay lifetime, τ_n, without the influence of non-radiative processes, would be:

$$\tau_n = \frac{1}{\Gamma} \tag{10}$$

τ_n can be calculated from the extinction coefficient, and absorption and emission spectra of a fluorophore (Lakowicz, 2006).

Fluorescence spectroscopy measurements can broadly fall into two categories: time-resolved and steady-state (see fig. 6). Time-resolved

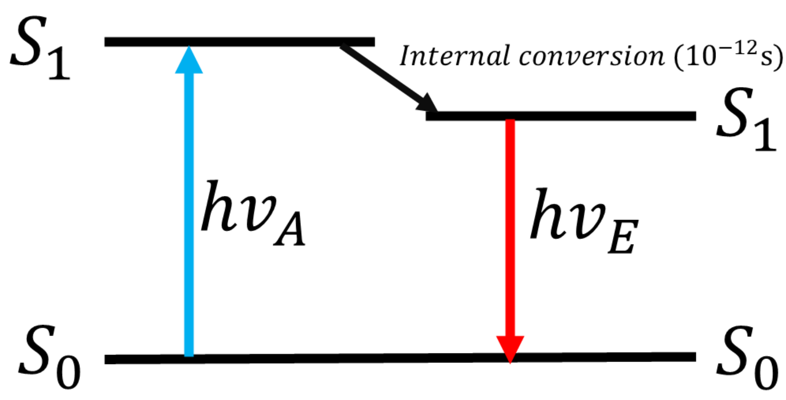

Figure 5: Jablonski diagram of fluorophore excitation and emission of photons during the fluorescence decay process. S_0 and S_1 represent the ground and singlet excited states, respectively. The blue arrow is the energy of the absorbed photon, whereas the red arrow represents the energy of the emitted photon, where v is photon frequency and h is Planck's constant at 6.63E-34 Js.

fluorescence spectroscopy is the technique used in this project, where the protein sample is excited with a light pulse and the subsequent intensity of fluorescence decay is recorded over time with a photodetection system. Steady-state measurements, on the other hand, involve the continuous illumination of the sample with a particular wavelength of light, then the time-averaged fluorescence decay intensity is calculated.

If a fluorophore is excited with pulse of light, an initial population of excited fluorophores, n_0, are generated. Then this population of excited fluorophores, $n(t)$, at time t after excitation, decays at a rate of $\Gamma + k_{nr}$, which is represented by the following differential:

$$\frac{dn(t)}{dt} = (\Gamma + k_{nr})n(t) \tag{12}$$

As every excited fluorophore has the same probability of emitting a photon in a set time after an excitation event, the random nature of the decay process can be described as an exponential decay of the population of excited fluorophores:

$$n(t) = n_0 e^{-\frac{t}{\tau}} \tag{13}$$

In fluorescence spectroscopy, rather than observing the number of excited fluorophores, the intensity of fluorescence decay is observed. This is proportional to $n(t)$. Therefore, by integrating eq. 12, substituting in eq. 13 and re-writing in terms of fluorescence intensity we derive eq. 14:

$$I(t) = I_0 e^{-\frac{t}{\tau}} \tag{14}$$

This can be applied to a given fluorophore with a single decay time (ns) of τ (eq. 9), and decay intensity at 0 ns, I_0. I_0, the intensity after the excitation pulse, is proportional to the concentration of fluorophores is a sample. The decay lifetime can be calculated as the gradient of $\log I(t)$ against t, however, this is more commonly achieved by fitting exponential decay models (Lakowicz, 2006).

Not all samples possess only one decay time and therefore eq. 8 cannot be applied to mixtures of species. Eq. 9, on the other hand, assumes a sample has multiple decay times – this concept is explored further with the mode TRF operation:

$$I(t) = \sum_i \beta_i \exp\left(-\frac{t}{\tau_i}\right) \tag{15}$$

The fractions of fluorophore in each environment can be represented by the pre-exponential factors β_i. TRF spectroscopy has the aim of recovering the decay times, τ_i and the amplitudes, β_i, through decay lifetime measurements (Lakowicz, 2006).

2.4. Decay Signal Processing

Whilst the high sensitivity of tryptophan residues to local environments makes them ideal candidates in the investigation of the quantities and biophysical behaviour of protein species. Grossweiner and Usui (1971) had been looking into photo-oxidised tryptophan residues during the flash photolysis of lysozyme, in which they were able to deduce the quantum yield of 1-2 tryptophan residues. Early work in evaluating fluorescence decay kinetics (1974) and the fluorescence decay of tryptophan (1976) came with studies by

Grinvald and Steinberg. They employed a method of least-squares to estimate a functional form of the decay data with the aim of minimising the sum of weighted squares of the residuals to obtain a best fit between decay data and the decay function. Back then the analysis of fluorescence decay data to obtain parameters that are characteristic of the decay process was described as “notoriously difficult” (Grinvald and Steinberg pp. 584, 1974; Lanczos, 1956; Grinvald and Steinberg, 1976).

Before them, Knight and Selinger (1971) had noted the problems of contending with decay curve distortion due to the finite pulse width of the excitation source and the truncated data that was generated. They concluded that whilst deconvoluting signals can offer a greater body of information they also had the propensity to increase noise. The challenge of deconvoluting decay data that has been distorted by the spectroscopic instrument response was also examined by Khidir and Decius (1962) and is a challenge that, whilst to a smaller degree, still exists today (Knight and Selinger, 1971; Khidir and Decius, 1962; Lee et al., 2022).

The often noise-prone decay intensity signals result in the need for complex signal deconvolution tools to distinguish minute differences between particular tryptophan conformations. One mode of interpreting fluorescence lifetimes is by statistically-fitting exponentials to the decay curves. This can provide information on the overall decay process that is species and biochemical

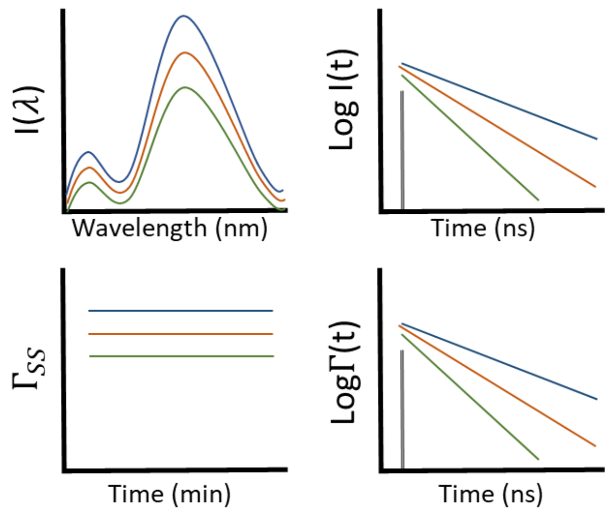

Figure 6: Differences in measurement domain between steady stage fluorescence (left plots) and time-resolved fluorescence (right plots).

environment-specific. Preliminary studies on the interpretation of tryptophan decay lifetimes had been conducted by Alcala et al. (1987) applied sum of exponential fitting on multi-frequency phase fluorimetry decay data from single tryptophan residues. However, instrumentation-based limitations exist in substantially sensitive instrumentation to capture fluorophore decay lifetimes in the nano-picosecond timescale (Alcala et al., 1987).

Time-resolved fluorescence (TRF) measurements are one of the most commonly used spectroscopic techniques, named so as decay behaviour is registered on the time domain and have been the focus of this project throughout. They rely on a sample being excited with a light pulse of a shorter lifetime than the fluorophores. The sample decays exponentially until excited by the next pulse of light. Widely used practises of measuring fluorescence lifetime events involve using photodetectors and photon-sensitive arrays (Sharma and Schulman, 1999). Early concepts on diffusion and molecular kinetics were solidifying in the late 18th century, forming the basis of fluorescence correlation spectroscopy (Ehrenberg and Rigler, 1974; Elson and Magde, 1974). Significant improvements to excitation, detection and computational technologies over the next decades reduced signal to background ratios by over 10^6-fold. Single organic dye molecules could be excited, and the resulting fluorescence recorded in fractions of milliseconds (Rigler, 1995; Mets and Rigler, 1994; Rigler and Mets, 1992) to picoseconds (Georghiou et al. 1985).

2.4.1. Convolution

To grasp the fundamentals of the signal deconvolution process, heavily used in this project to deconvolve quantity-describing decay fittings pertaining to different protein species, one first needs to start with its reverse counterpart: signal convolution. Convolution is a way of describing a linear system in the time-domain. Convolving the input signal to a system with its impulse response will generate an output that provides the performance characteristics of such a system.

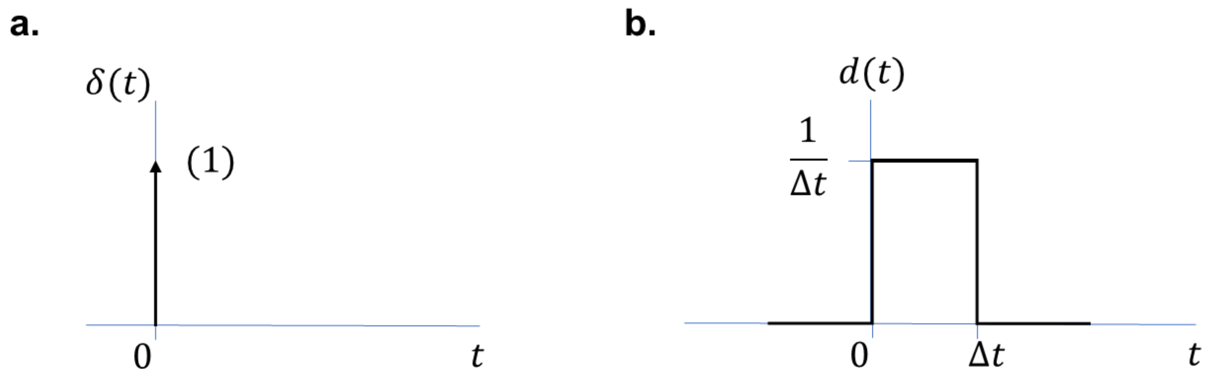

Figure 7: a) The impulse function and b) a rectangular pulse on the time domain.

The basics of signal convolution starts with an inverse Laplace transform of the system transfer function $H(s)$, to give the impulse response *h(t)* of a system in the time-domain:

$$h(t) = L^{-1}[H(s)] \tag{16}$$

The graphical notation for this can be found in fig. 7a. A signal occurring at time(s), *t*=0, with height infinity and a height of 0 at all other times, can be used to define the unit impulse $\delta(t)$:

$$\delta(t) \begin{cases} \infty \; if \; t = 0 \\ 0 \; if \; t \neq 0 \end{cases} \tag{17}$$

Integrating the unit impulse to obtain the area underneath it, will give 1. When this principle is applied to a rectangular pulse, *d(t)*, with start time, *t*=0 to *Δt* seconds and a height of 1/*Δt*, an area of 1 is again yielded upon integration:

$$\int_{-\infty}^{\infty} d(t)dt = 1 \tag{18}$$

A pulse width reduction will result in a height increase, though the area underneath the pulse will still remain to be 1, a summarised by eq. 19:

$$\delta(t) = \lim_{\Delta t \to 0} d(t) \tag{19}$$

Signal approximation can be achieved by the summation of a number of impulses – with approximation accuracy $\propto 1/\Delta t$. As pulse width, Δt, tends towards zero, d(t) tends toward the unit impulse. The approximation quality increases as pulse width is reduced. Therefore, a pulse at t = n *Δt* with height *x*(*n Δt*), equal to the signal at that point, can be described by the following relationship:

$$x(n\,\Delta t)d(t - n\Delta t)\Delta t \tag{20}$$

This is the basic pulse shown in fig 7b, amplified by $x(n\Delta t)\Delta t$ and delayed by $n\Delta t$ seconds, giving height $x(n\,\Delta t)$. Eq. 20 can be re-written as a summation of the pulses used in the approximation, $\hat{x}(t)$, of a signal waveform:

$$\hat{x}(t) = \sum_{n=-\infty}^{\infty} x(n\,\Delta t)d(t - n\Delta t)\Delta t \tag{21}$$

As $\Delta t \to 0$, the time interval *Δt* becomes differential $d\tau$, the pulse becomes an impulse at $n\,\Delta t$ and $n\,\Delta t$ becomes a continuous time variable, τ. The summation can now be described as an integration:

$$x(t) = \int_{-\infty}^{\infty} x(\tau)\delta(t - \tau)d\tau \tag{22}$$

To apply this impulse to a linear system we need to find the Laplace transform of input $\delta(t)$:

$$L[\delta(t)] = \int_0^{\infty} \delta(t)\exp(-st)\,dt \tag{23}$$

The one point the system has any value is at *t*=0, due to $\exp(-st) = \exp(0) = 1$. The Laplace transform of an impulse signal is therefore equal to its integrated form, which is 1.

$$L[\delta(t)] = \int_0^{\infty} \delta(t)(1)dt = 1 \tag{24}$$

When the Laplace transform of the input is multiplied by the system transfer function, we derive the Laplace transform of the output:

$$Y(s) = H(s)(1) = H(s) \tag{25}$$

The time-domain output is an inverse Laplace transform of Eq. (25):

$$y(t) = L^{-1}[Y(s)] = L^{-1}[H(s)] = h(t) \tag{26}$$

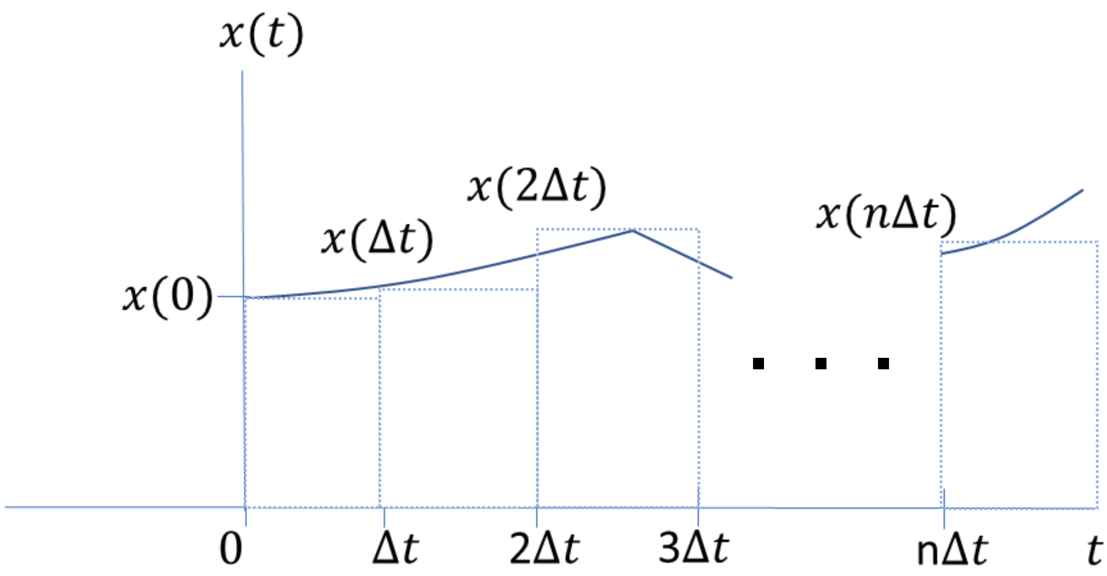

Figure 8: Signal summation and approximation using a packed pulse rectangular regimen.

Applying a unit impulse of $\delta(t)$ would therefore have impulse response, *h(t)*, as the output.

As indicated earlier with eq. 21, the approximation of input $x(t)$ can be achieved by summing delayed and appropriately scaled rectangular pulses as illustrated in fig. 8. The system response to such a pulse then becomes:

$$x(n\,\Delta t)h'(t - n\Delta t)\Delta t \tag{27}$$

Where *h'(t)* is the system response to the rectangular pulse, *d(t)*. Eqs. 21 and 27 can be superimposed on the time domain, the response to the summation of inputs in eq. 23 would therefore be:

$$\hat{y}(t) = \sum_{n=-\infty}^{\infty} x(n\,\Delta t)h'(t - n\Delta t)\Delta t \tag{28}$$

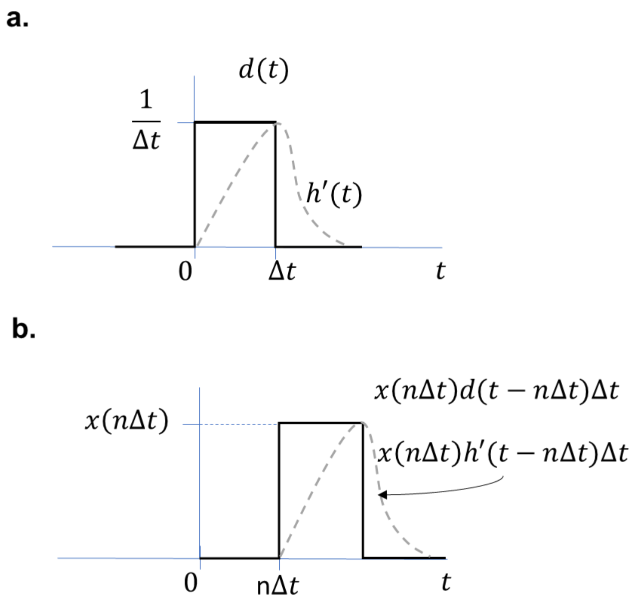

Fig 9: a) System response h'(t) to a single pulse d (t). b) typical pulse, $x(n\Delta t)d(t - n\Delta t)\Delta t$, used to approximate the input x(t).

As observed with eq. 21, as $\Delta t \rightarrow 0$, the pulse manifests as an impulse at $n\Delta t$ seconds, the product $n\Delta t$ becomes τ (the continuous time variable), the time step *Δt* becomes *dτ*, $h'(.)$ becomes impulse response $h(.)$ and the summation of inputs becomes an integration of inputs (see fig. 9). Thus, eq. 28 can now be written as the *convolution equation*:

$$y(t) = \int_{-\infty}^{\infty} h(t - \tau)x(\tau)d\tau \qquad (29)$$

Eq. 29 has a commutative property and can also be written in the following alternative term arrangement:

$$y(t) = \int_{-\infty}^{\infty} x(t - \tau)h(\tau)d\tau \qquad (30)$$

The convolution operation is commonly denoted with an asterisk (*):

$$y(t) = x(t) * h(t) = h(t) * x(t) \qquad (31)$$

Other properties include being distributive over addition (eq. 32) and associative (eq. 33) (see fig. 10a):

$$h(t) * [x_1(t) + x_2(t)] = [h(t) * x_1(t)] + [h(t) * x_2(t)] \quad (32)$$

$$h_2(t) * [h_1(t) * x(t)] = h_1(t) * [h_2(t) * x(t)] \quad (33)$$

Finally, a key property with applications in communication systems modulation, is that the product of waveforms in the time-domain are equivalent to their convolution in the *s* (frequency) domain, summarised by eq. 34 and eq. 35, respectively:

$$L[x_1(t)x_2(t)] = \frac{1}{2\pi j} X_1(s) * X_2(s) \quad (34)$$

$$F[x_1(t)x_2(t)] = \frac{1}{2\pi} X_1(\omega) * X_2(\omega) \quad (35)$$

Many linear system components such as inductors or capacitors rely on being readily amendable to transform-domain descriptions. Performing inverse Laplace transforms to the transfer functions of certain electronic arrangements to find the impulse response can be easier than directly working this out from the circuit. Situations where this would not be appropriate are when there is a time delay to the signal. In such cases determining its Laplace transfer function becomes more challenging. Starting with an evaluation of the impulse response instead and performing a Laplace transform on it can help with obtaining the desired transfer function (Mulgrew et al., 2003).

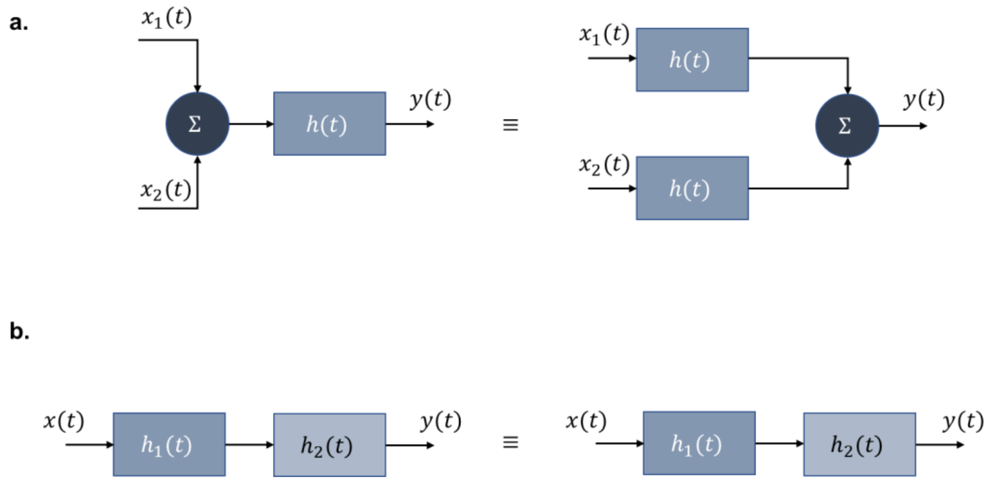

Fig 10: Illustrations of a) the summation and distributive, and b) the associative properties of convolution.

Being able to analyse decay functions unaltered by instrument-derived distortions is the target for the many biochemical fields that employ spectroscopic techniques. The majority of distortions arise from the finite width of the excitation pulse and the detection electronics. Whilst the sum of exponentials approach can be used to approximate the decay curve, a challenge remains in determining the decay parameters and exponential terms (Lakowicz, 2006; Demas, 1983). The programs used in this study generate accurate representations of decay times and other parameters which are explored in more detail in the next section. The choice of deconvolution program is dependent upon desired accuracy, algorithm complexity and speed of computations for the instrumentation at hand. The methods include (Apansovich and Novikov, 1990):

Perisamy (1988) outlined a means of using nonlinear least squares to fit data to *I(t)* (eq. 14) and obtain optimum decay parameters. This requires the convolution integral to be found (eq. 36) and the partial derivatives of the decay parameters.

$$F(t) = \int_0^t R(s)I(t-s)ds \qquad (36)$$

In 1990, Apansovich and Novikov presented a novel method for deconvoluting fluorescence decay data using single and double exponential decays, concluding that the double exponential decay has the highest accuracy when the decay constants are approximately equal to the registration interval and have a minimum factor of 2 difference between them.

Whilst computing fluorophore number and exact positioning for polymeric mixtures is an additional challenge due to the differences in fluorophores and their chemical environments, a variety of models can be tailored to fit data from mixtures of varying complexity. Djikanović et al. (2007) investigated an asymmetric log-normal and a combination of log-normal, and symmetric Gaussian models to analyse fluorescence spectra of biological molecules. They were able to deduce approximate probability densities for different fluorophore positions and structural information on compounds containing benzene rings. Fluorescence decay intensity signals for known samples can be used to deconvolute signals for unknown ones.

Even if a linear signal input-output relationship exists, a practical system will smooth the incident signal by applying a weighted mean over a small interval of the independent variable x. The magnitude of the output signal $h(x)$, is dependent on that of the incident signal $g(x)$. Green's (instrument) function $f(x)$ is a description of how the input at x is distributed along the observed range of x values, or instrument resolution. The signal at x, can be represented by the following convolution integral:

$$h(x) = \int_{-\infty}^{\infty} f(u)g(x-u)du \equiv f * g \tag{37}$$

Eq. 37 assumes that Green's function does not vary with x and t, and the system is therefore linear. It is termed the *convolution* integral in a nod to the "folding over" of the incident signal $g(x-u)$ with respect to Green's function $f(u)$. A simple example of this in action is with a wide-entrance and exit slotted scanning monochromator – the input of two rectangular functions results in an output that is a convolution of these. The resultant convolution being a triangular function. A linear invariant system convolutes the incident signal $f(u)$, which smooths it, reduces peak amplitude and spreads them out. Signal smoothing effects can be further pronounced when convolution is used in conjunction with a Gaussian smoothing filter (Davis et al., 2001).

2.4.2. Instrumentation

At the kernel of any fluorescence spectrometer are the excitation and photon detection sources. In the case of time-resolved fluorescence spectroscopy, the source of exciting photons is typically a laser that is required to work in synchronisation with the detection equipment for the correct registering of decay lifetimes.

Many of the first developed lasers in the 1960's would have had a fixed frequency of operation and single lasing wavelength which limited tuning to a narrow gain profile making them unsuitable for the majority of spectroscopic applications. The dawn of laser-based spectroscopy began with the advent of tuneable coherent dye lasers that allowed measurements to be made along a wide range of the electromagnetic spectrum.

Today the dye laser is operated with an organic molecular dye, suspended in a gain medium solvent. The variety of dyes ensure that laser emission wavelengths encompass around 320 nm to 1000 nm. Dye species are selected so that the generation of triplet states or non-radiative decay, which deplete fluorescence intensity, are minimised and exciting radiation is returned as fluorescence emission. The fluorescence quantum yield is the ratio of photons emitted by a laser dye candidate to the number of photons absorbed, the closer the value of the resulting fraction to 1, the more suitable a molecule for use as a laser dye.

Non-linear optical methods of increasing laser frequencies can extend the operating range of visible light lasers to include ultraviolet (UV) and infra-red (IR) regions of the electromagnetic (EM) spectrum. Second harmonic generation is one such method, where radiation with a wavelength of λ and frequency of v, is applied to a non-linear crystal, which then generates radiation at a wavelength of $\frac{\lambda}{2}$ and frequency of $2v$. Wavelength-dispersive prisms and dichroic mirrors can be integrated into the laser to separate co-propagating beams. To extend further into deep-UV territory, sum frequency generation is another non-linear technique that can be used. This involves laser frequencies v_1 and v_2 being mixed in a non-linear crystal which, in turn, generates a sum of the two frequencies. Compared to flashlamp pumped lasers, pulsed laser pumping offers greater input to output light conversion efficiencies, and greater flexibility with pulse repetition rates, pulse energy outputs, and pump wavelength.

The irradiance, *Ir* [Wm^{-2}], capabilities of a continuous laser can be described as the incident laser power per area that is irradiated, or in terms of power, *P* [W] for an area with radius, *r* [m] (McCoustra et al., 1995):

$$Ir = \frac{P}{\pi r^2} \tag{38}$$

For a pulsed laser, two types of irradiance need to be considered: the average irradiance, Ir_{AV} and the peak irradiance, Ir_{PEAK}. These terms are dependent on *E* [J], energy of each pulse and *R* [Hz], the laser repetition rate, summarised in the equations below:

$$Ir_{AV} = \frac{ER}{\pi r^2} \tag{39}$$

$$Ir_{PEAK} = \frac{E}{\pi r^2 \tau_{pulse}} \tag{40}$$

The laser pulse, τ_{pulse} [s], is often not constant and varies with time, so the instant of irradiance where the laser pulse has reached peak intensity, may exceed Ir_{PEAK}, which offers a rough measure of the term.

Lasers and the molecules they excite provide the source of photons that quantum detectors rely on to register measurements. By mode of operation, photodetectors can be divided into three main types: photovoltaic, photoconductive and photoemissive. The former two generate voltage gains by the conversion of incident photons on a photosensitive material into conductive electrons. Devices that operate in this way are aptly categorised as photon detectors as they convert photons into electrons (Long, 1977).

Sampling oscilloscopes can be used to trigger excitation sources and measurement events. For sampling, a slow sweep generator on a low setting is used triggering initiates a linear increase in the fast sweep generator. When a crossing event occurs between the slow sweep and the fast sweep ramp, this is detected by the comparator which strobes the sample and hold and records an analogue data point. The signal is held until the next triggering. (Sharma and Schulman, 1999).

Signals registered by an optoelectronic transducer often require conditioning before they can be processed further for recording n a computer. Conditioning is required to make them acceptable for subsiding circuitry, such as analogue to digital conversion, amplification or voltage division.

Fluorescent compounds emit photons at longer wavelengths than was used to excite them, also known as the Stoke's shift, and means that the excitation wavelength can be filtered out completely to the photodetector by the use of filtering optics and dichroic mirrors that allow a limited range of wavelengths to pass through and a limited range to be reflected at a specified angle (Sørensen et al., 2022; Lakowicz, 2006).

2.4.3. Fluorescence Spectroscopy in Biophysical Characterisation

To generate fluorescence decay signals, one first has to excite intrinsic or extrinsic fluorophores with energy supplied by a photon, the photon gets absorbed. The energy of which, is directly proportional to its frequency. And this energy is then transferred to an electron. Once an electron is excited there are several ways that energy can be dissipated, one of which is in the emission of photons with a lower energy than the exciting photon as demonstrated in the Jablonski diagram in fig. 5. The process is very fast lasting a matter of nano seconds, so faster-responding electronics are required for measurements.

Fluorophores can be described as either intrinsic or extrinsic. Intrinsic being those occurring in nature, and extrinsic are those added to samples so that it displays a more easily processable spectral profile. Tryptophan and tyrosine residues form major fluorophores in proteins, absorbing wavelengths near 280 nm with peak emissions near 320 nm (Neckers, 1973). As fluorophores are very sensitive to local chemical structures and as they absorb light along a particular direction with respect to the molecular axes, they are very useful for use in protein characterisation and polarization or anisotropy studies (Lakowicz, 2006; Sørensen et al., 2022).

The process is very fast lasting a matter of nano seconds, so fast responding electronics are required for measurements. Tryptophan has proven itself to be a very useful probe of protein histology and dynamics, however, its use in the study of protein-protein interactions has in the past been limited by the challenges in distinguishing fluorescence intensity signals in a mixture of proteins. To overcome this issue, 7-azatryptophan and 5-hydroxytryptophan have been used as extrinsic fluorophores which, with their distinctive spectral features, allow the selective excitation and observation of fluorescence emission (Lakowicz, 2006).

Whilst the vast majority (>99%) of intrinsic fluorescence in proteins can be attributed to tryptophan and tyrosine (Hales et al., 2021; Neckers, 1973), an array of different intrinsic fluorophores can be found in a typical bioprocess broth – including tryptophan, tyrosine, phenylalanine, NADH, FAD, pyridoxal phosphate and pyridoxamine phosphate (Lakowicz, 2006). These amino acids, coenzymes and vitamins correlate with cell metabolism and protein production, so measuring their quantities through fluorescence decay intensities would provide insight into the effect of critical process parameters (CPPs) on culture viability and species profiles (Graf et al., 2019).

2.5. In-line Process Analytical Technology

The identification and evaluation of an in-line method of quantifying species during bioprocessing has clear implications for the United States Food and Drug Administration (FDA) process analytical technology (PAT) regulatory framework. PAT can be defined as a system for performing manufacturing analysis and control through regularly timed measurements of CQA and CPPs to ensure final product quality exceeds regulatory standards (FDA, 2004). A key strategic driver of PAT technologies is the industrial target for transitioning from discrete batch sequential unit operations to continuous manufacturing. Regular in situ or in-line measurements would support the automated control of such a transformation. Continuous manufacturing has the advantages of reducing: process waste, plant energy footprints, manufacturing costs, requirement for off-line batch testing, and manufacturing cycle times. Whilst increasing manufacturing efficiencies, yields and product quality (FDA, 2016; Clegg et al., 2020).

In practice this can include the following associations:

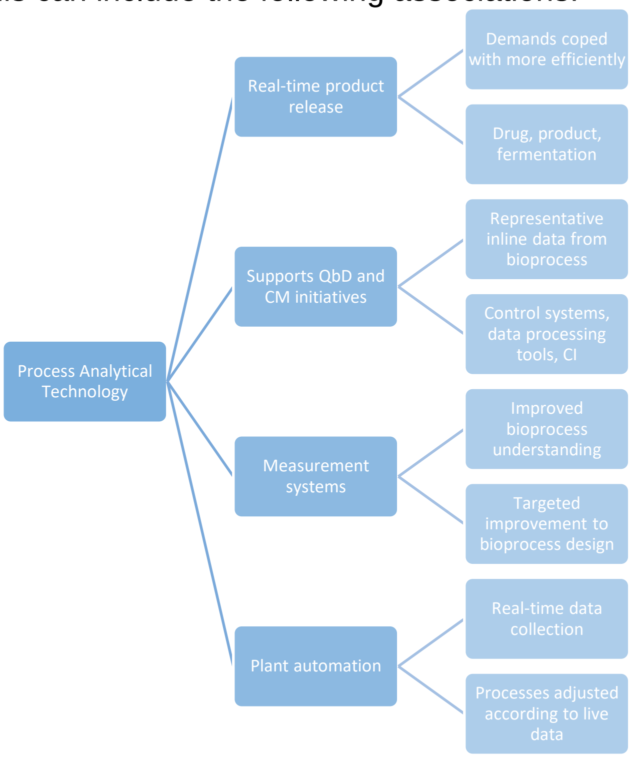

Figure 11: Diagram of the key characteristics and associations of process analytical technology.

As more companies are seeking to profit from the swelling market for biologics, an increasingly competitive research and development (R&D) environment is being fostered. This is driving innovation for improved quality of biological products, cheaper and more efficient production (Rolinger et al., 2020; Grilo and Mantalaris, 2019; Gagnon, 2012). Part of the improvements to production have come from the digital transformation of bioprocess lines – this has involved the implementation of PAT platforms and measurement sensors for process control (Grebe et al., 2018; Steinwandter et al., 2019; Rolinger et al., 2020).

Using spectroscopic sensors for bioprocess monitoring offers several advantages, such as eliminating the need for sample preparation, conditioning and destruction, as well as offering the opportunity for automation (Bakeev, 2010). Sensitivities to sample biochemistries and concentrations can be readily modified with modifications to system detectors and/or optics. With the use of multiple sensors improving accuracy and dynamic range – increasing the variety of product attributes that can be measured (Liggins et al., 2017; Rolinger et al., 2020). A linear correlation exists between cell culture fluorescence intensity and the concentration of biomass. When it comes to detection limits and dynamic ranges, these can easily be tuned to the bioprocess by component choice selection and would far exceed many other alternative analytical methods. With industrial ambitions to achieve continuous production cycles, in-line monitoring can allow multistage analytics, early fault detection, real-time product release and minimise contamination risks.

A major tool in multivariate data analysis (MVDA), multivariate calibration is the modelling of the relationship between the multitude of signals registered for a sample and the concentrations of constituents they correspond to (Eriksson et al., 2006). More recent work on testing in-line real-time methods of bioprocess sample monitoring have included adopting multivariate calibration and combining UV spectroscopy with partial least squares regression (PLS). This allows selected proteins to be detected and quantified in multicomponent mixtures. The variation in aromatic amino acid residues between protein species gives rise to variation in mid-UV absorption spectra. PLS can be used to calibrate models that correlate protein concentration with the mid-UV absorption spectra. This approach has successfully been used for high throughput chromatography systems and for the in-line quantification of co-eluting proteins post chromatography stages (Hansen et al., 2013; Brestrich et al., 2014; Brestrich et al., 2015).

Spectral measurements and selective protein quantification have also been performed for protein concentrations up to 75 mg/mL (Brestrich et al., 2018). These have been used to predict mAb concentrations in Protein A capture effluent. Other UV-based PAT methods have overcome the time delay limitations between sampling and results generation. Such as that designed by Bängtsson et al. (2010) for continuously determining the binding capacity of a chromatography column by analysing the differences in the feed and effluent UV absorbance signals (Patent WO2010151214A1; Rüdt et al., 2017). In-line UV absorbance measurements have successfully been applied to correlate absorption spectra with the concentrations of selected proteins for real-time monitoring. Brestrich (2014) combined a conventional AKTA® purifier chromatography system with a diode array-based detector and a Matlab software interface to deliver precise retention times and in-line protein quantification using spectral data (Brestrich et al., 2014; Brestrich et al., 2015). UV-vis spectrometry has also previously been used in the determination of reaction endpoints during fostamatinib disodium synthesis, Hart et al. (2015) used multivariate analysis and principal components analysis (PCA) to predict the purity of a reaction intermediate from manufacturing run data. PAT allowed overcharges of reactant to be observed, which in turn would have raised impurity levels beyond the acceptance criterion and the expensive loss of product (Clegg et al., 2020).

Graf et al. (2019) built an in-line system to report information on key variables involved with cell growth, based on fluorescence decay intensities measured after using different excitation wavelengths. The cell culture would be excited

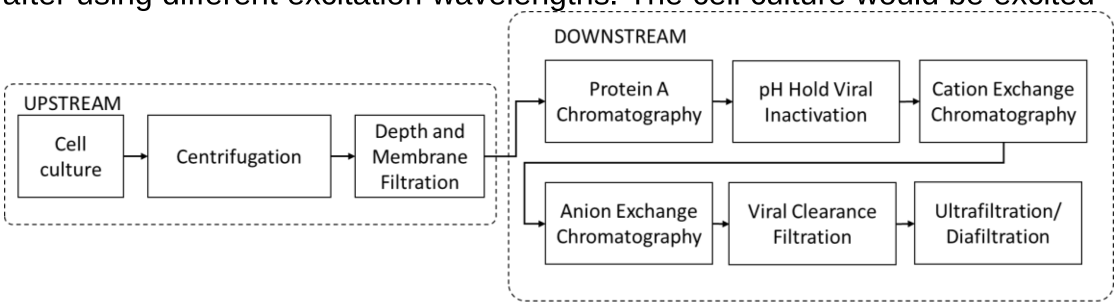

Figure 12: The division of upstream and downstream bioprocess for a typical mAb production line.

at different wavelengths to register fluorescence intensities pertaining to different protein markers of each variable. The instrument was divided into 2 parts – the sensor and a probe that they designed. The sensor consisted of 3 individually controlled light emitting diodes (LEDs) to excite the mammalian cell cultures. From each led a bundle of optical fibres connected to the probe head, which was inserted into the bioreactor. The detector was a back thinned CCD-spectrometer. They found that the combination of LEDs and CCD spectrometer they used, generated reproducible results with most of the intrinsic fluorophores present in the cell cultures traceable with their sensor. They found that compared to a previously used and discontinued BioView® system, the absence of multiplexers, and moving parts such as filter wheels improved dynamic range, instrument longevity and reduced the potential need for maintenance (Graf et al., 2019).

More recently, Sørensen et al. (2022) have investigated light-induced fluorescence spectroscopy as an in-line PAT tool for the quantification of low concentrations of pharmaceutical ingredients. They were able to measure the content of tryptophan with concentrations at 0.10 w/w%. Due to the non-linear relationship between their calibration and in-line measurements, employing a support vector machine regression (SVM-R) model was deemed to be a more robust choice compared to PLS. With SVM-R as the prediction model they achieved a correlation coefficient of R^2 = 0.997 for tryptophan concentrations (Sørensen et al., 2022; Igne et al., 2014).

2.5.1. In Bioprocessing

MAb biomanufacture can be divided into upstream and downstream unit operations. Upstream includes cell culture and harvesting, whereas downstream consists of a series of purification stages – formed by chromatography and filtration steps as shown in fig. 12. The product life cycle begins with the cell culture fed inoculum and expanded in bioreactors, before protein expression. For bacterial cultures a homogenisation step is required for product release and host cell debris are separated from the product by centrifugation and depth filtration. For CHO manufacturing lines, scales below 5000L seldom require centrifugation (J. Welsh 2022, personal communication, 5th September; Hong et al., 2018; Shukla and Thömmes, 2010; Kelley 2009).

Host cell protein (HCP) is further removed by a cascade of downstream purification stages, starting with mAb capture by Protein A (PA) chromatography and a subsequent virus inactivation pH hold step (PPH). MAb has a very high binding affinity to the protein A ligand, hence this first chromatography step results in the prevention of proteolytic degradation and the achievement of >98% product purity (Rüdt et al., 2017; Hong et al., 2018; Shukla et al., 2007; Shukla and Thömmes, 2010; Hahn et al., 2006). Process related impurities such as HCP and DNA pass through the column at a neutral pH, while the mAb elutes at an acidic pH. Off-line quantification of mAb is typically used before Protein A loading with dynamic binding capacity (DBC) studies to determine break-through curves for antibodies on particular columns. The columns can be loaded to 80% of their DBC which avoids significant losses of product – this can be scalable provided column length and linear flow remains the same (J. Welsh 2022, private communication, 5th September). However, the lack of real-time monitoring in batch loading mode results in an analytical bottleneck that forms a barrier to continuous mAb purification. The use of single wavelength monitoring measurements have the added challenges of mAb and impurity species both absorbing at 280 nm, with the size differences between mAb monomers and dimers as small as several nm. MAb titres in the harvested cell culture fluid are commonly determined through off-line methods, which need to be repeated for each batch due to cell culture variability and to adapt load volumes into chromatography columns (Rüdt et al., 2017; Gupta, 2002; Fahrner and Blank, 1999a; Fahrner and Blank, 1999b). The hold step at this low pH inactivates viruses. Aggregates, however, are not removed by Protein A chromatography, and the leached Protein A itself forms another impurity species (Rüdt et al., 2017; Jiang et al., 2009). Polishing chromatography steps follow – a common combination includes cation exchange (CEX) then anion exchange (AEX) chromatography. Hydrophobic interaction chromatography (HIC) can also be used to characterise protein product at various stages of bioprocessing or as a polishing step towards the end of mAb purification. It is effective in the clearance of HCP, aggregates, endogenous viruses and leached Protein A (Ghose et al., 2013; McCue et al., 2008). Operating conditions are selected to offer optimal impurity binding to resin and product flow through. Viral filtration involves the product feed passing through a membrane for virus removal. Product concentration and formulation is then achieved with ultrafiltration (UF) or diafiltration (DF) (Hong et al., 2018).

Challenges exist in measuring biological molecules with similar sizes and structures, as well as in measuring markers of complex biochemical pathways. Complex cell systems are highly sensitive to changes in pH, temperature, partial pressure and nutrients they are exposed to in bioprocessing, the process intermediates they go onto form may consist of only a small fraction of the desired proteins for separation. Underlining the importance of CPP optimisation through effective CQA monitoring at each bioprocess stage. The photophysical behaviour of tryptophan is equally if not more sensitive to the parameters listed above. These complexities have limited TRF studies to proteins with a single tryptophan residue such as ribonuclease, which simplifies fluorescence data interpretation and processing (MacKerell Jr et al., 1987; Axelsen and Prendergast, 1989). Different impurity species can have different retentions with chromatography membranes – major interactions can occur between mAbs and HCPs (Aboulaich et al., 2014; Rüdt et al., 2017). Despite requiring advanced control algorithms, real-time process monitoring supports the delivery of consistent product quality and the QbD approach with the greater process understanding possible using more accurate data-based models for each unit operation (FDA 2009; Hong et al., 2018; Wechselberger et al., 2010; Rathore, 2010; Rathore and Winkle, 2009).

Early work in automated sampling and analytical chromatography to monitor mAb titres had been performed by Chase (1986), Paliwal et al. (1993), Ozturk et al. (1995) and Fahrner and Blank (1999a). Whilst offering a plethora of commercial benefits such as long-term cost savings, the systems are expensive, may introduce contamination risks if on-line/at-line, and the time delay in sampling and the generation of analytical results can require processes be slowed down (Rüdt et al., 2017). PAT tools working in conjunction with mathematical modelling have been established and used with single wavelength univariate UV absorption measurements (Sørensen et al., 2022). Mendhe et al. (2014) had successfully developed a model using UV absorption measurements to make real-time pooling decisions based on the retention times of typical chromatogram peaks preceding product peaks.

However, for multicomponent processes, model-based sensitivity analyses present challenges with determining model parameters for each component (Brestrich et al., 2015).

With the greater body of bioprocess data extracted using PAT and more advanced feedforward and feedback control systems, reliable continuous

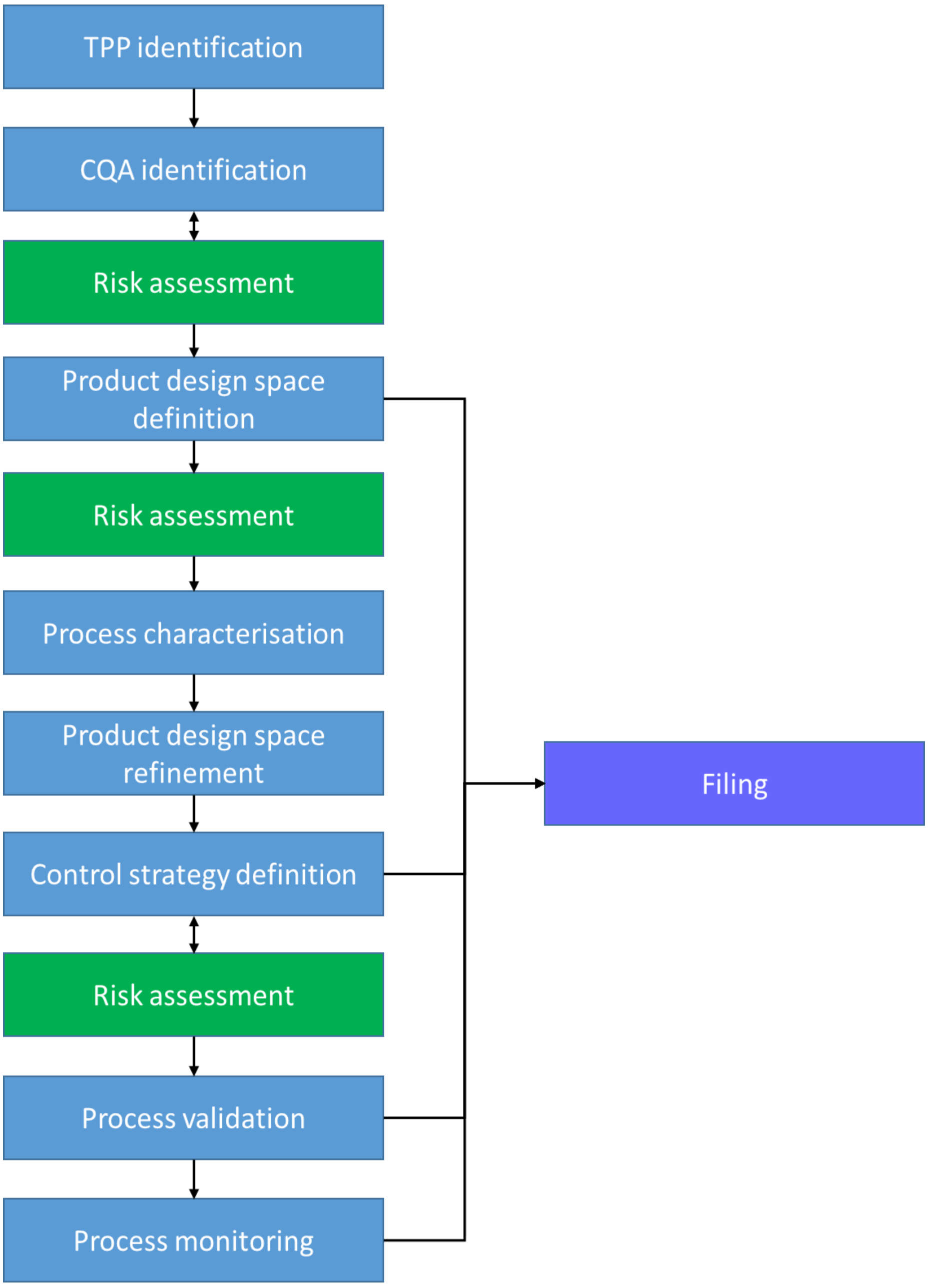

Figure 12: Overview of the key steps in the implementation of QbD (Rathore and Winkle, 2009).

modes of operation become possible. Industrial interest in end-to-end continuous biomanufacture has increased as of recent – with the end goals being able to manufacture and purify biological products quickly. Whilst continuous perfusion bioreactors have provided efficient methods of expanding cell cultures and performing basic purification after supernatant removal, continuous downstream processes have comparatively been limited in number (Konstantinov and Cooney, 2015; Hong et al., 2018; Lu et al., 2015).

Seamless PAT integration into the manufacturing line, together with a quality by design (QbD) approach and an improved understanding of the bioprocess can all reduce the requirement for off-line product testing, reduce inventories, production costs and support faster product release. In-process PAT can replace the tests required for final product specification and support the drive for continuous manufacture (Clegg et al., 2020).

The FDA-led QbD initiative forms another prominent driver of the industrial adoption of PAT. QbD is defined as a development approach that emphasises sound scientific understanding of the product, process and process control to allow effective steps to be taken quality risk management (FDA, 2009).

The implementation of QbD begins with the identification of the target product profile (TPP) which sets the bar on the target quality characteristics of a product that would ensure its efficacy and safety are realised. This includes product dosage, dosage forms and routes of administration. TTP identification goes hand in hand with critical quality attribute (CQA) identification, with the latter performed through a risk assessment as defined in the International Conference on Harmonisation of Technical Requirements for Registration of Pharmaceuticals for Human Use considerations (ICH) guideline Q9 (FDA, 2006a; FDA, 2006b). CQAs must meet strict acceptance criteria before licensing and approval as a commercial drug product (Velugula-Yellela et al., 2019; FDA 1999). This is followed by defining and refining the design space for the product based on studies with the product and similar products. The defining of a process design space involves risk analysis, use of design of experiments (DOE) to design experiments and an execution of studies using the DOE-derived parameters. Once complete, the purpose of process validation becomes a means to determine whether the product will be of acceptable quality if the process is operated within the parameter-bounds of the design space. A stronger understanding of the process design and the effects of each biomanufacturing stage on species quantities would provide greater flexibility with purification methods during process validation (FDA, 2008; Rathore and Winkle, 2009).

Regulatory filings involve the establishment of acceptable ranges of CPPs, control strategies, validation outcomes and the refined process and product design spaces (Rathore and Winkle, 2009). Finally, after the product has been approved, it would need to undergo process monitoring to ensure CQAs are being met and that the processes are performing within acceptable ranges of variability (Rathore et al. 2008; Rathore and Winkle, 2009).

Since 2004, an increasing trend has been reported in biologic license applications for product approval by the FDA. Given the expanding market and demand for biologicals, attentions have been drawn to improving CHO cell engineering and screening of the production line. However, it has been indicated that the advances in bioprocess feed strategy optimisation, automation and cell culture control have brought the most significant increases to product yield (Velugula-Yellela et al., 2019; Foltz et al., 2013; Kondragunta et al., 2010; Hmiel et al., 2015).

3. Methods

These methods were designed to test the laboratory-scale TRF-spectroscopy instrument to its protein quantitation limits and compare its performance against the quantitation methods currently standardised for use in industry. At the beginning of the project very little information was available on whether TRF spectroscopy could be used in the accurate, proportional quantitation of mAbs and HCP. Preliminary experiments had to be run to assess whether samples from industry fell within optimal concentration ranges for TRF spectroscopy and industry standards. Experiments were performed with samples that could be measured using both TRF spectroscopy and a comparative benchmark method. For the purpose of demonstrating in-line measurement and bioprocess retrofitting capabilities, it was ideal for sample formulations to remain as close to their original eluted form as shipped by Pall Biotech. Where sample reformulations were required for contrasting methods, they are indicated in this chapter.

3.1. Materials

3.1.1. Aggregate-fragment Analysis

All water used in sample and mobile phase preparation was ultrapure Milli-Q ® (Merck, US) with a resistivity of 18.2 MΩcm. MAb eluate samples were all supplied by Pall Biotech UK from the following bioprocess stages: Protein A capture and viral inactivation hold, CEX, AEX and UF. To obtain a breadth of total protein concentrations for linearity evaluation and to run HPLC-SEC within recommended column loading protein concentrations, all samples except for UF eluates underwent a 1:2 and 1:3 dilution with the original bioprocess elution buffer used as a diluent. For the UF eluates a 1:40 dilution was applied with its elution buffer.

3.1.2. HCP Detection

HCP-rich Protein A flow-through sourced from Pall Biotech (Portsmouth, UK) was used in the HCP-spiking of mAb samples. MAb pooled from post Protein A capture and post cation mixed mode chromatography was sourced from Pall Biotech (Westborough, USA). MAb post viral inactivation and post anion exchange chromatography was also supplied by Pall Biotech (Portsmouth, UK). K65M Fab eluates from Protein G capture, synthesised in E. Coli host cells were supplied by Cheng Zhang (UCL). The 60 mM sodium acetate elution buffer the Fab was suspended in was exchanged with 50 mM phosphate buffer for limits of detection measurements. For HCP-spiking measurements the buffer was exchanged with ultrapure, deionised MilliQ® water. These were used to run preliminary evaluations of the resolving capabilities of in-line TRF spectroscopy.

3.1.3. HCP Quantification Proof of Concept

The elution buffer in post UF mAb was exchanged with Milli-Q ® water using Vivaspin ® 20 (Sartorius, Germany) for 3 centrifugation cycles at 6000 rpm for 10 minutes, and a further 10 minutes to concentrate the sample further until 0.5 mL remained in the Vivaspin ® 20 tube. This was aliquot into two sets of 0.2 mL volumes of mAb suspended in Milli-Q ® water. Into each tube, the original UF elution buffer and Protein A flow-through was added to a quantum satis of 1 mL. The Protein A flow-through, which forms the initial bulk removal of process-related impurities was used as the source of CHO HCP. It was aimed that an accurate quantification of species would involve these samples exhibiting comparable signal properties for the mAb species and a reduction in signal intensity for the diluted Protein A flow-through after it had been mixed with a 0.2 mL volume of mAb.

3.1.4. HCP-Spiked and Un-spiked MAb

Post pH Hold and post anion exchange chromatography samples were added to 8 Vivaspin 20 centrifugal concentrators at the following volumes: 0.25, 0.5, 1, 1.25, 1.5, 2, 3, 4 mL. Post Protein A capture and post cation mixed mode chromatography samples were added to 8 Vivaspin 20 tubes in volumes of: 0.25, 0.5, 1, 1.25, 1.5, 2, 3, 4 mL. To reduce mAb loss through centrifugal concentration the samples were centrifuged at 3400 rpm for a minimum of 3 x 10-minute cycles. All stock mAb samples underwent 3 buffer exchanges with Milli-Q ® and were concentrated to a final volume of 0.5 mL. 0.2 mL of this stock mAb concentration was resuspended with 0.8 mL of the original elution buffer the sample was in and 0.2 mL was resuspended with 0.8 mL of HCP-rich Protein A flow-through. A HCP concentration-variable, mAb near-constant sample group was analysed using dilution ratios of 1:10, 1:20, 1:100, 1:1000, 1:5000 and 1:10000, protein A flow-through: mAb. Samples were measured with and without capillary cleaning, cleaning involved running capillaries with MilliQ® water, followed by Trigene disinfectant (Medichem International, UK), MIlliQ® water, Hellmanex® III (Hellma, Germany) for a minimum of 2 hours, followed by a final MIlliq® water wash and equilibration of capillaries with the mobile phase buffer.

3.2. FPLC-SEC-TRF Spectroscopy

FPLC-SEC was performed using the Superdex 200 Increase 10/300 GL SEC column (General Electric, USA) together with the Amersham Biosciences AKTA FPLC system as the mobile phase pump. Elution of sample constituents would occur in descending order of molecular weight; separated proteins would pass the TRF spectroscopy laser focal point and photodetector. Fluorescence decay intensities for the separated protein species in their respective buffers could then be registered and processed to obtain decay parameters. Constant flow rates of 0.3 mL/min were maintained for each sample injection and elution; mAb samples were injected into their original elution buffers as the mobile phase. Elution buffer mobile phases were: 25 mM sodium citrate for Protein A eluates, 25 mM sodium citrate and 40 mM sodium chloride for CEX eluates, and 18.75mM sodium citrate, 30 mM sodium chloride and 25 mM Tris for AEX and UF eluates. The column was equilibrated with a minimum of 2 column volumes (CVs) of mobile phase buffer before sample injections. The setup was designed for intermediate bioprocess eluates to be run without formulation modifications and dilutions. For this reason, the highest concentration UF eluates underwent a 1:4 dilution to prevent photodetector saturation. The optics and photodetector can be tailored to achieve wider desired dynamic ranges and sustain higher protein loads.

3.3. HPLC-SEC

The column used for HPLC-SEC measurements was the TSKgel SuperSW3000 (part no.: 18675, Tosoh Bioscience, Japan). Regulation of mobile phase flow rate, column pressure and sample injection were performed on the Knauer HPLC system (BIA Separations, Slovenia) and corresponding ClarityChrom control software (Knauer, Germany). UV absorbance measurements were obtained at 280 nm, bandwidth 8 nm. Sample injections into the HPLC-SEC column and TRF spectroscopy assembly for benchmarking studies were at 100 µL. Flow rates were maintained at a constant 0.3 mL/min using a mobile phase of 0.4 M Sodium Perchlorate and 0.05 M Sodium Phosphate at pH 6.7. This was degassed by vacuum pump for a minimum of 1 hr or by Helium gas sparging for a minimum of 30 min. The SEC column was equilibrated with 5 CVs of buffer mobile phase before samples were injected into it.

3.4. ELISA

A quadruple serial dilution of 1:10, sample: Abcam-supplied ELISA diluent was performed on the HCP-spiked mAb samples. Non-spiked mAb samples were diluted by a factor of 10 or serially diluted twice by a factor of 10. CHO HCP sandwich ELISA kits were supplied by Abcam (Cambridge, UK). The 96-well plates had been pre-coated with Rabbit anti-CHO HCP antibodies before 100 μL of the spiked and unspiked-mAb samples were added. The samples were incubated in the wells for 90 minutes at 300 rpm followed by a wash step with phosphate buffered saline and 100 μL of 5 μg/mL anti-CHO HCP antibody conjugated with biotin. The plate was then incubated for 45 minutes at 300 rpm. After a plate wash, 100 μL of Streptavidin-HRP conjugate at a concentration of 0.1 μg/mL was added to bind to captured biotin-labelled antibody. Any unbound conjugate was removed with a final wash step and 100 μL of TMB substrate was added. An incubation time of 10 minutes allowed sufficient colour development, after which, the reaction was stopped with the addition of 100 μL stop solution. The CLARIOstar (BMG Labtech, UK) microplate reader was then used to read the optical density of wells at a wavelength of 450 nm. ELISA tests were repeated until dilution ratios correlated with OD 450 measurements within the standard range for the kit. Equivalent HCP concentrations were derived in OrignLab by fitting a Langmuir binding isotherm model to the standard concentrations and OD450 readings. From this model, the OD450 values for unknown concentrations of HCP were derived which were then multiplied by the dilution factors applied at the start of the ELISA.

3.5. Mass Spectrometry

MAb eluates from protein A capture and viral inactivation, cation exchange and anion exchange underwent a buffer exchange with 20 mM triethylammonium bicarbonate to remove inorganic salts and increase the volatility of the samples. Liquid chromatography electrospray ionisation mass spectrometry (LC-ESI-MS) was performed on the Agilent 1100/1200 LC system followed by the 6510 A QTOF mass spectrometer (Agilent, UK).

3.6. Native PAGE

Samples were diluted with Novex™ Tris-Glycine Native Sample Buffer 2X (Thermo Fisher Scientific, US) and deionised Milli-Q® water (Merck, US) resistivity: 18.2 MΩcm. Then 7 µL of each sample was loaded onto a precast NuPAGE™ 7% Tris-Acetate gel (Thermo Fisher Scientific, US). Samples were run from anode to cathode due to the mAb isoelectric point (pI) being found to be over pH 8. The gels and power set-up were placed in a cold room set to 4 ˚C, which was where the electrophoresis was run. Native PAGE was run for 210 minutes at 150 V, in a running buffer comprising of 25 mM Tris base and 192 mM glycine. Running buffer pH was adjusted to 6.5 with hydrochloric acid.

3.7. TRF Spectroscopy

For this project, fluorescence decay intensities of protein samples were obtained using the TRF spectroscopy optical assembly outlined in Hales et al. 2021 and shown in fig. 13. The assembly focused UV wavelengths at 266 nm from a frequency-quadrupled neodymium-doped yttrium aluminium garnet (Nd: Yag) laser (Crylas, FQSS 266-50), through a polymer-coated UV-fused silica capillary (Molex, TSP300665) to excite tryptophan and tyrosine residues with samples. The pulse width of the laser was 1 ns and the pulse energy was set to 50 µJ, with a repetition rate of 100 Hz. Any excitation energy variability between pulses did not detract from the study. Emission wavelengths were reflected by an ellipsoidal collimator (Newport, Ellip-2) towards the active area of an ultrafast photodiode (Alphalas, UPD-200-UP). Raw fluorescence emission intensities were translated into a current output by the photodiode then converted to a voltage signal through a 2.2 GHz transimpedance amplifier (Femto, HSA-X-I-2-40) and 12 GHz sampling oscilloscope (Pico Technology, PicoScope 9211A) to generate a digitised intrinsic fluorescence decay lifetime trace for the samples injected. This had a sampling clock of 120 ps, which, together with a 16-bit voltage resolution, enabled 256 excitation pulses to be registered in less than 5 s.

The digital signal $I_j(t)$ derived from the fluorescence decay intensity contribution of the *j^th^* protein species can be modelled in the form of the convolution equation as described earlier:

$$I_j(t) = \int_0^{\theta} R(t) * S_j(t)dt \tag{41}$$

Where θ is the width of the sampling oscilloscope time window, $S_j(t)$ is the impulse response of the sample for N protein species (eq. 42), and $R(t)$ is a convolution of the detector impulse response and excitation pulse of the laser (eq. 43).

$$S(t) = \left\{ \sum_{j=1}^{N} \gamma_j \left(\frac{\beta_j}{\tau_{j_1}} e^{-\frac{t}{\tau_{j1}}} + \frac{1-\beta_j}{\tau_{j_2}} e^{-\frac{t}{\tau_{j2}}} \right) \begin{matrix} if\ t<0 \\ if\ t\geq 0 \end{matrix} \right\} \tag{42}$$

$$R(t) \sim \sum_{i=1}^{2} \alpha_i \delta(t - \varphi_i) \tag{43}$$

β, defines the contribution of the first fluorescence decay component and can be further represented as $= \frac{\beta_{j_1}}{\beta_{j_1} - \beta_{j_2}}$. As a sum of the pre-exponential factors of the *j*th protein species (where *j*= 1,2), γ_j is a constant proportional to the species quantity and can be described by $\gamma_j = \beta_{j_1} + \beta_{j_2}$. τ_j forms the fluorescence decay time for each decay component, α_i is the signal amplitude and φ_i is the temporal offset of the excitation pulse .

Eq. (41) can therefore be summarised as:

$$I_j(t) \sim \sum_{i=1}^{2} \alpha_i \gamma_j \left[\beta_j \left(1 - e^{\frac{\varphi_i - \theta}{\tau_{j1}}} \right) + (1 - \beta_j) \left(1 - e^{\frac{\varphi_i - \theta}{\tau_{j2}}} \right) \right] \tag{44}$$

Eq. 44 forms the basis for processing raw measured fluorescence intensity signals to quantify and identify proteins. The decay times τ_1 and τ_2 are intrinsic to the protein being quantified and were obtained by plotting fitted decay lifetime measurements against elution volume (Hales et al. 2021).

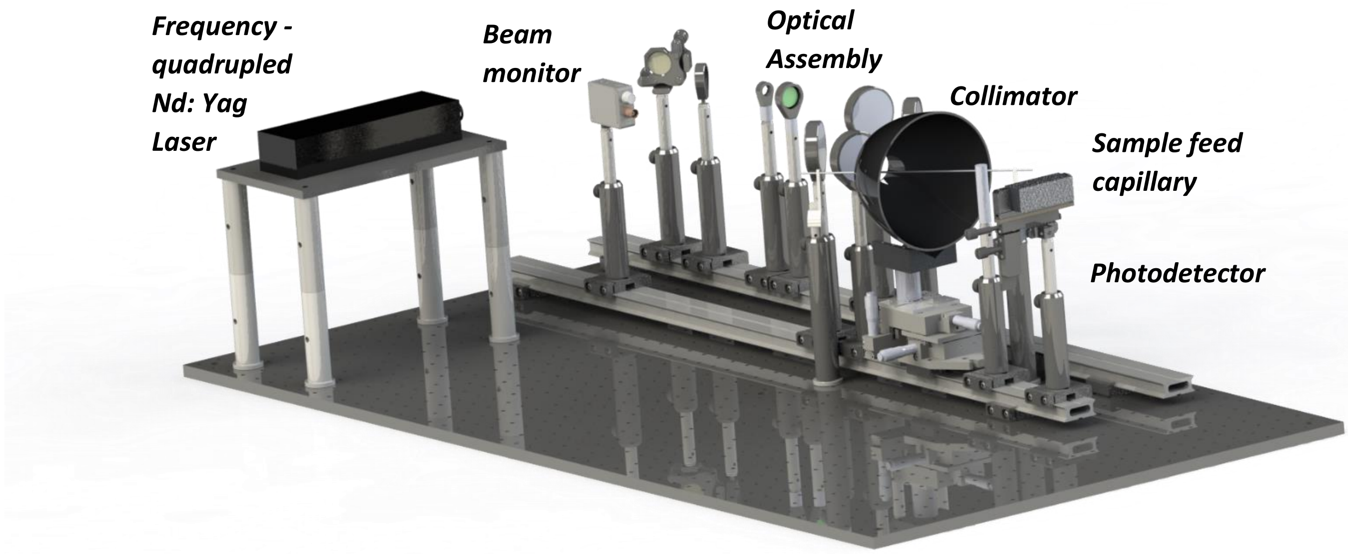

Figure 13: Render of the spatial arrangement of components that were used to characterise the intrinsic fluorescence lifetime of the protein mixtures inline without a SEC column (produced by Samir Aoudjane, UCL).

Decay associated chromatogram (DAC) peak traces defining the fluorescence intensity contributions of two species with contrasting decay parameters can be generated using Eq. 44. Measurements were designed to assess whether the areas under each DAC signal are proportional to the quantity of the species in the sample. OriginLab was the data processing platform throughout for the generation of decay parameters and integration of DAC peaks to obtain species proportions.

Decay parameters could be established for the separated species constituents of samples using the setup outlined in fig. 13. Decay parameters are unique to species and chemical environments; hence, the purpose of the initial preceding FPLC-SEC step was only to ensure that the fluorescence decay of pure species were being logged for decay parameter calibration. For subsequent measurements no chromatography column was used, samples were directly injected into the capillary running through the TRF setup. The decay parameters τ_1 and τ_2 (ns), and β, are intrinsic to each protein species being quantified and were obtained from decay lifetime measurements across the span of species elution volume. When these decay parameters are plotted as a function of elution volume they converge to a limited range of values at the points where a particular species is eluting. They were used in the fitting of double exponentials to the total fluorescence intensities to generate individual decay contributions for each species to the total fluorescence intensity, even where multiple species were co-eluting such as mAb monomers and aggregates (Hales et al., 2021).

Specialised decay intensity contribution calculating software as presented in Hales et al., 2021 was run on OriginLab. This generated decay parameter signatures for each sample, which were then used to fit double exponentials on the raw data. From the resultant decay associated chromatogram (DAC) traces, relative quantities of each species could be calculated as peak areas trough-to-trough for each species trace.

Decay parameters were extracted from the points of convergence to a narrow set of values for the product-related impurity analysis – plotting the rolling variance (n=5) for the desired elution regions enabled decay parameters to be selected where variance was lowest. For the process-related impurity analysis, mean decay parameters were calculated using a set of decay parameters from the elution regions of each species of interest. This set was first generated using the method outlined in Hales et al. (2021) then input into a prototype python program built by John Hales (UCL). The program simulates a decay fitting function for the sum of two exponential decays over a range of time values to calculate the mean decay parameters for that time range. Table 1 summarises the stages involved in data collection and processing.

Table 1: Key stages involved in decay associated chromatogram generation.

1. Acquire raw fluorescence intensities	2. Compute decay parameters for fluorescence intensity	3. Compute average decay parameters	4. Exponential fitting (DAC plot generation) using decay parameters
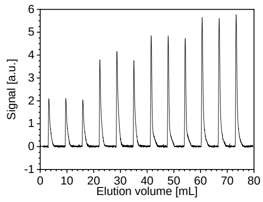	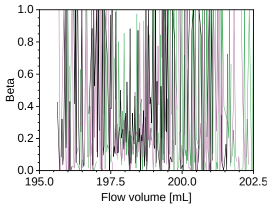	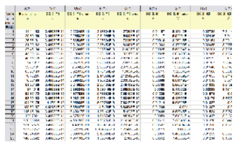	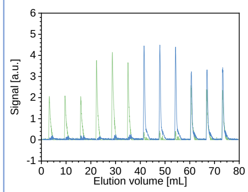
Samples injected into photodetector pathway. Tryptophan and tyrosine in protein molecules excited with deep UV wavelengths (266 nm).	Identify elution volume time windows (peak width), run decay parameter fitting software.	Select decay parameters from regions of signal convergence or run signal averaging software to obtain decay parameters for data in elution region.	Perform integration on DAC peaks with desired species.

The experiments conducted and materials used are outlined below in Tables 2 and 3 for reference.

Table 2: Summary of experiments that were conducted.

Experiment	Hypothesis for Evaluation	Equipment Used	Samples (suspension buffer)	Results Output	Data Processing
Decay parameter determination					
FPLC-SEC-TRF Crude Sample Decay Analysis	Decay parameters converge to narrow range of values during species elution time windows.	Superdex 200 Increase 10/300 GL SEC column (General Electric, USA) Amersham Biosciences AKTA (Cytiva, US) FPLC system.	***IgG1 eluates from:*** PH Hold (25mM sodium citrate, pH 4.5), S Hypercel CEX (25 mM sodium citrate and 40 mM sodium chloride, pH 6.5), Mustang Q AEX, UF (18.75 mM sodium citrate, 30 mM sodium chloride and 25 mM Tris, pH 7.5).	Raw total fluorescence intensity chromatogram (Voltage against time).	Fitting of exponentials, mean decay parameter computation, deconvolution of total fluorescence intensity to confirm accuracy of decay parameters.
Head-to-head Analysis against TRF Spectroscopy					
HPLC-SEC	UV (280 nm) absorbance peak areas positively correlate with TRF spectroscopy DAC peak areas.	TSKgel SuperSW3000 (part no.: 18675, Tosoh Bioscience, Japan).	***IgG1 eluates from:*** PH Hold (25mM sodium citrate, pH 4.5), S Hypercel CEX (25 mM sodium citrate and 40 mM sodium chloride, pH 6.5), Mustang Q AEX, UF (18.75 mM sodium citrate, 30 mM sodium chloride and 25 mM Tris, pH 7.5). ***Mobile phase:*** 0.4 M sodium perchlorate and	UV absorbance chromatograms.	Area extraction from chromatogram output.

			0.05 M sodium phosphate, pH 6.		
ELISA	HCP concentrations positively correlate with TRF spectroscopy DAC peak areas.	Abcam (Cambridge, UK) 96-well ELISA kit. CLARIOstar (BMG Labtech, UK).	Protein A flow-through (25 mM sodium citrate, pH 4.5), UF mAb (18.75 mM sodium citrate, 30 mM sodium chloride and 25 mM Tris, pH 7.5)	OD450 reading	Fit Langmuir binding isotherm to standard curves.
Mass Spectroscopy	MAb fragments are present in samples.	Agilent 1100/1200 LC system, 6510 A QTOF mass spectrometer (Agilent, UK).	PH Hold, S Hypercel CEX and Mustang Q AEX (20 mM triethylammonium bicarbonate).	Histogram of molecular mass.	Mode molecular mass.
Native polyacrylamide gel electrophoresis (PAGE)	MAb monomers and aggregates are present in samples.	Novex™ Tris-Glycine Native Sample Buffer 2X, deionised Milli-Q® water (Merck, US), NuPAGE™ 7% Tris-Acetate gel (Thermo fisher Scientific, US).	Same as FPLC-SEC-TRF.	Protein gel imagery.	Evaluation of protein band positioning.

Pre-processed decay parameter data is displayed for the samples below in fig. 1, Appendix.

Table 3: Details of samples tested and methods used.

Sample	Bioprocessing Stage	Source manufacturing line	Protein details	Methods of Analysis
MAb	Protein A	Pall Biotech - Westborough	Trastuzumab, IgG1 humanised monoclonal antibody, CHO cell derived	TRF, ELISA
	Viral inactivation	Pall Biotech - Portsmouth		TRF, HPLC-SEC, ELISA, LC-MS, native PAGE
	Cation exchange	Pall Biotech - Portsmouth		TRF, HPLC-SEC, ELISA, LC-MS, native PAGE
	Cation exchange mixed mode	Pall Biotech - Westborough		TRF, ELISA
	Anion exchange	Pall Biotech - Portsmouth		TRF, HPLC-SEC, ELISA, LC-MS, native PAGE
	Ultrafiltration	Pall Biotech - Portsmouth		TRF, HPLC-SEC, ELISA, LC-MS, native PAGE
HCP	Protein A affinity chromatography flow-through during mAb manufacture	Pall Biotech - Portsmouth	Mixed range, CHO cell derived	TRF, ELISA
Fab	Protein G affinity chromatography	UCL – Department of Biochemical Engineering (produced by Cheng Zhang)	K65M surface mutation, E. coli derived	TRF

4. Product-Related Impurity Analysis

Aggregates and fragments constitute major product related impurities in the biomanufacturer of mAbs, that can detriment final product efficacy and safety (Wälchli et al., 2020) (see Chapter 2). Challenges with current analytical methods involve achieving sufficient resolution between mAb monomers, dimers and fragments which can possess very similar hydrodynamic radii (Vajda et al., 2015; Vlasak and Ionescu, 2011). Additionally, aggregate species typically make up <5% of eluates in the polishing stages of manufacture (Li et al., 2019). HPLC-SEC is an important tool for analysing the process related impurity content of industrial eluates. The proportionality between species quantities derived from off-line HPLC-SEC and in-line TRF spectroscopy are evaluated here.

4.1. Results and Discussion

The decay parameters for each mAb eluate are summarised in Table 4 – these were extracted from the decay parameter fittings after FPLC-SEC-TRF. Tables 9-10, Appendix display the concentrations of samples tested. Figs. 14 and 15 demonstrate how the decay parameter variance converges towards zero across the elution volume for a particular species, near zero exists the true decay characteristic values. This convergence to a constant can be analysed visually in the DC decay parameter traces in fig. 14 for one monomer and aggregate peak post FPLC-SEC-TRF spectroscopy. Fig. 16 displays the DAC traces for the mAb monomer (green) and mAb aggregate-fragment (purple) species for the cation exchange eluates when passed through FPLC-SEC-TRF, counterpart column-free decay associated chromatography plots can be found in fig. 2, Appendix. Fig. 17 (show that the decay parameters extracted from the DC aggregate elution window yield DAC traces outlining the quantity of the aggregate species as well as a third fragment species post-monomer elution during FPLC-SEC. The LC-ESI-MS plots in fig. 22 also identify the presence of 3 species with molecular weights corresponding to mAb monomers, dimers and Fab-Fc fragments.

UV absorbance areas for the HPLC-SEC cases (see Appendix) were calculated by ClarityChrom and plotted directly against the TRF fluorescence decay contribution-based peak areas integrated in OriginLab. Integration windows were kept constant for each triplicate and varied between samples due to the differences in the elution volume between fluorescence intensity peaks and troughs to baseline. No smoothing was applied to the fitting of results used the concentration calibration curves to keep them precise.

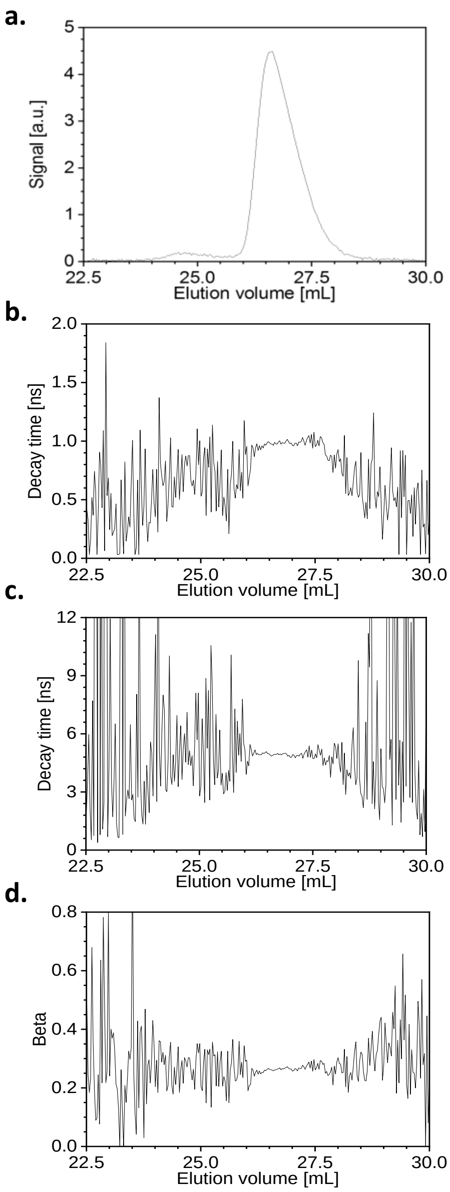

Figure 14: a) Pre-processed raw total fluorescence decay intensity for UF aggregate (22.5-25.8 mL) and monomer (25.9-30 mL) species. With decay parameters used in exponential fittings: b) τ_1 , c) τ_2 and d) β values. All are shown across the elution volume for the mAb sample injected.

Fig. 23 displays the plots of HPLC-SEC chromatogram peak areas for the monomer and dimer species corresponding to the same samples independently quantified using TRF-derived DAC species signal traces. For the low concentration, low laser power rating test regimens, Pearsons R^2 values were 0.85 for the monomer and negligible for the aggregate-fragment species between the peak areas plotted against each other. For the low concentration, high laser power rating conditions R^2 values of 0.999 and 0.64 for the monomer and aggregate-fragment species were respectively observed. Lastly, for the low power rating, high concentration settings, R^2 values were 0.96 for the monomer species and 0.69 for the aggregate-fragment species. This demonstrates that strong positive correlations can be achieved by TRF spectroscopy when directly compared against HPLC-SEC, for resolving the monomer species amongst a mixture with product related impurities. A positively correlating linear relationship also exists between the two modes in the measurement of aggregate-fragment proportions.

Table 4: The decay parameters used in the exponential fitting of species decay intensities for the different test regimens followed.

Test regimen	Bioprocess stage	Species class	Decay parameters		
			β	τ_1 [ns]	τ_2 [ns]
Original sensitivity, *high* concentration (4.70 mg/mL > total protein concentration > 1.41 mg/mL Low laser pulse power: 40 µJ	Protein A, pH Hold	Monomer	0.384	1.35	4.97
		Aggregate-fragment	0.281	0.952	5.20
	S Hypercel™	Monomer	0.343	1.35	5.43
		Aggregate-fragment	0.340	1.04	5.27
	Mustang Q™	Monomer	0.329	1.32	5.37
		Aggregate-fragment	0.317	0.905	4.63
	Ultrafiltration	Monomer	0.251	0.923	4.82
		Aggregate-fragment	0.220	0.750	3.62
Original sensitivity, *low* concentration (1.10 mg/mL > total protein concentration > 0.31 mg/mL) Low laser pulse power: 40 µJ	Ultrafiltration	Monomer	0.251	0.923	4.82
		Aggregate-fragment	0.260	0.647	5.02
Sensitivity-improved (2.82 mg/mL > total protein concentration > 0.28 mg/mL) High laser pulse power: 50 µJ	Mustang Q™	Monomer	0.251	0.923	4.82
		Aggregate-fragment	0.260	0.647	5.02

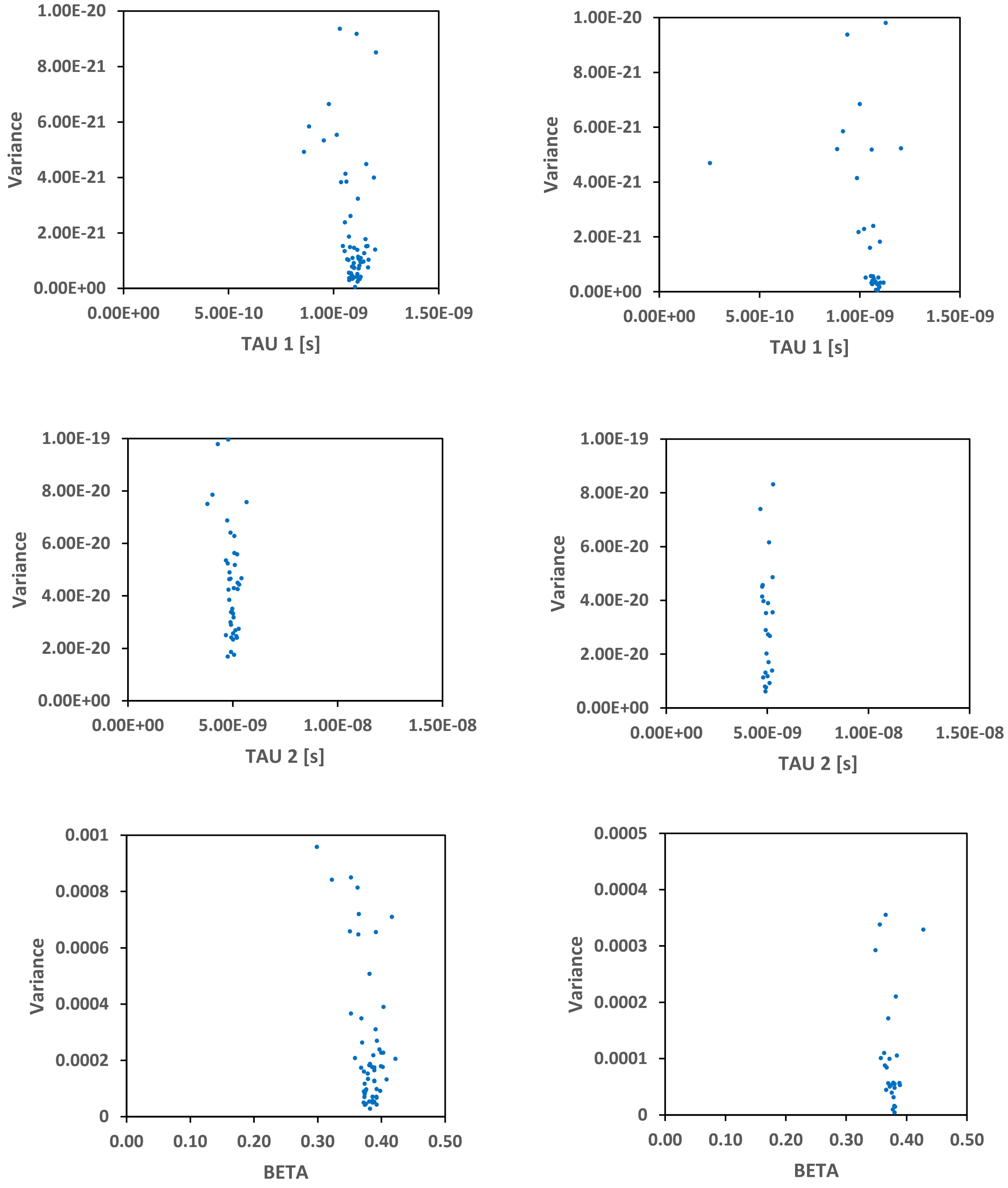

Figure 15: Rolling variance (n=5) of decay parameters for the monomer and aggregate species.

The final calculated decay-associated species quantities are dependent on the decay parameters that are extracted for each test run at a particular set of conditions – these include: chemical composition, buffer conditions, local functional groups, fluorophore shielding and temperature (Lakowicz, 2006). Therefore, a greater body of information can be extracted from a decay intensity fitting than a UV SEC absorbance chromatogram. When a mixture of species are excited at a particular wavelength, the resultant decay profile can be described by a set of parameters that include the times between excitation and emission, as well as the proportional factors used in exponential models.

It can be seen that these decay parameters converge to a narrow set of values where we have a single pure species eluting, for example, where we have the mAb monomer and where here we have the aggregate (figs. 14-15). It has been previously demonstrated that these decay parameters can be used as a signature for different protein species and different mixtures in Hales et al. (2021). Through signal convolution the exponential model used to describe *N* protein species can be solved and the fluorescence decay intensities that are proportional to species concentrations can be generated. The basic method of extracting accurate decay parameters from the regions of greatest signal convergence and stability has been shown to corroborate with expected species profiles. The application of several decays per fit has smoothed noise-prone signals – particularly for concentrations that generate signal intensities close to the baseline. With lower concentrations the contribution of noise to decay intensities increases, which can give rise to erroneous, negative and weak correlation coefficients. By reducing the noise contribution to the total fluorescence, signal smoothing presents a temporary measure at gauging species-representative positive correlations for concentrations below 0.28 mg/mL. Signal smoothing runs the risk of increasing the decay contribution of noise as well as reducing it. Therefore, forgoing signal smoothing remains the ideal option for the greatest quantification accuracy. Plotting decay parameters against a rolling variance has been shown to be a useful tool in identifying decay signal convergence points, especially where concentrations are low and associated fluorescence decay intensity signals have large noise components. The benefit of selecting the decay parameter with the lowest variance amongst a cluster of variances and evaluating its decay associated chromatogram output, is that it can be readily implemented into neural network and deep learning systems.

The decay associated chromatograms present the deconvoluted total fluorescence intensities into its constituent decay intensity contributions – the areas underneath these signal traces describe positively and linearly proportional quantities of proteins when compared with UV SEC absorbance.

The presence of two independent DAC signal traces that follow the monomer and aggregate total fluorescence intensity elution curve are indicative of decay parameters that describe their decay times accurately. By separating the mixture of monomer and product related impurities by FPLC-SEC, decay parameters for the individually eluting species could be obtained at the first instance. TRF decay characterisation indicates the presence of a fragment species eluting together with the monomer. FPLC-SEC does not generate a sufficient separation of monomers and the fragment species, and their retention times overlap (figs. 16-17). But we did not know that the aggregate and fragment species would have very similar if not the same decay properties, but these figures indicate that aggregate and fragments can be quantified together. The generation of mAb aggregates and fragments have been described as indicators of degradation (Vázquez-Rey and Lang, 2011; Wang, 1999) and their presence in the samples could have been due to high SEC pressure and shear forces in manufacture or the variety of mobile phase pH changes during capture and purification.

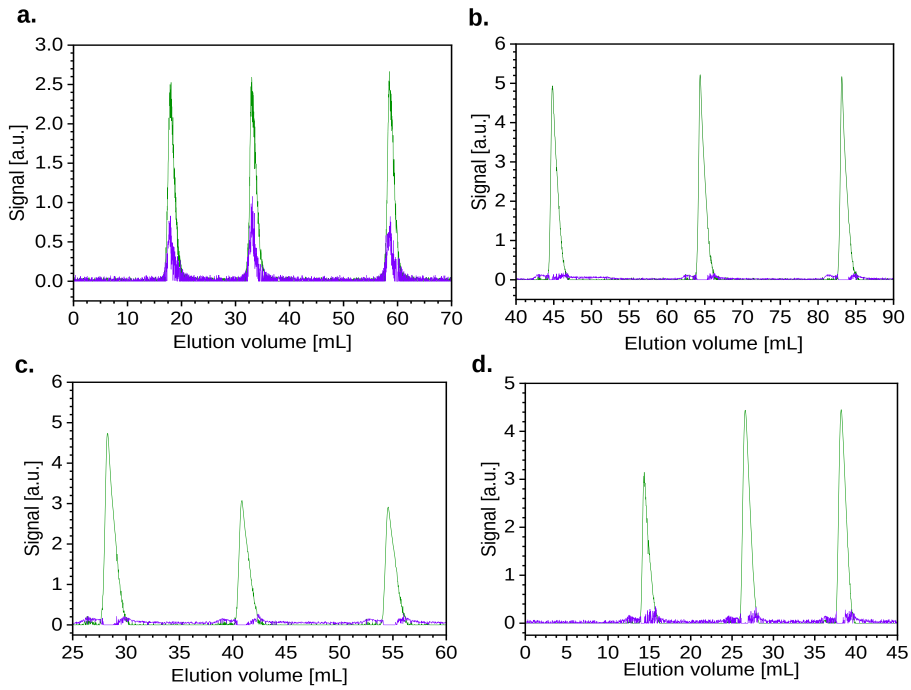

Figure 16: Decay contributions of the aggregate-fragment (purple trace) and monomer (green trace) using the decay parameters extracted from fig. 1. a) pH Hold, b) S Hypercel™ , c) Mustang Q™ and d) Ultrafiltration eluates were run through FPLC-SEC for weight separation.

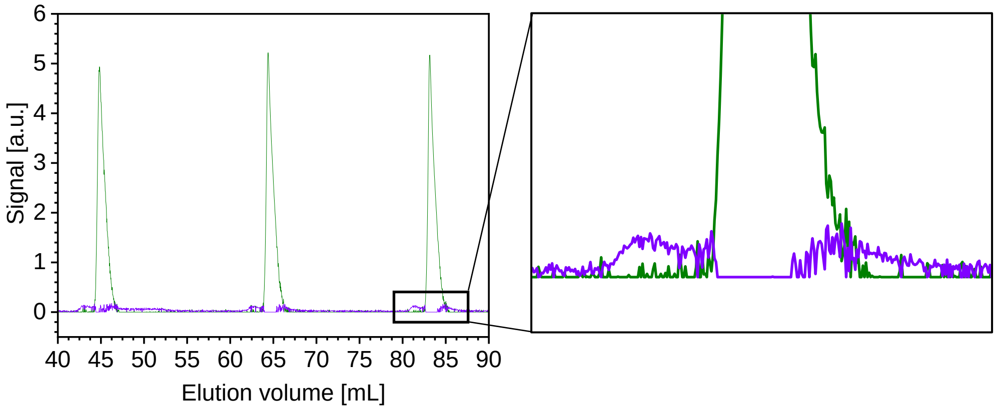

Figure 17: A DAC plot of the results of decay parameter testing for a CEX, FPLC-SEC-TRF mAb eluate. The purple trace encompasses the aggregate and fragment elution regions, the green is present only when a monomer species is eluting.

Two clear protein bands were visible for the native gel electrophoresis in fig. 18, for the monomer and dimer species present in all the bioprocess samples measured but the fragment concentration is far too low for the resolution of the gel. The pI of the mAb samples were far too high to enable them to be run together with the protein ladder at supplier-recommended pH values. The smearing of bands in the native-PAGE can be attributed to a number of possible factors including species denaturation during electrophoresis, contamination of original samples or the presence of species with varying molecular weights (Kaer et al., 2008). The configuration of anode and cathode to facilitate the migration of bands laterally are indicative of the mAb monomer and aggregate species having isoelectric points above the pH of 6.5 used for the running buffer. Testing a running buffer with a pH that is closer to the mAb isoelectric point resulted in poor band migration over the 210 minutes of a single run. The thickness of the bands in the native PAGE gel indicates that the mAb has been overloaded. Whilst deliberately overloading can allow the visualisation of low concentration aggregate, dimer and fragment species, this was not successful in fig. 18. Alternatively, employing staining techniques with greater sensitivity such as silver staining or SYPRO® Ruby can achieve a sensitivity of 1 ng and detection limits of 0.25-1 ng (Molecular Probes, 2007). A gradient PAGE gel with varying polyacrylamide concentrations can improve the resolution of bands of a broad range of protein sizes and proteins of similar sizes by separating them more efficiently. For samples consisting of oligomers, dimers, monomers and fragments, a greater low-high polyacrylamide percentage range would facilitate a greater "sieving" effect to produce sharp bands for all expected species. For the native-PAGE in fig. 18, a running buffer of 25 mM Tris base and 192 mM glycine was used at a pH of 6.5 instead of 8.5 (manufacturer recommendation), and samples were run from anode to cathode as the mAb pI was found to be above 6.5. In addition to protein overloading, the application of 150 V for 210 minutes could be the cause of denaturation which would contribute to the band smearing observed.

For TRF spectroscopy, the presence of a fitted decay intensity contribution peak where the mAb dimers had eluted and towards the right shoulder of the monomer peak (fig. 17), suggests that the fluorescence decay times for the dimer and fragment species are very close. FPLC-SEC did not generate a sufficient separation of monomers and the fragment species, their retention times overlapped, or the SEC column did not possess sufficient resolving power for the fragments in sample. MS and HPLC-SEC both detected the presence of mAb aggregates and fragments which were aligned with the aggregate-fragment DAC traces generated by TRF spectroscopy. Two clear protein bands were visible for the native gel electrophoresis, for the monomer and dimer species present in all the bioprocess samples used in fig. 18, the fragment concentration is far too low for the resolution of the gel and could have also been introduced to the sample through the high pressures and forces the mAbs are subjected to during the chromatography steps.

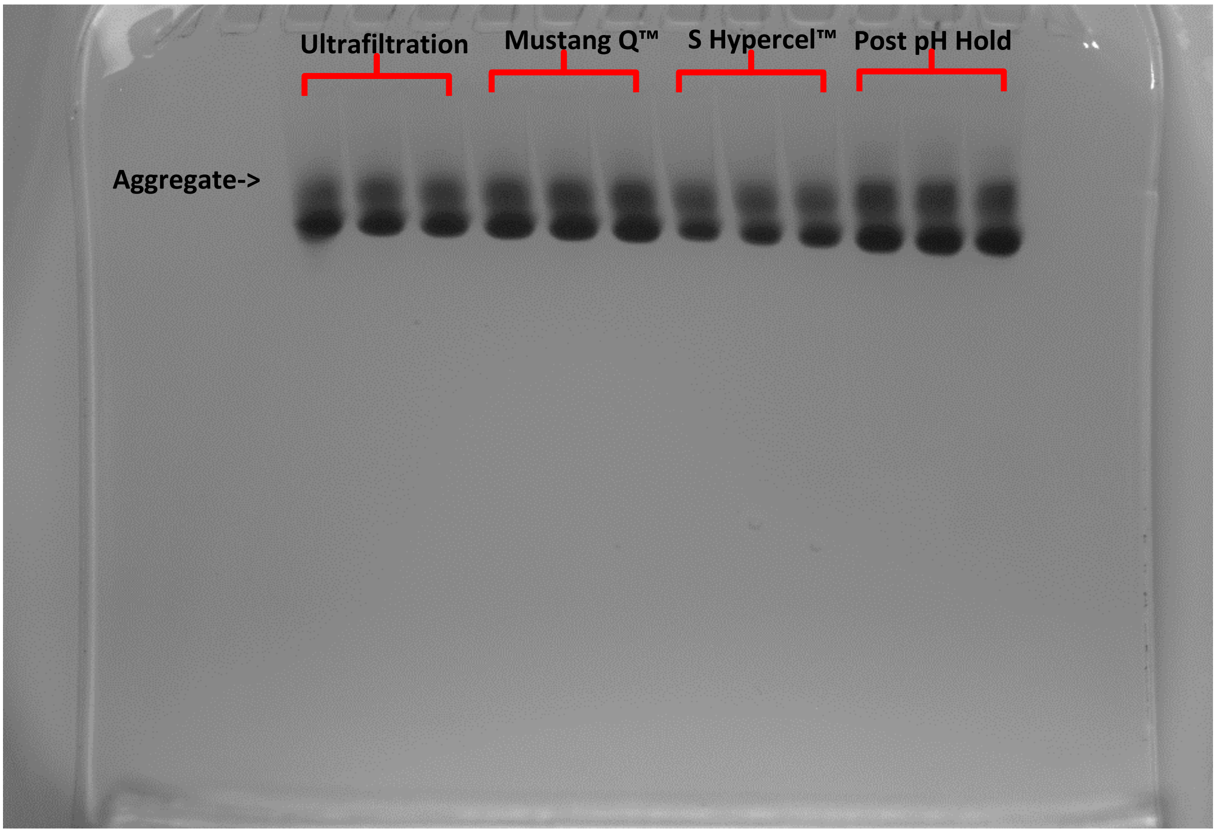

Figure 18: Native gel electrophoresis of mAb samples sourced from Pall Biotech, ran at a temperature of 4˚C, potential difference of 150 V, for a total of 210 minutes on a 7% Tris-Acetate Gel with a 25 mM Tris base/192 mM glycine running buffer.

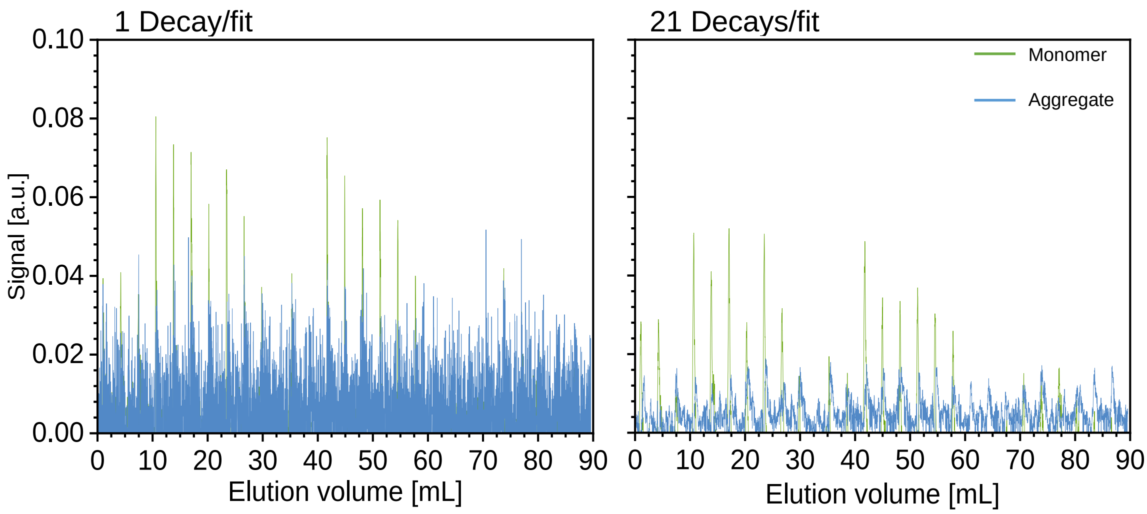

Figure 19: Side-by-side comparison of DAC plots for low concentration samples at the low 40 μJ pulse power, with no signal averaging (left) and averaging at 21 decays/fit.

Any variability in the fluorescence intensities of individual sample injections in figs. 19 and 20, can be attributed to the settling and sedimentation of mAb samples in HPLC vials during the wait for injection turn compounded by system noise and Brownian motion in the capillary. In a continuous mode simulation without the batch injection of samples, any variation would be due to the Brownian and Taylor dispersion of proteins in flow. Some strides have been made in reducing these effects for single molecules (Cohen and Moerner, 2008), however, the high protein concentrations and non-laminar flow rates used in bioprocessing, we found that increasing the pulse power rating to generate sufficiently high signal intensities that did not vary greatly with random noise fluctuations.

The low signal to noise ratio is particularly prominent for the aggregate and fragment species signal in fig. 19. As expected, the low concentrations lead to decay intensity contributions and UV absorbances that are more variable without a clear linear relationship. We can see that this is **not** the case for the mAb monomer species, where we have correlation coefficients above 0.9 between SEC absorbance and DAC, which meets regulatory requirements. USP reference standards for the validation of compendial methods (USP <857>) describes acceptable signal to noise ratios as being either 2:1 or 3:1 for **detection limits**, which we are being met for the monomer even at the low concentrations and laser power ratings. We can achieve them for the aggregate species at the lower concentrations with higher pulse power ratings, and at higher concentrations more typically used in industry. For **quantitation limits** a regulatory ratio of 10:1 is put forward which we can achieve with mAb concentrations at and above 2 mg/mL, with around 9 mg/mL being the concentration observed between downstream purification stages in industry (USP <1225>).

ICH recommends that to establish the linearity of the detection of an impurity, a minimum of 5 concentrations be used and that the concentration ranges be 50 – 120 % of the specification. For a specification of 9 mg/mL, then for samples tested under 1 mg/mL for the aggregate species we are quite far from the final industrial specification of the instrument (USP <1225>). For future measurements requiring the quantification of concentrations below 0.28

mg/mL, a fitting of system noise itself can be quantified and subtracted from species DAC traces through software.

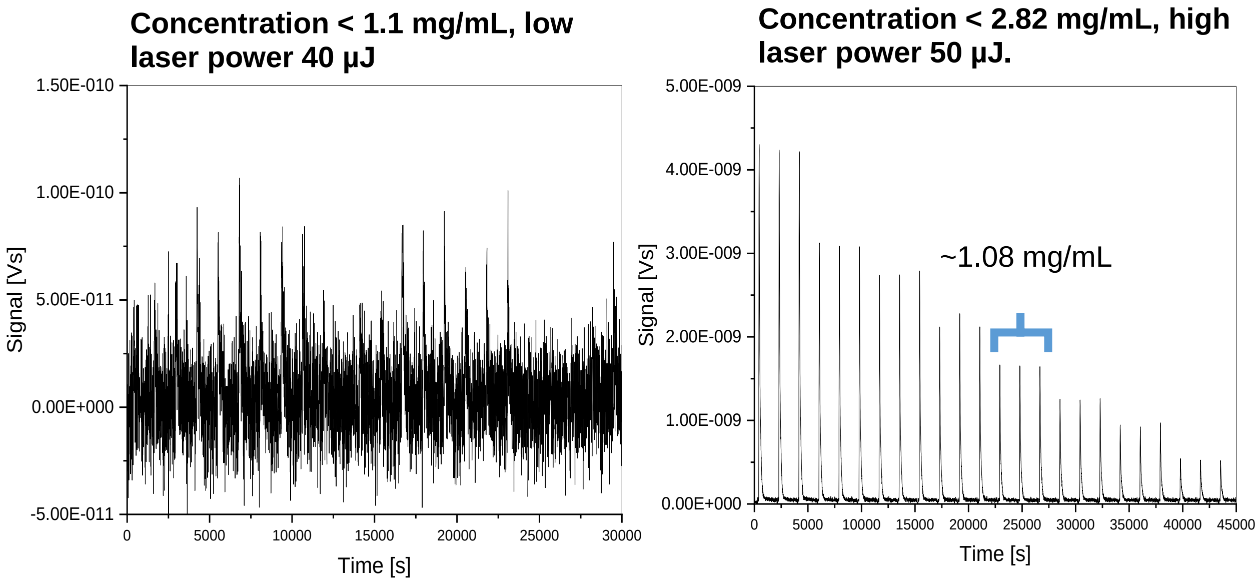

Figure 20: Differences in fluorescence decay intensity of mAb with an increase of the laser pulse power rating.

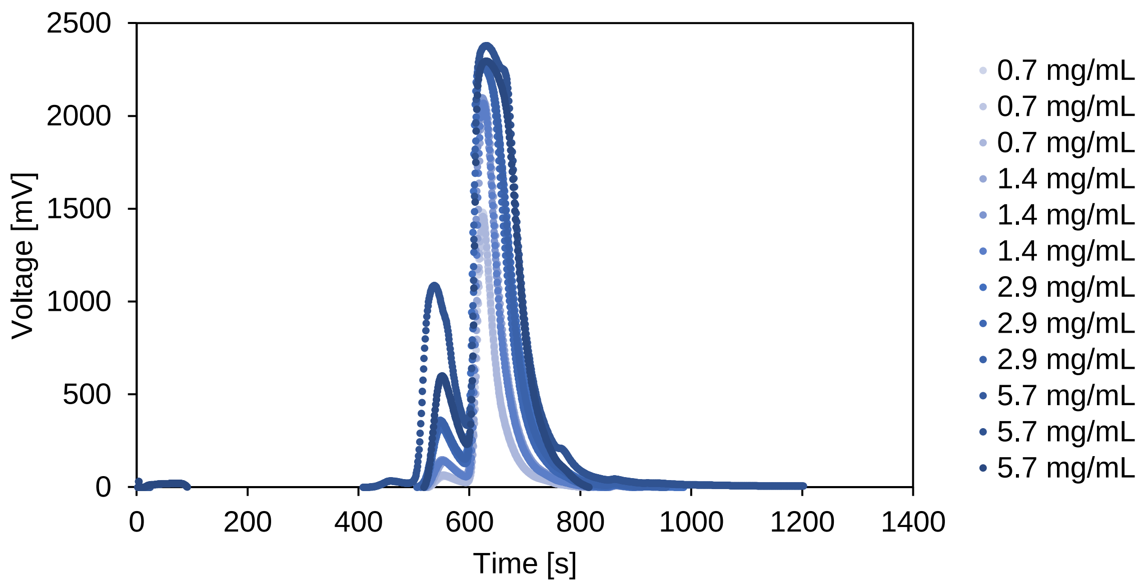

Figure 21: Peak truncation and tailing with UV SEC absorbance at higher protein loading concentrations. Darker data points correspond to higher mAb concentrations.

Peak truncation and tailing were observed for HPLC-SEC at concentrations beginning from 2.9 mg/mL, for TRF spectroscopy quantification accuracies increased closer to the original sample concentrations. The signal smoothing effect of increasing the number of decays per fitting (fig. 19) can aid with identifying very low concentrations of analyte and reduce the need for applying other smoothing models. With the 50 µJ power rating, no need for smoothing was required for concentrations down to 0.28 mg/mL. HPLC-SEC chromatograms can be found in figs. 3-8, Appendix.

Using the more chaotropic sodium perchlorate salt instead of NaCl in the mobile phase – as identified by Wang et al. (2017), was found to offer the most superior improvement to peak shape. With faint aggregate peaks, the original running buffer of sodium phosphate and NaCl for the column did not produce chromatograms that were truly representative of the species in the samples. Including 0.4 M sodium perchlorate in the HPLC-SEC mobile phase facilitated high chromatogram resolution, reduced peak tailing and sharper aggregate and fragment peaks. Any future tests can include this buffer component and would ensure consistency is maintained across measurements. When it came to peak area calculations, we found the OriginLab integrate gadget which applies the trapezium rule to the entirety of your chosen data region, to have adequate ease of use and offer adaptability when incorporated into user-designed programs for the generation of DAC peak areas. Likewise, for the UV absorbance chromatogram peak areas, ClarityChrom sufficed with automatic peak area calculations. Using the peak analyser or multiple peak fitting tool can cause some peaks to be missed if they do not fall within certain size thresholds, and of course this can compromise the accuracy of quantification. The OriginLab Integrate Gadget which applies the trapezium rule to the entirety of the user-selected data region allowed a more accurate selection of peaks corresponding to sample injections.

The results of LC-MS also indicate the trace presence of fragment species. But unlike LC-MS, where the original sample buffer needs to be exchanged with a volatile solvent which can influence mAb biochemistry and species profiles, TRF spectroscopy required them to simply be run in their original form through the unit. This can be achieved in-line or on-line depending on manufacturing constraints.

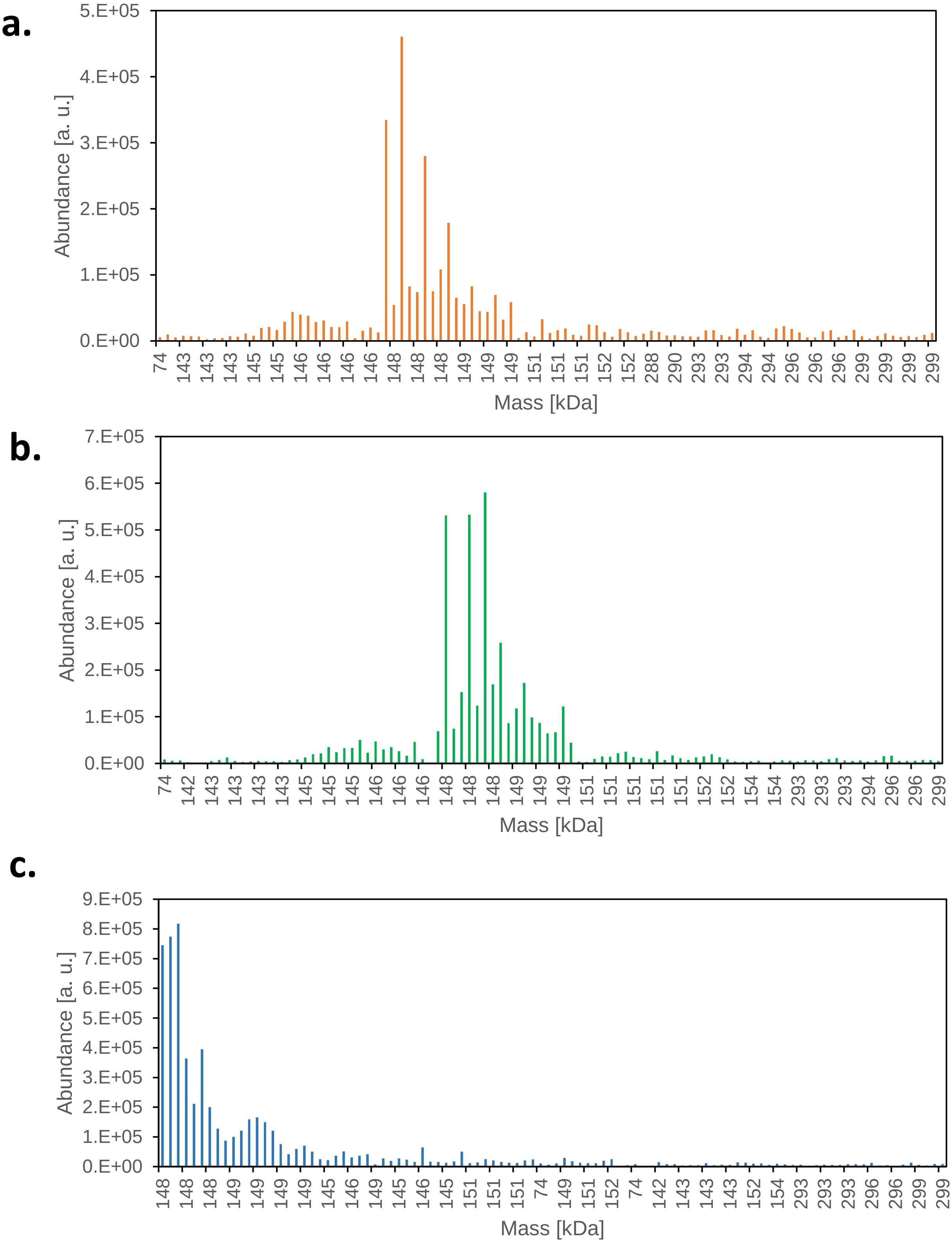

Figure 22: MS species analysis for eluates from a) Protein A capture and virus hold, b) cation exchange, c) anion exchange.

Positive proportionalities were achieved between TRF spectroscopy and HPLC-SEC in each parity plot in fig. 23, demonstrating the strong potential of using in-line-measured fluorescence decay intensity contributions as an alternative to conventional off-line-measured UV absorbance. Even at concentrations <2.8 mg/mL, a strong positive correlation (R^2=0.999) exists for the decay associated peak areas obtained by in-line TRF spectroscopy and SEC UV absorbance chromatogram peak areas for the monomer species. A positive relationship (R^2=0.64) is also observed between the two analytical systems for the aggregate-fragment species.

At greater concentrations this correlation improves for the aggregate-fragment species as these result in greater decay intensity signal to noise ratios. When the mAb samples were tested on TRF spectroscopy at the lower laser power rating, without an SEC column, fluorescence decay profiles could still be obtained for both the monomer and dimer species. The DAC peak areas for the monomer species displayed a positive correlation coefficient of 0.85 with SEC absorbance peak areas. However, the lower laser power rating was found not to be a sufficient yielder of fluorescence emission for the aggregate and fragment species. HPLC-SEC indicated that the samples had the lowest fragment content out of all species. Aggregates on the other hand, form much larger structures than monomers, hence can be prone to fluorophore shielding. The lower power rating was therefore found to not be suitable for resolving the decay contributions of the larger molecules such as aggregates and molecules with low concentrations. For the power rating of 50 µJ, the higher correlation coefficients above 0.9 indicate in-line TRF spectroscopy is a strong contender for meeting the regulatory USP threshold for a spectroscopic analytical technique against the industrial standard of HPLC-SEC.

The linear model predicts that at concentrations where SEC-absorbance does not register a signal, it is predicted that TRF spectroscopy will (aggregate-fragment) and vice versa (monomer). A portion of this can be attributed to inherent system noise for both methods and the target concentrations they are designed to analyse. To directly compare TRF spectroscopy against HPLC-

SEC, samples had to be diluted by at least 3-fold. The dynamic range of TRF spectroscopy was found to be far superior than HPLC-SEC.

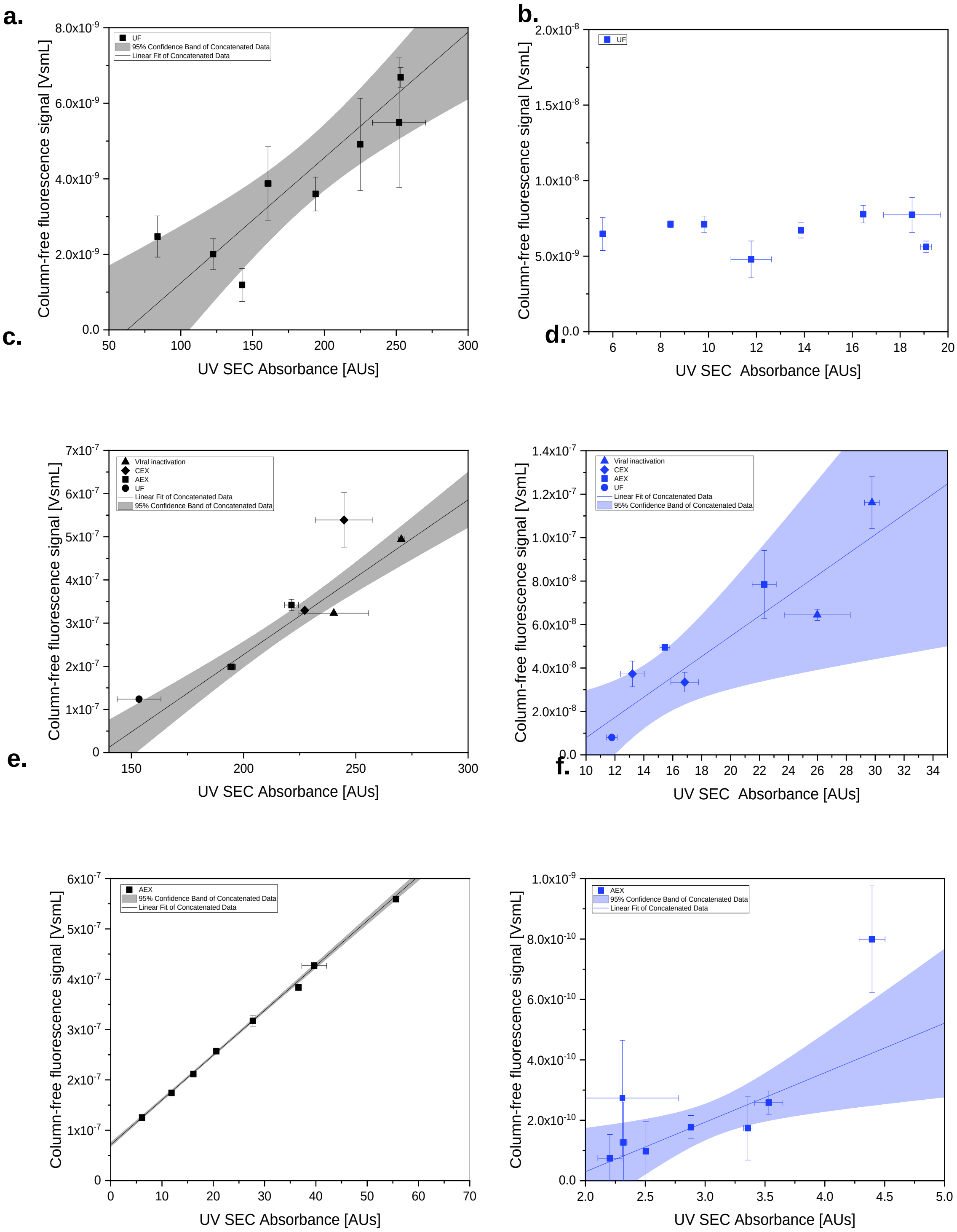

Figure 23: Parity plots comparing peak areas derived by HPLC-SEC UV absorbance and column-free TRF spectroscopy decay contribution intensity, for: a) b) low laser pulse power, low concentration, c) d) high laser pulse power, low concentration, and e) f) low laser pulse power, high concentration.

The generation of mAb aggregates and fragments have been described as indicators of degradation (Vázquez-Rey and Lang, 2011; Wang, 1999) and their presence in the samples could have arisen due to high SEC pressure and shear force exposure during the head-to-head analysis against TRF spectroscopy. The subjugation of mAb samples to a variety of mobile phase pH changes during capture and purification can also contribute to residual levels of aggregation and fragmentation (Mazzer et al., 2015). Several studies have reported that the peptide bonds in the hinge region are particularly susceptible to hydrolysis (Liu et al., 2008; Xiang et al. 2007; Vlasak and Ionescu, 2011). Proteolytic enzymes in milieu of residual HCP species from manufacture can also play a role in peptide bond hydrolysis (Gao et al. 2010; Sandberg, 2006). Due to their immunogenicity and potential mediator of adverse drug effects, mAb fragmentation and aggregation will continue to remain major concerns during manufacturing (Rodrigo et al., 2015; Lee et al. 2018; Song et al. 2014). The need for accurate, bioprocess-representative, sustainable, and cost-effective quantification methods are underlined here. In-line TRF spectroscopy eliminates the requirement for the routine SEC analysis of CQAs and the subjugation of mAb eluates to differing biophysical conditions. Instead, direct measurements are performed on bioprocess feeds/eluates in original mobile phases and at original concentrations. As samples are not removed for off-line analysis, the possibility exists for a significantly greater number of measurements in a given time frame compared to the typically 30-60 minutes of analysis required for HPLC-SEC.

As the mobile phases return a near-zero voltage signal, any peak attributed to a mAb sample can be taken as a positive control and the protein-free mobile phase as the negative control, improvements to the experimental set-up can include real-time HPLC-SEC pooling of sample fractions as they pass TRF spectroscopy and fraction collection of proteins, aggregates and fragments for further analysis. Challenges to this include achieving sufficient initial separation between the mAb monomer species and similar-sized aggregates post HPLC-SEC column elution as dead volume and curved capillaries between the SEC column and the TRF spectroscopy detector can encourage the remixing of separated components.

Time-resolved fluorescence spectroscopy has demonstrated candidacy at paving the way for a streamlined, in-line method of quantifying multiple protein species in industrial biomanufacture. There is a clear market demand for such technology, not only from a financial standpoint given the time and material savings it offers but also from a sustainability front as well, since it can reduce the amount of waste single use items through off-line quantification methods.

With the competing method of HPLC-SEC, when we reach 2.9 mg/mL we can observe peak truncation and asymmetry due to a surpassing of column and UV absorbance detector limits. The total protein concentrations need to be limited in head-to-head analyses between in-line TRF spectroscopy and off-line HPLC-SEC. Again, the minimal formulation constrictions with TRF spectroscopy meant that similar detector saturation effects were not observed in samples sourced pre-UF.

1 decay per fit provides the most accurate species quantity estimates. However, the quantity describing signal traces can be very noise prone, in such a case, the option for signal smoothing exists which can help with identifying a pattern and temporarily assessing the proportionality of a system.

With the sensitivity-improved TRF spectroscopy system, signal smoothing and artificial baseline noise removal techniques were not required to artificially raise signal to noise ratios and correlation coefficients.

We see this greater signal to noise ratio reflected in the benchmarking results of improved-sensitivity TRF spectroscopy against HPLC-SEC. Here the results of the improved sensitivity TRF spectroscopy configuration had a much greater or comparable correlation with off-line HPLC-SEC – this was despite testing the samples at lower concentrations than those tested with the original configuration. For each sample and test configuration case the positive relationship between the decay associated, and UV SEC absorbance peak areas are much stronger for the monomer species. This can be explained by their greater concentration compared to the impurity species which typically forms less than 10 % of the sample.

The propensity of mAbs to form aggregates is a major regulatory concern – particularly their unpredictable in-vivo nature that may cause life-threatening immunological and toxicological responses (Bucciantini et al., 2002; Hermeling et al., 2004; Engelsman et al., 2011). This has led to strong scrutiny of aggregate detection, quantification and monitoring methods (Berkowitz et al., 2012). Aggregates can form at any point of the biomanufacturing line, storage, shipping and delivery. Environmental stressors, for example, pH, agitation, and temperature, have been investigated as aggregate inducers. Freezing and solution contact with certain surface materials have also been identified as initiators of aggregation (Mahler et al., 2009: Hawe et al., 2009). Whilst SEC is a primary analytical tool in aggregate quantification, opted for robust, sensitive and reproducible aggregate quantification. SEC columns are critically limited in the total protein concentrations that can be loaded – exceed this, and the UV absorbance detectors become saturated and generated chromatograms inaccurate. There is also an upper limit to the aggregate sizes that can be resolved, as the largest can be filtered out by system frits, and pore and bead sizes can provide resistance to flow. They also have a very limited mobile phase options – often the samples either require re-formulation or suspension into non-matching mobile phase solvents. Since the aggregative nature of mAbs is sensitive to pH it then becomes difficult to discern the true aggregate quantities in the bioprocess (Philo, 2009; Engelsman et al., 2011).

Table 5: Industrial advantages of TRF spectroscopy over standard HPLC-SEC.

Specification	*Bioprocess Method*	
	Off-line high pressure liquid chromatography-size exclusion chromatography (HPLC-SEC)	**In-line time-resolved fluorescence (TRF) spectroscopy**
Frequency of measure	40 samples/run	User defined, can be unlimited
Quality of results	Dependent upon separation efficiency provided by SEC, reduces over time.	Greater robustness, in-line measurement system has lower risk of contaminating feedstream.
Required labour	Sample buffer exchange and dilutions. Column equilibration and storage.	Switch on device components and run unaltered samples in buffer of choice.
Sample test time	20-60 mins/sample	Flow rate-defined, total fluorescence intensity can be < 1 minute/sample.
Cost considerations	Regular replacement of SEC column, cleaning validation for sample valves and column, samples to waste.	Cleaning validation for connected tubing, no regular replacement of parts necessary, long-term cost savings.

Benchmarking the UCL TRF analytical assembly with commercially available HPLC-SEC has been key to meeting the aim of demonstrating its quantification capabilities. The major practical differences observed between them are summarised in Table 5. HPLC-SEC performs off-line measurements, with each sample typically requiring 20-60 minutes of analysis time. This is in addition to the time required for maintaining high separation efficiency, column preparation and equilibration which requires several hours per mobile phase change. Buffer-types and protein concentrations are limited to the specifications of the SEC column in use, all of which reduces processing efficiency and increases costs.

TRF Spectroscopy on the other hand can be inherently in-line, where the generated decay associated chromatograms resolve the proportions of multiple co-eluting species. Mixtures containing multiple species can be run without a requirement to wait for individual species to elute, unlike HPLC-SEC. This allows for much quicker analysis times, as well as less limitations on the concentrations, protein range and buffer conditions that can be run.

With the exponential growth in approved monoclonal antibody (mAb)-based therapeutics to meet an equally exponentially growing clinical demand, biomanufacturing has had to adapt with improved productivities to sustain higher product titres (Shukla and Thommes, 2010). These have been achieved with more efficient capture technologies, greater analytical capabilities and an increased understanding of the bioprocess. With the majority of costs accounted for by downstream processes, optimising the efficiency of product recovery and impurity removal by use of in-line analytics are key focus areas by industry seeking to lower manufacturing costs (Guiochon and Beaver, 2011; Levy et al. 2013).

5. Process-Related Impurity Analysis

Similar to aggregates and fragments, the presence of HCP in mAb solutions can induce severe immunogenic responses and undesirable side effects (Singh, 2011). As CHO cells are the host cell for production of mAb used in this thesis, CHO HCP will be present at its highest concentrations in earlier chromatographic recovery stages. Their total content can be quantified industrially by ELISA, however, HCP species cannot be identified without an additional method geared towards structural analysis such as gel electrophoresis or mass spectrometry (Levy et al., 2014). The studies in this chapter had the aim of demonstrating the capabilities of TRF spectroscopy in quantifying two very different protein solutions mixed together; increasing concentrations of HCP in mAb mixtures were quantified using TRF spectroscopy and ELISA to chart proportionality, and therefore accuracy of the former.

5.1. Results and Discussion

5.1.1. *E. Coli* HCP DAC Signal Discrimination

The ability of decay fitting program to separate the optical signals pertaining to two completely different species was first tested with: Fab and protein G flow through, separate, and in a mixture (see fig. 24). When there is no protein G flow through the decay associated signal describing its quantity in red formed baseline noise, and the blue signal describing the quantity of Fab is still being detected at concentrations as low as 0.025 mg/mL. Whilst the red trace is not exactly on zero due to baseline noise contributions from instrument components, biomanufacturing lines typically operate at concentrations that are a magnitude of 10^3 greater than the concentrations tested here.

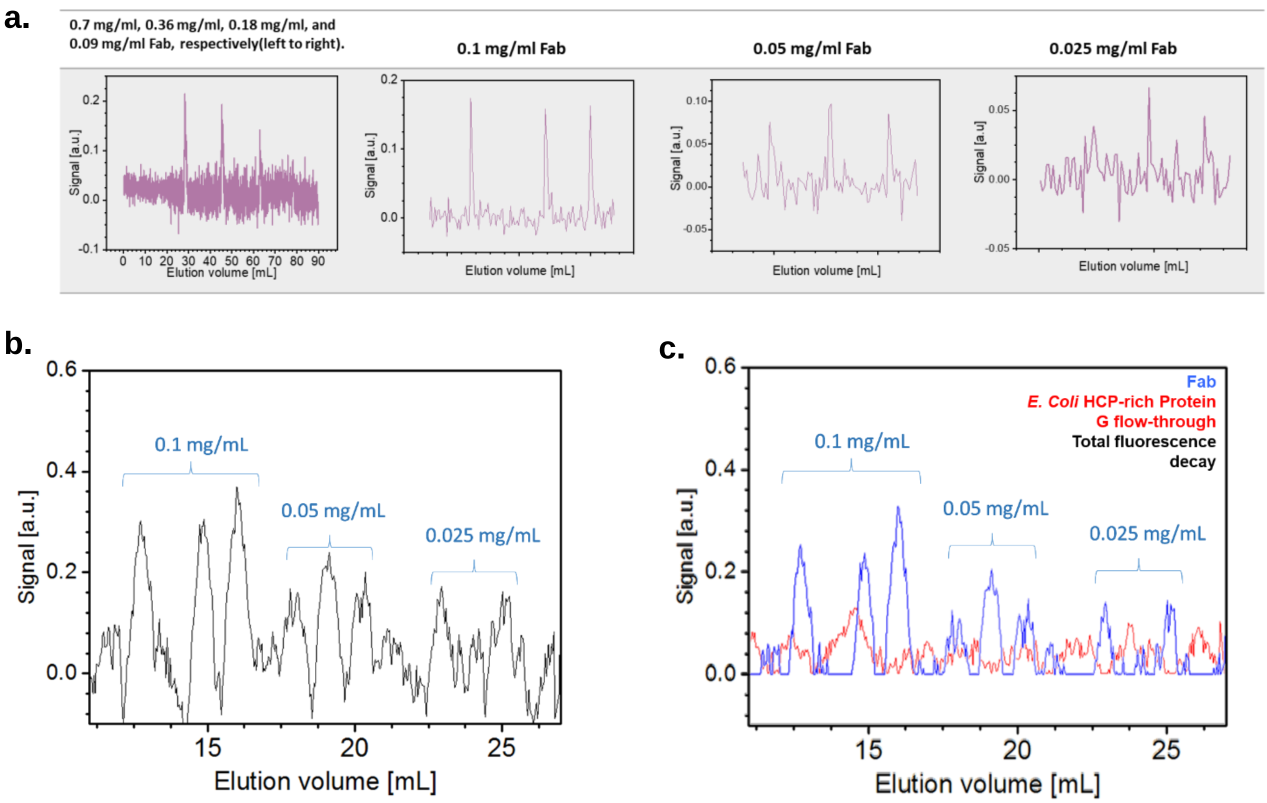

Figure 24: a) limits of total fluorescence intensity detection for Fab samples measured at successively decreasing concentrations. b) Total fluorescence intensity at points of Fab sample injection. c) DAC traces describing the quantity of Fab when it was injected through the column-free system and HCP when it was not run through.

In figure 24, a positive relationship can be observed between the known Fab concentrations run through the device and the peak amplitudes registered with the software. This positively proportional concentration-decay intensity relationship can also be observed with the CHO HCP and mAb injections.

For the DAC plot in fig. 25e, presenting the quantities of mAb and CHO HCP as a green and purple trace, respectively, for each sample injection, the peak areas under both signal traces are aligned with the concentrations injected. The concentration of HCP-rich protein A flow-through used to spike the mAb samples remained the same for each mixture and the concentrations of mAb in each even set of triplicates was formulated to be equal.

The decay contribution of HCP residues building up on the capillary at the point of emission detection has the ability to increase baseline noise and sample fluorescence intensities. Successive amplitude increases with each Protein A flow through sample were not observed where 24 sample injections were separated with a capillary CIP protocol. Where residue build-up becomes noticeable through calculable decay amplitude increases with successive sample injections, the increasing baseline can be modelled as a function to determine the ideal point CIP introduction.

The mAb DAC trace for peaks *w* and *z*, in fig. 25b was representative of samples that had been aliquot from the same stock volume, had the same concentrations and the same dilution applied. Figs. 25b-d therefore demonstrate the proof of concept for HCP-rich Protein A flow-through quantification within mAb mixtures. DAC peak areas were closest to 0 where mAb or HCP species were not injected. The first triplicate and last triplicate This indicated that the proof-of-concept experiment conducted with one mAb concentration could successfully be translated to more concentrations and more bioprocess stages. The protein-free mobile phase negative control and positive control of either ultrafiltered mAb or HCP-rich protein A flow-through facilitated a visible signal distinction between flow times where no sample was injected, and times where only mAb or HCP were injected. The DC decay parameter plots in fig. 25g show clear regions signal convergence for a mAb and HCP-representative peak (figs. 25g1 and 25g2 respectively). This allowed an accurate selection of decay parameters that were exclusive to each species mixture and therefore concentration-reflective DAC signal peak could be obtained (fig. 25). The addition of a clean in place protocol midway through sample measurements (fig. 25e) was associated with a lower baseline HCP-rich Protein A flow-through signal. Without capillary cleaning, the HCP baseline DAC signal would increase in intensity as the experiment progressed (fig. 25f), indicating the buildup of HCP-based foulant on the capillary.

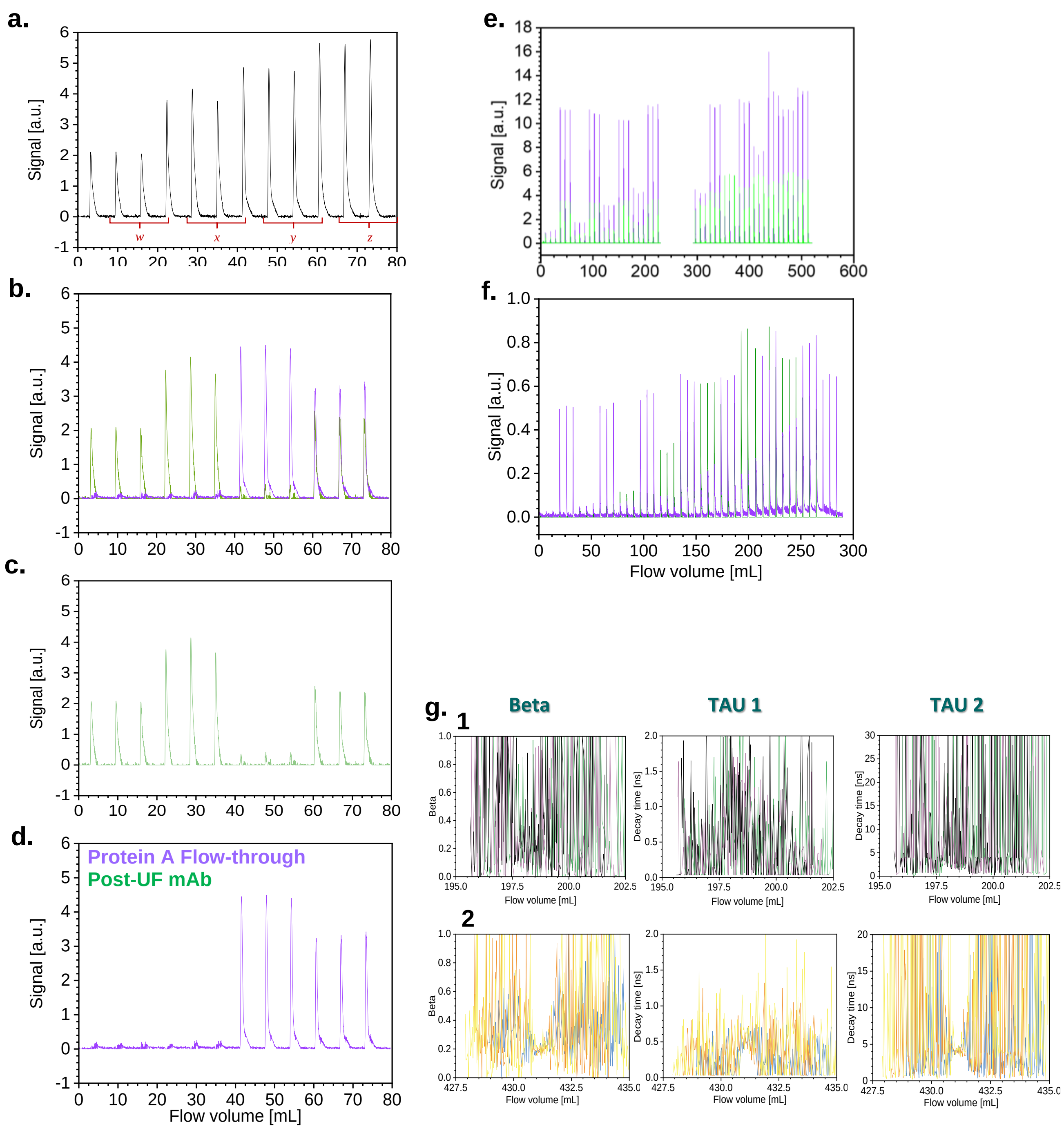

Figure 25: Discrimination of fluorescence decay intensity signal for mAb samples and mAb mixtures with Protein A flow-through. The elution of the mAb (green) and the protein A flow-through (purple) can the independently traced. a) Total fluorescence intensities for each of the samples tested as a proof of concept for HCP detection. The samples in alphabetical order are: *w*, mAb aliquot from dialysis tube and therefore diluted with water as well as its original buffer, *x*, mAb diluted with only its original elution buffer, *y*, Protein A flow-through, and *z*, second mAb aliquot from dialysis tube resuspended in Protein A flow-through. b) DAC traces for the mAb (green) and Protein A flow-through (purple) species displayed together. Displayed separately in c) for the mAb decay intensity contribution, and in d) for the Protein A flow-through. This proof of concept experiment was repeated on a greater scale with more mAb concentrations spiked with HCP (one example shown in e.). Each odd triplicate represents unspiked mAb, the following triplicate represents the same concentration of mAb, albeit spiked with HCP. Capillary cleaning occurred between flow volumes: 200-300 mL. f) MAb and HCP-rich Protein A flow-through mixtures run through TRF spectroscopy without cleaning protocol. g) Superimposed (n=3) decay parameter signal traces for: a) mAb eluates from UF, b) HCP-rich protein A capture column flow-through.

5.3.2. CHO HCP DAC Signal Discrimination

The β, $\tau_1$and τ_2 values for the mAb were 0.29, 1.07 ns, and 5.05 ns, and for the HCP-rich Protein A flow-through, were 0.291, 7.38 ns, and 4.66 ns. The fluorescence decay contributions of the mAb and Protein A flow-through species are presented in fig. 6. The average mAb DAC trace peak area for peaks *w* and *z*, where the samples had the same concentration of mAb (measured to 2 s. f.) are 2.83×10^{-7} Vs(S. D.: 3.56×10^{-9}, n=3) and 3.28×10^{-7} (S. D.: 5.29×10^{-9}, n=3) (3 s. f.), respectively. The *y*-peaks have an average peak area of 5.63×10^{-7} (S. D.: 1.04 x10^{-8}, n=3) for the Protein A flow-through DAC trace and 2.87×10^{-8} (S. D.: 3.71×10^{-9}, n=3) for the mAb DAC trace. For peaks *w* and *x*, the Protein A flow-through signal peak areas are 3.41×10^{-8} (S. D.: 1.47×10^{-9} , n=3) and 3.83×10^{-8} (S. D.: 7.95×10^{-9}, n=3) (3 s. f.), respectively. The total fluorescence intensity in fig. 5A are a sum of the integrated peaks in fig. 5B calculated by the TRF spectroscopy set-up. The greatest average total fluorescence intensity peak area can be observed in triplicate *z*, at 7.79×10^{-7} (S. D: 8.34×10^{-9}, n=3) (3 s. f.). A 21.5 % (3 s. f.) reduction in the average peak area for Protein A flow-through is observed between triplicates *y* and *z*, the latter of which represents samples with an 80% volume of Protein A flow-through and a 20 % volume of mAb suspended in elution buffer.

5.1.2. HCP-Spiked and Unspiked MAb Sample Analysis

Peak areas analysed under the unspiked mAb DAC trace returned strong positive correlations with ELISA-derived HCP concentrations. Correlation coefficients for the post Protein A, post cation mixed mode, post pH hold and post anion exchange DAC mAb trace peak areas against ELISA HCP concentrations (shown in figs. 10a-b, Appendix) were respectively as follows: 0.87392, 0.85977, 0.91887, and 0.99747. Unspiked mAb populations had a greater ELISA-derived concentration variance along the x-axis, with variances of 6.58E5, 2.52E6, 3.28E4, and 1.16E8 $(ng/mL)^2$ for AEX, PPH, CMM and PA eluates, respectively. Variances of TRF spectroscopy-derived species proportions along the y-axis were considerably lower, in the same order as before: 1.20E-14, 9.27E-14, 1.42E-15, and 1.20E-13 $(Vs)^2$, suggesting that the noise floor may have been reached. HCP-spiked mAb samples exhibited greater variances overall along the ELISA concentration x-axis: 5.11E9, 1.61E10, 3.12E9, and 1.77E9 $(ng/mL)^2$ for AEX, PPH, CMM and PA samples, respectively. Likewise, along the TRF spectroscopy y-axis differences were no greater than an order of 10 (in the same order): 1.68E-14, 8.50E-14, 6.05E-15 and 3.43E-14 $(Vs)^2$. The greater orders of magnitude in ELISA concentrations reflect the HCP-Protein A flow-though that was added to each mAb sample, however, this is not observed to the same degree along the y-axis. To assess whether the noise floor and thus lower limit of HCP measurements had been reached for the TRF spectroscopy instrument data points for HCP-altered mAb were also added and all datapoints were combined (fig. 27). This way it could be deduced whether the positive proportionality for unspiked-concentrated mAb samples was due to the concentration of residual HCP or an artefact in the measurement process at these low concentrations. The greater variance of 2.82E9 $(ng/mL)^2$ for ELISA assumes that the minimal change in measurement magnitude for TRF spectroscopy (variance: 4.46E-14 $(Vs)^2$), despite an HCP dilution range by the order of 10^3, is due to the lower limit of its dynamic range being reached.

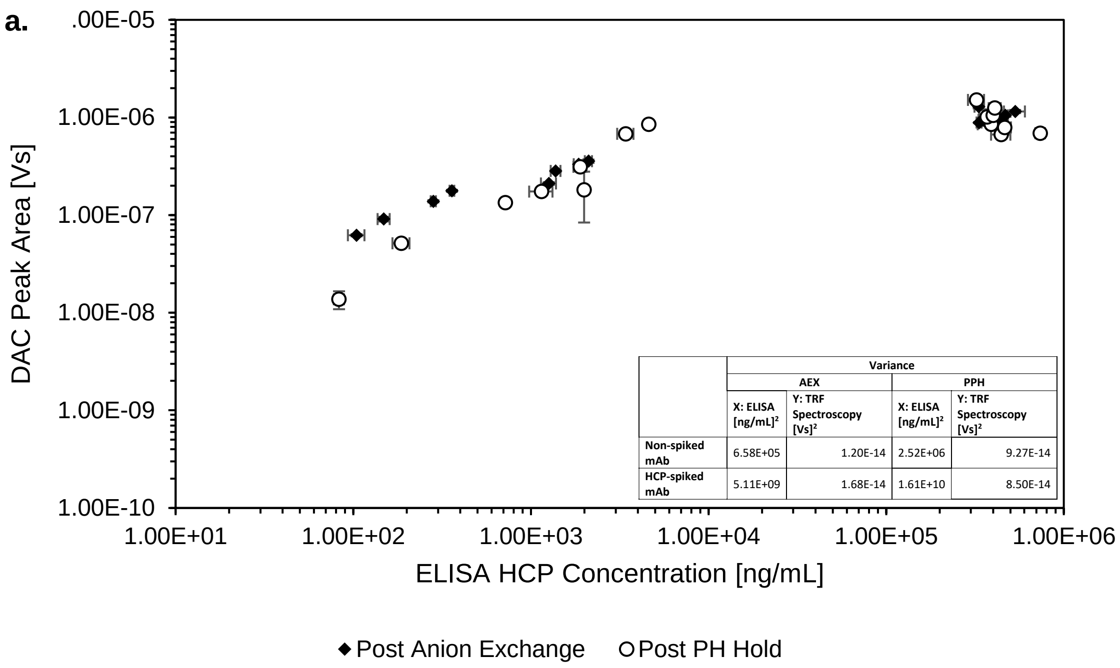

	Variance			
	AEX		PPH	
	X: ELISA $[ng/mL]^2$	Y: TRF Spectroscopy $[Vs]^2$	X: ELISA $[ng/mL]^2$	Y: TRF Spectroscopy $[Vs]^2$
Non-spiked mAb	6.58E+05	1.20E-14	2.52E+06	9.27E-14
HCP-spiked mAb	5.11E+09	1.68E-14	1.61E+10	8.50E-14

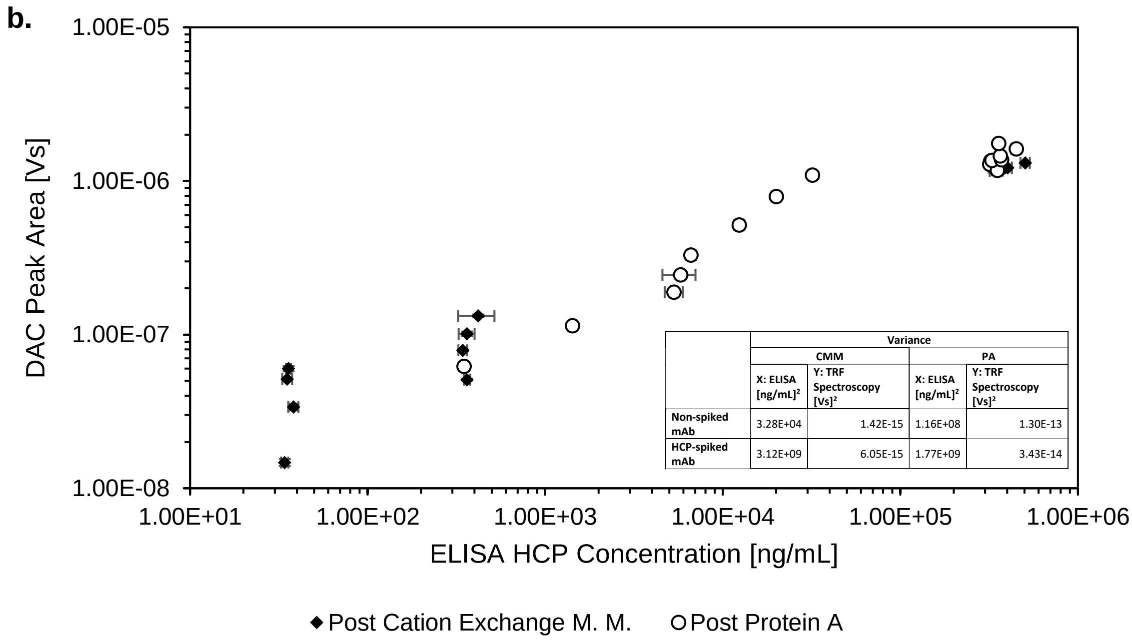

	Variance			
	CMM		PA	
	X: ELISA $[ng/mL]^2$	Y: TRF Spectroscopy $[Vs]^2$	X: ELISA $[ng/mL]^2$	Y: TRF Spectroscopy $[Vs]^2$
Non-spiked mAb	3.28E+04	1.42E-15	1.16E+08	1.30E-13
HCP-spiked mAb	3.12E+09	6.05E-15	1.77E+09	3.43E-14

Figure 26: Decay associated chromatogram (DAC) peak areas for HCP-rich protein A flow-through plotted against ELISA-derived HCP concentrations with variances for the unspiked and HCP-spiked mAb samples. Unspiked mAb eluates were sourced from 2 different biomanufacturing lines, either: a) anion exchange and pH hold or b) cation exchange mixed mode and protein A chromatography.

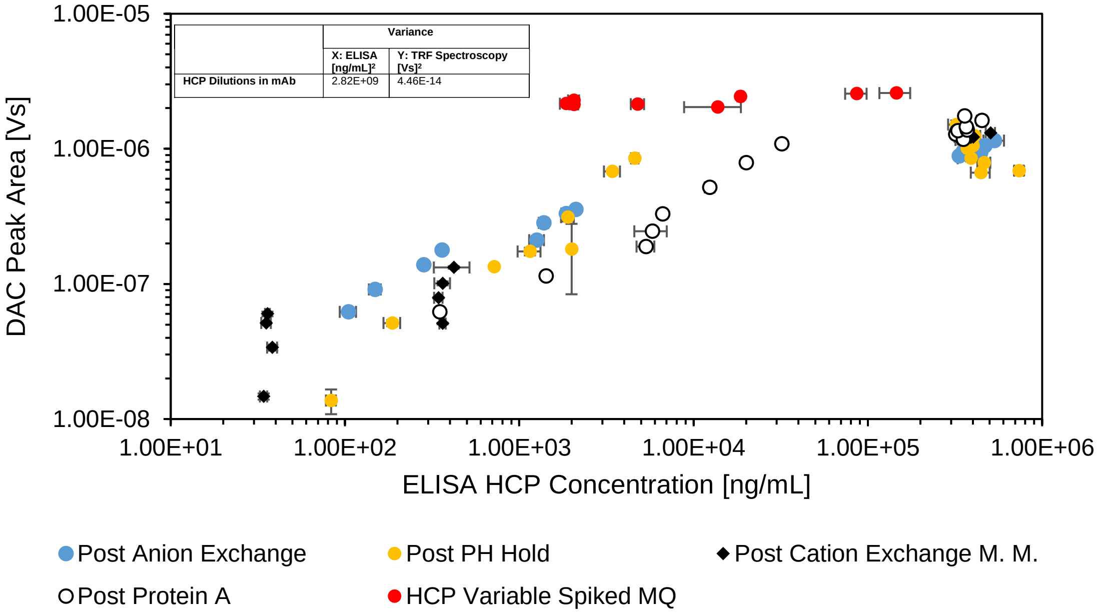

Figure 27: Decay associated peak areas for HCP-rich protein A flow-through plotted against HCP concentrations obtained from ELISA for all samples altogether including mAb-varied HCP-spiked samples (blue, black, clear and yellow data points) and HCP-varied mAb-spiked samples (red data points).

The peak areas for the HCP DAC traces increased with increasing mAb concentrations, despite spiked-protein A flow-through concentrations remaining equal. To further investigate this increase in registered HCP in the mAb samples an ELISA was run on each – the standard curves fitted with Langmuir binding isotherm models can be found in fig. 11, Appendix. Figs. 26-27 show clustering for both test methodologies for the mixed samples and a positive correlation for the mAb signal trace peak areas and HCP content. In fig. 25e-27, the unspiked mAb samples display increasing ELISA and TRF-derived HCP quantities with increasing mAb concentrations (figs. 26-27) – this is reflective of residual HCP centrifugal concentration together with mAb. However, in fig. 27, the HCP-varied samples have not yielded comparable DAC peak areas for HCP and ELISA-derived HCP concentrations. For the former, there is very little change in peak areas despite dilution factors having a difference of 4 decades in the log scale. For both manufacturing lines, the downstream samples returned lower HCP DAC trace peak areas. For the Westborough biomanufacturing line, the downstream samples had lower TRF spectroscopy and ELISA-returned HCP quantities. For the Portsmouth biomanufacturing line, expected trends were only reflected through TRF spectroscopy – highlighting its greater accuracy over commercial ELISA. Underestimated Portsmouth HCP concentrations can arise due to the reduced affinity of capture and reporting antibodies with bioprocess specific HCP species.

The process of concentrating mAb samples concentrates impurities and products of mAb degradation. In particular, a colour change has been observed upon concentration. Post-translational modifications (PTMs) as described in Li et al. (2014) can detriment the product purity, quality and biological activity. Increasing aggregate percentages have previously been observed for mAb exposed to near UV-visible light (300-700 nm) wavelengths. Increasing light exposure time has also been associated with increased oxidation of mixtures and resultant hydrophilicity. The degree and length of time of light exposure of the mAb samples prior to receipt is unknown, and whether any discolouration to samples can be attributed to photodegradation. The yellow discolouration of light-exposed mAb samples can be due to photodegradation-induced chromaphore formation on the mAb. Reversed phase HPLC-SEC would be required to identify the biological structures the yellow chromophores are associated with, this could be used in conjunction with HPLC-SEC to assess aggregate, monomer and fragment levels. Tryptophan has a number of oxidation products and pathways (Simat and Steinhart, 1998; Reubsaet et al., 1998; Li et al., 2014), each with their own absorption spectra and fluorescence decay properties. Li et al., identified kynurenine, N-formylkynurenine and hydroxytryptophan as the tryptophan oxidation products responsible for light-induced mAb sample colour change. Whilst the structural information of PTMs is limited, another area of use for TRF spectroscopy can be in improving understanding in the relationship between mAb stability and changes in sample colour through the abundance of particular tryptophan oxidation products (Li et al., 2014).

Overall, the dynamic range of TRF spectroscopy was found to be over 10-fold of what can be achieved using HPLC-SEC in the previous chapter and 10000-fold of what can be detected using ELISA – meaning its species resolving capabilities can be applied to a greater range of bioprocessing scenarios. ELISA requires a number of sample dilution ratios to be tested against OD450 values, however, it was found that only a dilution was required to UF eluates to generate decay parameters that were not distorted by photodetector saturation. HCP-spiked mAb samples formed clusters where they had been spiked with the same volume and stock of HCP-rich protein A flow-through. But they had a greater range along the x-axis (ELISA-derived concentrations) and minimal change along the y-axis (TRF spectroscopy) for the varying dilutions of HCP-rich protein A flow through in the mAb solution. At present, indicating that HCP DAC concentration measurements as part of a mixture with mAb, lose accuracy at concentrations below the Protein A flow-through that was supplied by Pall Biotech. These results set the precedent for further research into the capabilities of TRF spectroscopy at quantifying HCP in-line against conventional off-line methods. Biological therapies in requirement of CQA analysis are not limited to mAb-based platforms, they can also include cytokine receptors, growth factors and protein biosimilars. In all cases, product efficacy is highly dependent upon specificity with patient target sites (Shepard et al., 2017). As decay parameters form a signature profile that is unique to different biochemical arrangements of tryptophan and tyrosine residues (Hales et al., 2021). It has been demonstrated that TRF spectroscopy-based species quantification can be extended from product related impurities to process related impurities and other protein mixtures – once individual decay signatures have been obtained for a species at a set pH, they can be applied to a range of mixtures of different protein concentrations.

The replacement of batch ELISA-based analytics with TRF spectroscopy, would eliminate the requirement for costly HCP capture and reporting antibody-tailoring and significant formulation modifications to bioprocess samples. The application of serial dilutions to samples are often necessary to achieve measured HCP concentrations that fall within the standard range of the ELISA kit in use. The running of bioprocess samples through HPLC-SEC requires the dilution of post-elution samples in non-matching mobile phases, with upstream samples posing an increased risk of column fouling. As sample modifications are not necessary for TRF-spectroscopy analytics dilution errors are greatly reduced and species quantifications are more representative of the bioprocess stage under investigation. This supports QbD approaches by improving the understanding of the direct effects of critical performance parameters on the concentrations of different species. Future goals for TRF spectroscopy would require the identification of routes for technology adoption by industry and further testing on more protein samples to form a library of decay parameters ready for use on unknown protein mixtures.

6. A Scale-down Route for Industrial Retrofitting

6.1. Introduction

TRF spectroscopy has recently demonstrated its capability to distinguish intrinsic fluorescence decay lifetimes of co-eluting species in-line, thereby allowing their quantification without a need for time-consuming off-line methods in the evaluation of CQAs in mAb manufacture. Standard analysis of mAb aggregate and fragment species – key product-related impurities, and HCP– a key process-related impurity, are greatly limited in the ranges of concentrations and formulations that can be tested. The industrial standards of HPLC-SEC and ELISAs are the first point of call in the quantification of product and process-related impurities due to their robustness, reliability and grounding in literature. However, they require several hours of preparation and formulation constraints to be applied to original bioprocess samples, which limits the information that can be gained on the influence of CPPs on manufacturing efficiency.

Transforming the manufacture of protein therapeutics into a continuous process stream can significantly increase the efficiency of production and reduce the time to market and operational costs. The application of PAT would allow the accurate real-time monitoring of product critical quality attributes, in particular purity and concentration to ensure that they remain within acceptable bounds, and that any parameters that adversely affect these, such as aggregation and degradation are negligible (Read et al., 2010).

This project set out with the goal of assessing, identifying, developing, and implementing an in-line analytical method capable of quantitating the percent antibody monomer during the biomanufacturing process. This voyage was embarked upon to map out a path to eventually replace the current off-line size-exclusion HPLC method of assessing aggregates at Pall Biotech.

Whilst the current bench-top assembly has demonstrated the strong candidacy of in-line TRF spectroscopic techniques for multistage bioprocess implementation there are severe limitations in its mobility.

Achieving this would involve engineering the current UCL prototype instrument into a portable module that can sustain the pressures, flow rates and concentrations in mAb biomanufacture. The data processing and instrument control software would ideally be centralised to one software platform. Integrating TRF spectroscopy into a PAT system would involve it being part of a closed-loop control system, providing real-time monitoring, sample-time selection and automated responses to measured signals.

An evaluation of the robustness of the instrument on a range of different separation challenges, such as different protein types, chromatography types, and in batch vs continuous modes would be necessary before industrial implementation. As was observed for the current bench-top optical assembly, module enhancements would need to be carried out post-performance testing.

At the initial stages of development, the following design considerations were taken:

- Samples of chromatography feeds/eluates typical of industrial manufacturing, would need to be tested on the scale down system to evaluate detection capability and limitations.
- Flow cell size: seamless assembly with current manufacturing and chromatography rigs, in-line, therefore minimal contamination concerns.
- Dynamic range: the levels of detection across a wide range of protein concentrations including Pall specified ranges.
- Cost and energy footprint: long term cost saving projection from the reduced/eliminated need for ELISAs and HPLC-SEC and the waste they generate.

Design and testing cycles for performance using standard/model samples would be carried out to achieve the quantification of CQAs.

Work has involved the designing of the spectrofluorometer assembly to meet the specifications set by Pall. The quantification of the fluorescence decay rates of tryptophan residues within the protein products can be performed on the frequency domain involving the excitation of the sample at 266nm and the detection of emission intensity by a PMT, or on the time domain with components that readily allow single photon counting. The key aim has been to optimise this for protein concentration, where time-correlated single photon counting could offer a more economical assembly and accurate detection of proteins at low concentrations, frequency domain processing using a laser excitation source could accurately detect proteins at concentrations above 50 g/L.

The use of light emitting diodes (LEDs) are beginning to gain traction in fluorescent spectroscopy techniques. Their compact nature, versality, low power consumption and long operational lifetime make them ideal choices for use individually or as part of an array to excite a wider range of molecules (Hart et al., 2002; Landgraf, 2004; Lakowicz, 2006). Their small size and convenient interfacing through USB ports, simplify their installation and transport considerably when compared to lasers.

Photomultiplier tubes (PMTs) offer good sensitivities and wide quantum responses. The range of designs on offer can be tailored to the application and time responses required. In general, the shorter the distance in electron travel along the dynode chain, the faster the time response. However, like many detectors dark current can be a problem. This is the current running through the device, generating a signal when no light is incident on it and can arise due to excessive light exposure and voltage application.

Charge-coupled devices (CCDs) have an original purpose in imaging detection, but with their linear dynamic range and remarkable sensitivity have also developed a use in fluorescence spectroscopy. They typically consist of over 10^6 pixels, where each pixel accumulates charge in proportion to the total exposure of light, that is, each pixel is a detector in its own right. This generates a 2D image of the incoming emission and the charge at each pixel can be logged individually. Signals can be collected via fibreoptic cables, and when used with LEDs, a solid-state device is created (Lakowicz, 2006; Epperson and Denton, 1989; Hiraoka et al., 1987; Bilhorn et al., 1987).

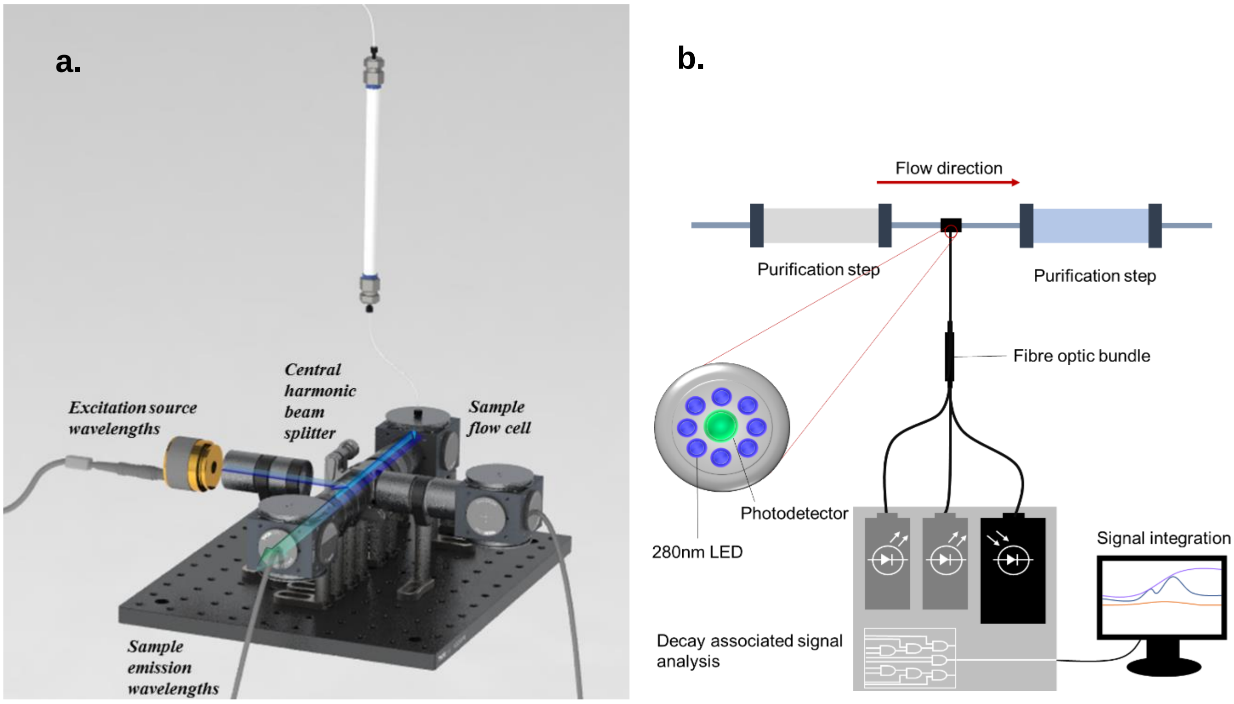

Figure 28: Two possible scale-down configurations for a standalone inline TRF spectroscopy instrument, a) frontal-sagittal flow and b) optical fibre probe.

6.2. Design

Key results have involved the design and optimisation of components for a scale-down fluorescence spectroscopy instrument. The design was created for an instrument to occupy a surface area near the size of an A4 piece of paper and be versatile in its potential future positioning. Fig. 28a illustrates the basic arrangement of components in a spectroscopic system that is capable of time-resolved and time-correlated photon analysis. Components were selected to meet biomanufacturing specifications and offer signal: noise that exceeds 10: 1 sample: background and good resolving power. The system can be used in TRF and time correlated photon counting (TCSPC) modes – the former in an in-line with the greatest sample concentrations, and the latter is an existing option for characterising the decay parameters of species in a mixture. In overview, pulsed light from the LED is collimated and focused onto a dichroic beamsplitter at 45 degrees, which reflects the wavelengths required for excitation into the flow cell carrying the protein samples, then the longer emission wavelengths are transmitted through the beamsplitter, through a long pass filter, and focused into a photodiode for detection. Details of the individual component choices are summarised below.

6.2.1. Excitation Source

The current bench-top instrument excites tryptophan and tyrosine residues with an Nd: Yag at 266 nm. The laser provides a high dosage of power and excitation intensity, which in turn, yields highly resolvable fluorescence decay intensities for species at lower concentrations. However, at this excitation wavelength other residues such as phenylalanine are also excited. Tryptophan has been reported to have the greatest absorbances near 280 nm (Anthis and Clore, 2013).

The fluorescence properties of tryptophan can be modified by the environment the residues reside in, for example, a blue-shift can be observed when tryptophan is buried amongst hydrophobic protein cores. The key problem here is being able to determine the origin of multiexponential tryptophan decays when in solution. Proteins can have a range of different conformational states. Some studies have attributed the presence of rotamers or particular protein conformations as the root of bi or multiexponential decays – with each exhibiting one fluorescence lifetime. The decay lifetime of a rotamer is the result of quenching interactions in fluorophores. The transfer of charge from excited indole moieties to carbonyl groups in peptide bonds, proton transfer, excited state electrons, and quenching have all been identified as being responsible for tryptophan deexcitation. Common decay lifetimes for tryptophan are 0.4-0.5 ns and 2-4 ns, therefore, an excitation source was selected to be capable of producing pulse widths below these times (Albani, 2014; Chang et al., 1983; Kuszaj et al., 1999; Antonini et al., 1997).

Excitation wavelengths of 280 nm are generated by a Horiba N-280 LED with pulse width < 1.2 ns and pulse power 1-2pJ. Easily adjustable repetition rates include 10 kHz, 25 kHz, 50 kHz, 100, kHz, 250 kHz, 500 kHz and 1 MHz allowing cyclical measurements to be made in a matter of nanoseconds for time-resolved and time correlated single photon counting (TCSPC) modes. Versatile and light weight at 1 kg, LED head is connected to the control module with a cable of sufficient length for flexible TRF module manoeuvring to achieve in-line monitoring. The USB PC interface helps with control centralisation to one PC screen. A wide range of samples can be analysed with a simple change of the LED head – with wavelengths ranging from 250 nm – 1310 nm. The plug and play configuration allow easy maintenance, wavelength modification and measurement logging.

6.2.2. Optics

Wavelengths under 280 nm are separated from wavelengths above 355 nm by the #37-721 beamsplitter. Wavelengths ≤280 nm are reflected into the beam monitoring photdetector and wavelengths ≥ 340 nm are reflected into the emission photodetector. Therefore, the Horiba N-250 and N-260 LEDs can also be used as excitation sources for measuring the emission of phenylalanine residues. For mAb and HCP quantification applications we have found measuring the emission from tryptophan and trace tyrosine residues to be sufficient in generating results aligned with industrial analytical standards. As such the design is presently, primarily aimed at delivering the excitation wavelengths for, and measuring the emission wavelengths of tryptophan. The FB340-10 bandpass filter (Thorlabs, US) removes undesired fluorescence intensity contributions above 340 nm and associated noise.

Table 6: Optics selection for emission and excitation wavelength collimation and focusing for a scale-down system.

Brand	***Part no.***	***Specifications***
Thorlabs	**LB5284**	CaF_2 Bi-Convex Lens, Uncoated
	LA5763	CaF_2 Plano-Convex Lens, Uncoated
	LA5042	CaF_2 Plano-Convex Lens, Uncoated
	LBF254-040	N-BK7 Best Form Lens, Uncoated
	FB340-10	Bandpass Filter, CWL = 340 ± 2 nm, FWHM = 10 ± 2 nm
Edmund Optics	**#37-721**	355nm T, 266nm R Harmonic Separator, Stock #37-721.

Table 7: Optical transmissions at wavelengths of interest for scale-down instrument lenses (Thorlabs, UK).

Part no.	*Total Optical Transmission (%)*			
	265 nm	**280 nm**	**340 nm**	**360nm**
LB5284	92.924847	93.134775	93.243498	93.36908226
LA5763	92.924847	93.134775	93.243498	93.36908226
LA5042	92.924847	93.134775	93.243498	93.36908226
LBF254-040	0.004771	1.601412	87.234047	90.420784
FB340-10	4.38E-05	6.96E-05	35.56144	0.50554
#37-721	<1	<1	>95	>99

Uncoated CaF_2 lenses have been selected for their high laser damage threshold, high transmissions in the UV spectral ranges (see Tables 6-7), and low refractive index (varying between 1.35-1.51 with wavelength ranges of 180 nm-8 um). It is also adequately chemically inert for spectroscopic applications and offers the greatest hardness when compared to other fluoride candidate compounds (Thorlabs, 02022).

6.2.3. Photodetection

Photodiodes have the advantage of being a smaller size to photodetector compartments, so much so, they can be readily soldered onto a circuit and come in a variety of mount materials, frequency cut-offs, photosensitive areas, spectral responses and connector pin configurations (Hamamatsu, 2022a). Fast response times below 1 ns, high sensitivities and suitable quantum efficiencies along the UV spectral wavelength range can all be achieved using a hybrid photodetector. Photodiodes can be combined with photosensor amplifiers to amplify weak photocurrents with low noise and high accuracies. This can be achieved with optical fibres that guide emission waves to the photodiode. Power is supplied via an AC adapter or dry battery, high resolution (16-bit) digital signals can be processed on a serially connected computer, analogue measurements can be made using a BNC-connected oscilloscope and processed according to user preference.

Sensitivities can be switched from “high” to “low” modes based on in-line protein concentrations to achieve current-voltage (I/V) conversion and amplification that meets the dynamic range of subsequent emission registering components. This can be achieved with a basic range-switchable photodetector amplification circuit comprising of a wide-range photodetector connected to two or more I/V conversion amplifiers providing two or more sets of voltage outputs for analysis. The total protein concentration will be positively proportional to fluorescence intensity and therefore the registered voltages. Desired voltage outputs can be controlled by a connector switch between the conversion amplifier circuits (Hamamatsu, 2020).

Silicon (Si) detectors are composed of PN junction photosensitive areas fabricated onto a Si substrate. The cross section in fig. 29 shows the

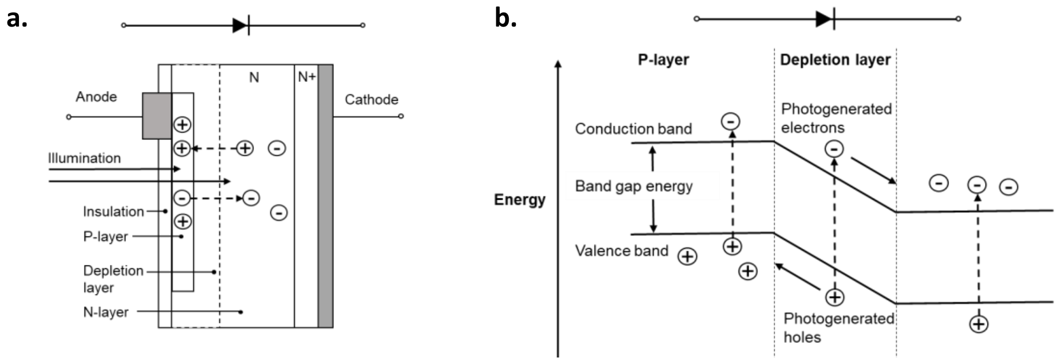

Figure 29: a) the charge operation of the Si photodiode in the scale-down device. b) the valence and conduction band junction.

arrangement of the photosensitive P-layer and the substrate-side N-layer. The spectral response of the photodiode can be controlled by the thicknesses of the P, N and N+ -layers and the dopant concentrations. The PN junction site of Si photodiode is illustrated in fig. 29. If the energy of incident light exceeds the band gap energy, the electrons in the valence band become excited to the conduction band, leaving holes in their original valence positions. Electron-hole pairs are generated through the P, depletion and N-layers. An electric field across the depletion layer accelerates the flux of electrons towards the N-layer. The electrons-holes are diffused throughout the layers and collected in the valence band of the P-layer. Resulting in a overall positive charge for the P-layer and a negative charge for the N-layer. As the detector is connected to an external circuit, supplied electrons will flow away from the negative N-layer and the electron-holes will flow towards the opposing electrode – this electron-hole pair diffusion across a Si photodiode, generates a measurable current.

They are capable of high-speed responses with frequencies above 10 MHz typically offered and an extremely linear photocurrent with respect to incident illumination intensity – for light ranging from 10^{-12} to 10^{-2} W, a range of linearity above 9 orders of magnitude can be achieved. The upper limit of this linearity will be dependent on the reverse voltage and load resistance whilst the lower limit is on the noise equivalent power. Ultimately, linearity degrades with increased in-series resistance (Hamamatsu, 2022b).

The output current generated by the circuit of a Si photodiode (fig. 30) can be summarised as:

$$I_O = I_L - I_D - I' = I_L - I_S\left(\frac{\exp(qV_D)}{kT} - 1\right) - I' \tag{45}$$

When the current output, $I_O = 0$, the open circuit voltage, V_{OC} becomes:

$$V_{OC} = \frac{kT}{q} In(\frac{I_L - I'}{I_S} + 1) \tag{46}$$

Assuming that the shunt resistance current, $I' = 0$, the photodiode reverse saturation current, I_S increases exponentially with increasing photodiode temperature, T. We also find that V_{OC} is proportional to $\log I_L$ and inversely proportional to T. This does not, however, apply for low light cases. When the load resistance, $R_L = 0$, and the output volage, $V_O = 0$, the current of this short circuit, I_{SC} can be calculated through the following expression:

$$I_{SC} = I_L - I_S \exp\left(\frac{q.I_{SC}R_S}{kT} - 1\right) - \frac{I_{SC}R_S}{R_{sh}} \tag{47}$$

The limit of linearity between I_{SC} and illuminance, are therefore dependent on

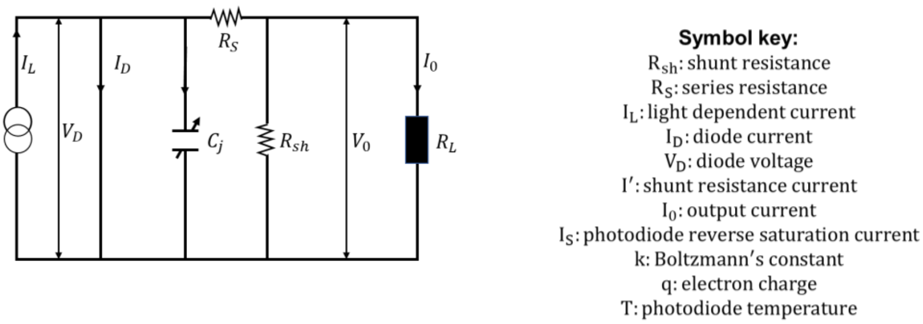

Figure 30: The equivalent circuit of a Si photodiode (Hamamatsu, Japan). Terms in eqs. 45-47 are defined in the symbol key.

the last two terms of eq. 47. Over a wide range in resistance these terms become near negligible. Fig. 31 plots the current versus voltage relationship for three different incident light intensity scenarios – as this intensity increases, the function is translated further along the negative y-direction.

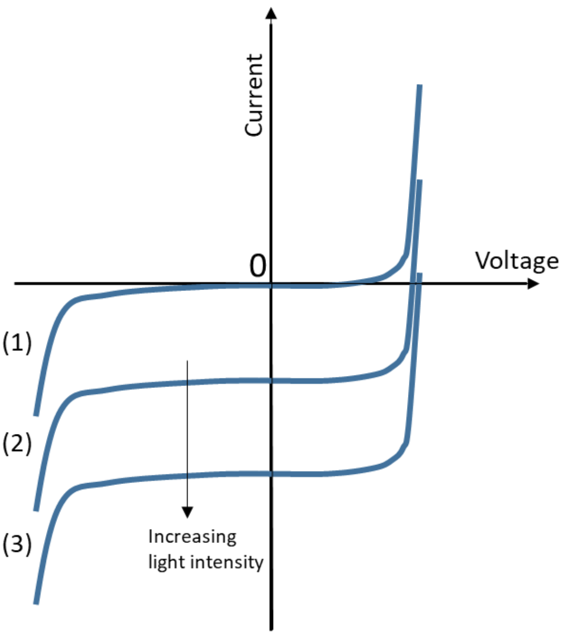

Figure 31: Current-voltage response of a Si photodiode at 1, the dark state, 2, when light is incident on the photodiode, and 3, when the light intensity is increased.

Table 8: Selected photodetectors for the beam monitor and sample emission measurements.

Part no.	*Specification*	*Photosensitive area(mm)*	*Photosensitivity (A/W)*	*Rise time(μs)*	*Terminal capacitance(pF)*
S12053-02	Si APD	φ0.2	0.42	0.0388	2
S1226-44BQ	Si photodiode	3.6 x 3.6	0.10-0.12	1	500

6.2.4. Digitisation

The analogue signals registered by the photodetector need to be converted to digital before further processing on a computer.

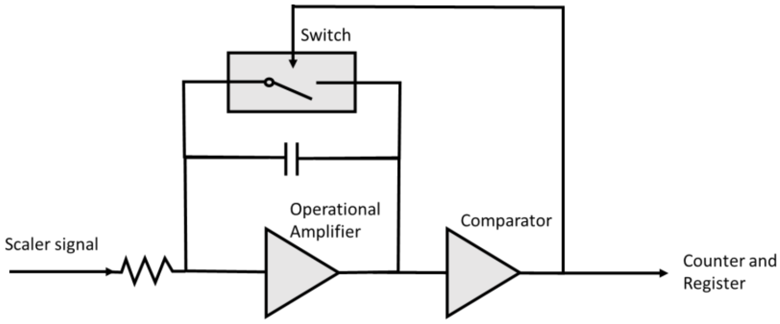

Figure 32: Basic arrangement of a V/F A/D converter.

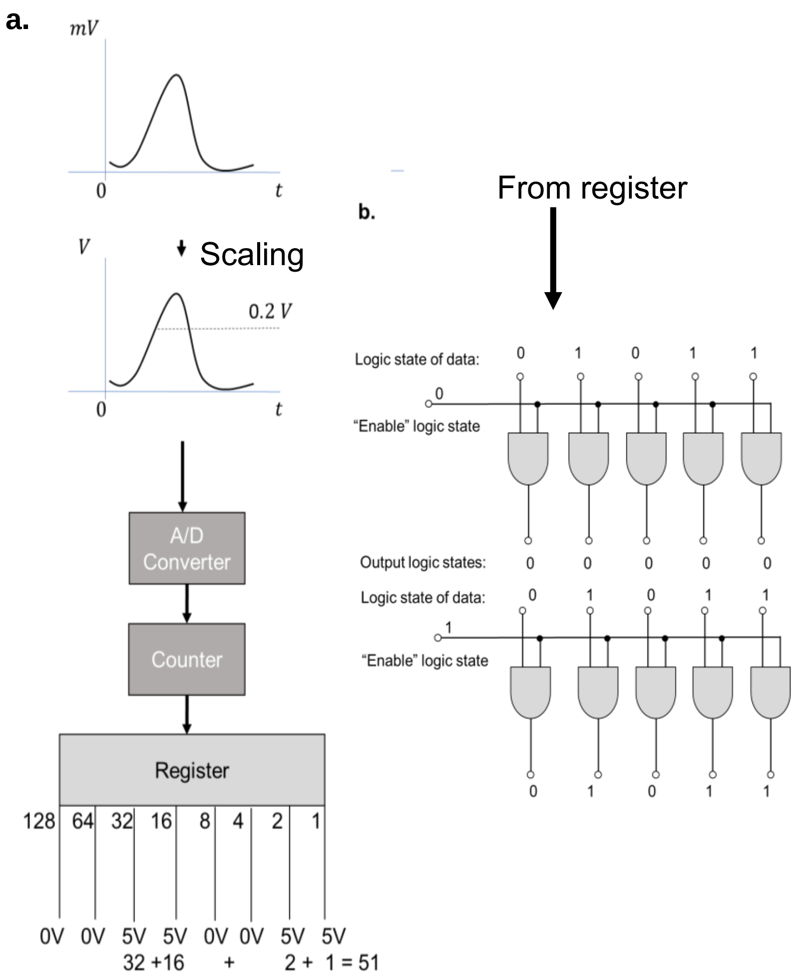

Figure 33: a) The process of signal scaling, digitisation, counting and registration. b) The peripheral interface adapter of a computer involved in data transfer.

Detectors can have output ranges that are significantly lower, often ranging below 100 mV, than the operational input into Analog-to-Digital (A/D) converters which can reach several Volts. In such a case, measurements in mV would need to be scaled to V – a simple process with the use of a linear scaling amplifier. Once scaled, the emission signal can be digitised using several methods such as single slope integration, sample and hold approximation, and voltage-to-frequency (V/F) conversion.

For basic V/F A/D conversion, the integrator, consisting of an operational amplifier and a feedback capacitor, provides input into the comparator which activates a switch to pass information to a counter and register. The switch is activated when a threshold potential across the capacitor is reached, after which, a pulse is passed to the counter and the capacitor is discharged. The process repeats again. Capacitor charge time is inversely proportional to the input voltage – subsequently, the pulse frequency from the comparator will be proportional to the input voltage. The counter samples the frequency of pulses at regular intervals and transfers the frequency count to the register in binary format. The magnitude of this binary number is dependent on the number of bits employed by the computing system. Fig. 33, provides an example of the stages involved in data acquisition for an 8-bit register, for which the largest decimal number of counts will be 255. The significant bits can be counted to give a total of 51 in decimal notation. If a voltage of 1V was the maximum that could be amplified to, then working backwards, we can deduce that $\frac{51}{255} \times 1V = 0.2\ V$. The higher the bit rating, the smaller the discrimination that can be made between any two numbers and the greater the precision of measurements. An 8-bit system would be capable of $\frac{1}{255} \times 100 = 0.4\%$ number discrimination which is typically more than adequate for contemporary applications. Another important feature for A/D converter selection is the rate of data acquisition. Signal peaks consisting of less than 20 data points are prone to serious distortion and poor accuracies. To assess the required data acquisition rate, f_A, can be obtained by calculating the following basic operation:

$$f_A = \frac{20}{w_B} \tag{48}$$

The minimum number of data points required for a satisfactory peak accuracy, needs to be divided by the narrowest peak base width, w_B, in seconds. After A/D conversion, the data is transmitted to a computer through either serial or parallel modes. In serial transmission mode, the digital data is transferred one bit per time unit. As a binary counter generates output bits in parallel format, where each has its own output channel, and their values are simultaneously available. To use the serial data transmission configuration, this parallel output scheme first needs to be changed to serial. This can be accomplished by using a Universal Asynchronous Receiver/Transmitter (UAR/T) – at the heart of its operation is the strobing of the shift register by a computer signal that displaces each bit of the binary number, one at a time from register to computer. This mode has major uses in multi-detector A/D converter systems where information is transferred to a computer over medium to long distances. Advantages include good immunity to noise, easy implementation, and reliability. The speed of transmission is limited to several kilobytes/sec for the generation of chromatographs, however, this has improved greatly over the years with the development of solid-state devices.

For parallel data transmission, the counter outputs are directly connected to a peripheral interface adapter (PIA), which itself is connected to the computer data bus. This data bus comprises of parallel rows of conductors through which binary data from the A/D converter is transferred. In the computer itself, it forms the transmission points for binary data between the central processing unit (CPU), memory units and peripheral circuits. The transfer of data from different levels is accomplished by a series of dual input, tri-state output AND logic gates, for each bit. The data bus otherwise cannot be continuously connected to the A/D output register. With an AND gate, data from its input can only appear at its output upon the reception of a computer signal. The logic state of the output of an AND gate will be identical to the input if the second input has a logic state of 1. Fig. 33b demonstrates the operation of AND gates in a PIA. The digital output of the A/D converter arrives as one input into each AND gate. Whilst the other input remains inactive, the output is zero. Upon activation of this other input with a logical 1 voltage, the output logic states become the same as the first input. The data can then be read by the computer and transferred from is accumulator to either its random-access memory (RAM), buffer store or hard/solid-state drive. As for the AND gates, with the enabling voltage removed, the gate outputs are reset to zero, the digital output of the A/D converter is isolated from the computer and the process can repeat again. When compared to serial, the parallel data transfer configuration offers very fast data transfer times (5 G/s achievable). A number of connections are required between the A/D converter and PIA, so applications are limited to cases where the A/D converter and computer are in close proximity. This is a common option for analyses involving built-in PCs. In chromatography, such data acquisition systems can have chromatographs stored in binary format in computer memory. Each detector output at a given time can be represented by a binary word – the period of time between consecutive binary words represents the intervals between samplings. The chromatogram is therefore a reconstruction of the detector readings at given times. A chromatogram with an analysis time of 20 minutes and 5 data points/second, could typically occupy 12000 binary words (2 words/data point) (Beesley et al., 2001).

To carry this out, it was important to select a system that had a peripheral component interconnect express (PCIe) system that could sustain the fast transfer of large amounts of data, be of a size that could slot into a majority of PC towers and possess a dynamic range to support the quantisation of molecules at <1 % of total concentrations and species with concentrations upwards of 50 g/L.

6.2.5. Time-resolved Decay Analysis

As outlined in the Background, the measurement of fluorescence decay intensities involved the measurement of the impulse response function, as this would be the observed fluorescence decay when a sample is excited with an infinitely sharp pulse. Reminding ourselves of the convolution of the impulse response in eq. 31, we can represent the observed fluorescence decay, $F_O(t)$, as the convolution of the excitation pulse, $L_P(t)$, with the fluorescence response, $F_R(t)$, of a system:

$$F_O(t) = L_P(t') * F_R(t - t')dt' \tag{49}$$

$$f_O(t) = \int L_P(t - u)f(u)du \tag{50}$$

The decay fitting software used in the quantitation of mAb product and process-related impurity species can be used to simulate the fluorescence response function through the convoluted data. $F_O(t)$ can be calculated through this way, as three exponentials are used, avoiding a case of invalidation to e^{-1} where a single exponential is used.

It is recommended that the excitation pulse time distribution is measured in short time intervals to the fluorescence lifetime. (Sharma and Schulman, 1999).

The convolution theorem can be used to represent products on the Laplace domain through two independent functions. Whilst the Laplace transform of the true fluorescence can be generated by dividing the observed fluorescence, $f_O(t)$ by the Laplace transform of a function, $L(s)$:

$$F(s) = \frac{f_O(s)}{L(s)} \tag{51}$$

Where s, is an arbitrary value.

For time-resolved, single-photon counting and fluorescence decay characterisation applications (Liu et al. 2012) least-square analysis has been applied widely. Least-square analysis is an iterative convolution method that can be applied to single photon counting applications and has had wide use in In-line fluorescence spectroscopic techniques. For this, the decay times are modified until a best fit can be arrived at; the difference of squares between $f_O(t)$ and $R_c(t)$ are minimised with the following equation:

$$X^2 = \sum_{in} \omega_{in}\left(f_O(t) - R_c(t)\right)^2 \tag{52}$$

The statistical weighting factor of the error in each value of $f_O(t)$ is $\omega_{in} - 1/f_O(t)$. The minimum value of X^2 would signify a best fit. In the ideal weighting:

$$\omega_{in} = 1/\sigma \tag{53}$$

Where σ, forms the standard deviation of $f_O(t)$.

However, the weighting of the fit can lead to errors that reach up to $\pm 15\%$ for single-exponential fitting and higher for more complex data. Its validity has come into question as it cannot be used in the analysis of data with low photon counts due to the Poissonian data distributions, rather than Gaussian (Turton et al., 2003; Lakowicz, 2006; Maus et al., 2001). Simulating the decay curve, can eliminate artifacts and improve the reliability, repeatability, precision and accuracy of fits. The application of exponential decays uses the definition introduced in the Background:

$$I = \sum_j A_j \exp\left(-\frac{t_i}{\tau_j}\right) \tag{54}$$

A key consideration is the inclusion of background counts, which can worsen precision as it requires more decay parameters to used and reduces the dynamic range if the background count exceeds the signal (Turton et al., 2003). Therefore, single photon counting arrangements can most accurately be performed in a photon-free environment. Achieving this in practise is challenging due to the presence dark counts and currents, in addition to the possibility of photon pile-up events for higher intensities (Han et al., 2020). However, improvements have been made to spectral response ranges, photon-resolving capabilities and signal-to-noise ratios, including the development of new technologies using zero-dimensional quantum dot resonant tunnelling diodes (Blakesley et al., 2005), one-dimensional photogating and quantum nanowires (Luo et al., 2018; Gibson et al., 2019) and two-dimensional materials that employ van der Waals forces (Ghosh Dastidar et al., 2022; Wang et al., 2022).

6.2.6. Control System

A digital closed-loop control system can be used in the timing of measurements and begins with a reference input set point (fluorescence decay) input to a CPU, where it undergoes A/D conversion, before moving onto the controlled system for further processing, then returns to the set point after a D/A conversion to original format, as depicted in fig. 34. For its robust performance, stability, wide dynamic range of CPPs and functional simplicity,

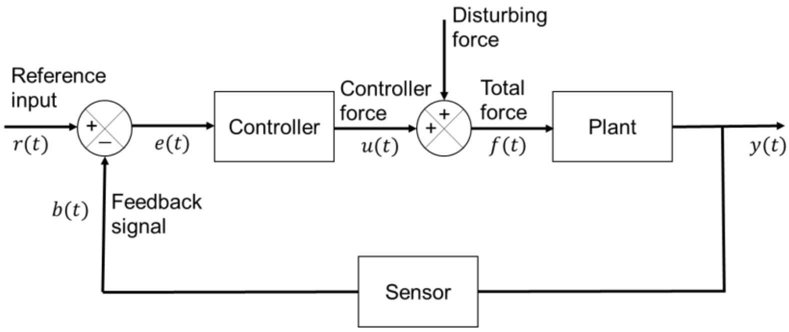

Figure 34: A basic digital closed-loop control system with a sensor and error detector.

implementing a proportional integral derivative (PID) controller remains the optimal option. *T*, the sampling period, is influenced by the time constant of the transfer function for the closed loop system. An interrupt service routine (ISR) can be incorporated, that is triggered by the D/A converter output. Such a closed-loop control system can facilitate the alteration of LED frequencies and intensities, or active circuits according to the estimated total protein concentration and desired mode of analysis. Applying the ISR procedure, results in the actuation of *u(n)* to the D/A converter. If the variable *u(n)* is not sent to the D/A converter sufficiently quickly, the system can witness unstable control systems and transport delays. To reduce instrument noise, signals, such as *y(t)* can be frequency attenuated using an anti-aliasing filter (Galan, 2022; Meirovitch, 1985). The control of CPPs, such as fluid flow, are performed on separate equipment modules.

6.3. Discussion

UCL has created and constructed an optical bench-based analytical instrument that has demonstrated the capability for in-line monitoring of chromatographic eluates, and real-time optical deconvolution of multiple protein species with overlapping peaks. This has enabled even completely overlapping species peaks to be separately quantified, which is not possible using post-processing of chromatograms. “On the fly” results generation is possible with software centralisation and automation. This would also require less memory and has applications in process control where the rapid generation of results is required to assess production stages. Peaks can be identified and have integration applied to them automatically through Originlab, so long as a threshold signal amplitude is specified for the peak start and species-associated signal amplitudes are above this threshold, to prevent baseline noise traces from being integrated.

TRF-based analysis has been identified as an ideal route for a scale-down system due to the ease of its use with a wide dynamic range of fluorescence intensities and concentrations observed in the bioprocessing line. Its high versatility in species types that can be quantified allow easy integration into theoretically any bioprocess stage. A range of optical component choices can be used to overlap the spectral profile of the species in the bioprocess stage of interest. The calculation of decay parameters from separated species can be performed on a standalone system not connected to the main production line with pure samples of the target species or a mixture of species separated by molecular weight using a preceding SEC column. The option for generating these decay parameters through an on-line species separation system also exists, however, once decay profiles for targeted species have been identified for set bioprocess chemical conditions these options will no longer be necessary. Decay parameters can be referenced from a library and applied in the subsequent decay fitting calculations. This leads to a truly SEC-free, in-line system of quantification.

The current bench-top system has demonstrated signal: noise ratios that exceed USP reference standard requirements when used with the total protein concentrations in mAb biomanufacture. This method has also been able to sustain the fluorescence intensities in downstream purification, which would not be possible with current UV absorbance and single photon counting systems without significant dilutions. As achieving high product titres forms a major industrial goal, the proportion of system and instrument noise on the final analysis is expected to be minimal (<0.01% total peak area). As has previously been seen in Claßen et al. (2019), the delivery and measurement of respective excitation and emission wavelengths through flexible optical fibres housed in the same probe would have the simplest method of installation, involving only the insertion of the probe into analysis ports – made liquid-tight through a valve. Alternatively, a TRF spectroscopy instrument can be positioned so that the flow of eluates is on its sagittal and frontal plane, effectively flowing right through it. The light-tight flow cell would consist of a reinforced UV-transparent glass flow chamber, capped with steel valves either end. Integrating with the previous and subsequent bioprocess stage will be more challenging as fittings will need to demonstrate they can sustain the flow rates and pressures the feedstream. This will require in-depth computational fluid dynamics analysis to ensure shear forces on the glass and fittings are within acceptable ranges. A leakage detector system and automatic shutdown will also be needed. The flow cell-incorporating design makes testing the response of optical components much easier in laboratory small-scale bench-top format with eluates syringe pumped through the instrument. The probe-head design will need testing with either a laboratory-based ultra-scale down chromatographic bioprocess train or with the large-scale bioprocess feed itself. The latter requires probe fittings to be designed to the dimensions of bioprocess equipment, incorporated to these between current purification stages and tested with several production cycles. The use of each excitation wavelength would require validation against an industrial reference standard. A single photodetector with a wide quantum response can be programmed to begin sampling the bioprocess feed every set number of minutes to generate a user-defined number of data points, the inputting of pre-determined decay parameters, decay function simulation, decay fitting, and species proportion calculations would be completed until the next sampling. Rather than performing the integration and analysis of decay intensity associate peaks against a mobile phase background, a stable signal for constituent species would be measured during the production run – any peaks and troughs to species concentrations would be indicative of CPP changes such as the switching of a mobile phase.

The in-line technique has shown promise in the continuous monitoring and quantification of a particular target protein eluted from a chromatography column even if there was co-elution with contaminant proteins. Whilst this technology might have further-reaching impact as a tool for the quantification proteins within mixtures and the assessment of formulations, there is a clear and immediate need for the adaptation of this technology to aid the in-line quantification-separation of protein products from side-products in an industrial bioprocessing context.

7. Conclusions

HCP and the products of mAb degradation will continue to form major impurities during the mAB biomanufacture. The current industry-standard methods of assessing them can be improved in efficiency.

The key problems this project set out to address included:

1. Evaluating the capabilities of in-line TRF spectroscopy for the measurement of CQAs during mAb manufacture.

2. Identifying a route for this technology to be retrofitted to industrial bioprocessing rigs.

Benchmarking the UCL TRF analytical assembly with commercially available HPLC-SEC and ELISA has been key to demonstrating its quantification capabilities for product and process related impurity analysis, respectively. An overview of the major practical differences between them is provided in Table 8. With HPLC-SEC and ELISA measurements are performed off-line. With HPLC-SEC each sample typically requires 20-60 minutes (HPLC-SEC), in addition to the time required for maintaining high species separation efficiency, column preparation and equilibration which requires several hours per mobile phase change. Buffer-types and protein concentrations are limited to the SEC column in use. For the most accurate HCP analysis, the binding affinity of antibodies in ELISA kits would need to be optimised with the HCPs observed in a biomanufactuing line. These can vary between cell batches and the mAb types that are produced. The ELISA process requires samples to be diluted in manufacturer-supplied diluents and typically lasts around 7 hours. This sets a barrier to achieving high-throughput analytics, in turn, reducing processing efficiency.

TRF spectroscopy on the other hand has been successfully used to perform inherently in-line measurements, with the DAC plot in Table 8 summarising the nature of analysis. Mixtures containing multiple species can be run without a requirement to wait for individual species to elute, allowing for much quicker analysis times, as well as less limitations on the concentrations, protein range and buffer conditions that can be run.

Table 8: Comparison of the key features of TRF spectroscopy and the current industrial standards for measuring process and product-related impurities.

TRF Spectroscopy

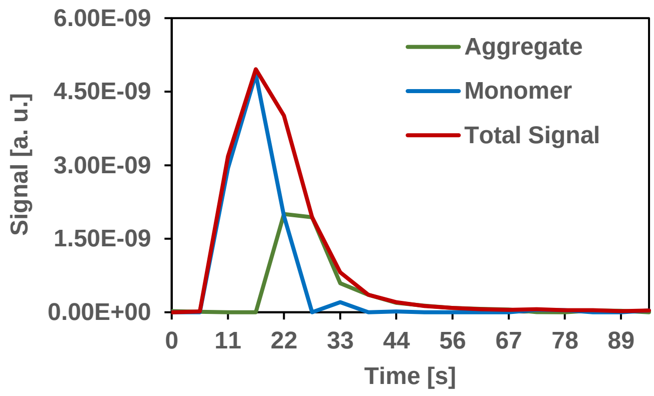

Output	Analysis time	Species	Sample preparation	Mode
Peak deconvolution	<20 minutes for an unaltered sample	99% of proteins	Less limitations on mixture complexity – no risk of column fouling. Higher concentrations can be tested.	In-line

HPLC-SEC

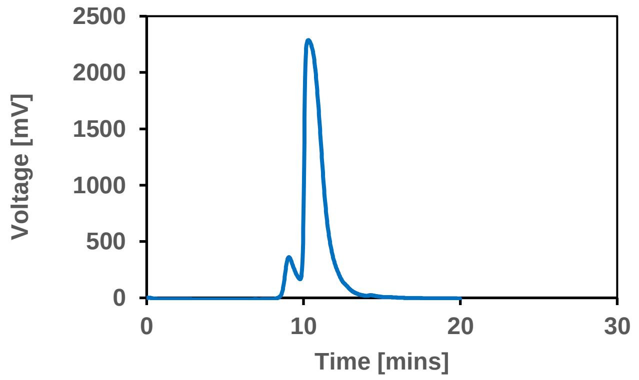

Output	Analysis time	Species	Sample preparation	Mode
UV absorbance chromatogram	20-60 minutes species elution wait time + column equilibration	Monomers, aggregates and fragments	Concentration limits for column used. Column fouling with upstream samples.	Off-line

ELISA

	1	2	3	4	5	6	7	8	9	10	11	12
A	4.858	1.723	1.61	1.5	4.989	0.293	1.377	0.311	0.209	0.223	0.25	0.23
B	4.882	1.793	1.623	1.528	4.924	0.27	1.355	0.312	0.223	0.203	0.26	0.225
C	4.934	1.892	1.648	1.653	4.921	0.28	1.345	0.298	0.33	0.3	0.338	0.345
D	4.956	1.617	1.633	1.661	4.957	0.276	1.375		0.534	0.557	0.664	0.572
E	1.793	1.747	1.645	1.411	0.321	0.318	2.457	0.82	1.164	1.187	1.264	1.171
F	1.695	1.69	1.558	1.334	0.327	0.291	2.409	0.769	2.656	2.594	2.73	2.615
G	1.701	1.608	1.543	1.393	0.323	0.302	2.59	0.808	4.521	4.598	4.603	4.518
H	1.528	1.625	1.437	1.402	0.337	0.299	2.464	0.8	4.981	4.941	4.983	5.172

Output	Analysis time	Species	Sample preparation	Mode
Optical density	~4 hour procedure + time for sample dilutions	Primary capture mAb-specific HCP	Serial dilutions and optimisation required to meet standard concentration range.	Off-line

Results have shown that for each DAC processing run, decay parameter signatures for the separated species can be extracted from volumes of signal convergence and then applied to unknown mixtures containing those species, enabling their quantification. In Table 8, the DAC signals have been clearly resolved for the aggregate species in red and for the monomer species in green for SEC and no SEC cases.

Fragment species have been detected in the samples through LC-MS and HPLC-SEC, particularly for the post pH hold and post S Hypercel™ bioprocess stages. This supports the hypothesis that the DAC signals observed for a species eluting at a time slightly offset to the monomer, is indeed an antibody fragment. In which case, the decay parameters selected from where an aggregate elution occurred are also shared by the fragment species.

A compilation of the processed DAC and HPLC-SEC data indicated that there is a very clear positive correlation between the two technologies. The HPLC-SEC chromatograms indicate the presence of a separate fragment species eluting post monomer. This finding is reflected in the DAC profiles obtained for the same samples.

The correlation coefficient between TRF DAC and industry-standard HPLC-SEC UV absorbance can be improved further with iterations to the instrumentation to increase sensitivity.

To summarise, the head-to-head analysis of the UCL analytical instrument and industry standard HPLC-SEC demonstrate that we can achieve a good positive correlation between the two. This was despite each of the samples used in benchmarking having total protein concentrations below 3 mg/mL to not overload the SEC column and cause chromatogram artefacts. The dilutions that had to be applied would also dilute the detectable mAb impurities within samples. Greater quantification accuracies and r-square values are likely to be achieved on our in-line TRF spectroscopy-based approach with much higher mAb concentrations such as those handled in the biomanufacturing line. This is by virtue of stronger signal components against noise for each eluting aggregate and monomer species – this is the opposite of HPLC-SEC where dilutions are often necessary for accurate analysis.

For the HCP study, the results demonstrate that the analytical software can distinguish decay intensity contributions of mAb, HCP-rich Protein A flow through and the mixture of the two in the same run. The software accounts for the effect of dilutions on species quantities and shows that they are representative of the expected compositions.

A key proof-of-concept experiment involved running post UF mab samples, Protein A flow through and a mixture of the two, on in-line TRF spectroscopy without a SEC column. The idea was that despite the differences in mixture these should still register a similar amount of mAb using TRF.

This experiment demonstrated that our measurement and processing method could successfully quantify mAb within a HCP-rich mixture. The reduction in signal intensity for the protein A flow-through in the last triplicate (fig. 25), was due to the buffer exchange at the beginning, where the mAb was suspended in water ***before*** the protein A flow-through had been added to it, meaning it would have been diluted to some degree. This showed that the software accounted for the effect of a 20 % dilution in the quantification of a species in a mixture – showing that they are representative of the expected compositions.

By analysing the fluorescence decay intensity contributions of multiple species within mixtures we can extract detail on protein aggregation, conformational state, degradation as well as the effects of mobile phase pH changes. TRF spectroscopy therefore provides us with more information on bioprocess samples than the current off-line batch sampling mode HPLC-SEC and ELISA. The in-line nature of TRF spectroscopy makes it very versatile, allowing species quantity analysis to be achieved at a fraction of the time and without the sample formulation limitations that would be required using industrial standards. Not only does this allow the direct assessment of the effect of any bioprocess stages on protein species distribution, but it also provides industry with a greater insight into the influence of CPPs on CQA proportions, facilitating a quality by design approach to therapeutic product manufacture.

8. Future Work

8.1. Viral Vector Quantification

This work has demonstrated that our method can be used to assign decay parameters to tryptophan and tyrosine residues in mAb and HCP particles.

In-line viral detection applications are also another area of great industrial interest. During mAb manufacture this can involve the evaluation of viral inactivation and removal steps and simplify the development of less aggregation-inducing methods. The manufacture of lentiviral (LV) and adeno-associated virus (AAV)-based therapeutics require similar resolving powers to that of the currently used system and can potentially be used in the detection of recombinant, partially filled and empty capsids – the latter two of which reduce the safety and efficacy of the product. This forms an emerging area where accurate, quality control-friendly, and rapid analytical techniques are required to determine full: empty capsid ratios for release testing (Li et al., 2020).

Viral vectors are a rapidly emerging area of therapeutics that can facilitate gene transfer to target cells or tissue for their modification and expression of genes (Naldini et al., 1996). Several virus types can be used for such applications – from retroviruses, adenoviruses, adeno-associated viruses, poxviruses, herpes simplex viruses, and baculoviruses. The selection will depend on desired recoveries, production ease, safety, stability, toxicity and the efficiency of transgene expression that can be achieved. A widely researched viral vector, lentiviruses fall into genus of retroviruses, which includes the human immunodeficiency virus, with which they share many physiological features. They are spherical and have a diameter around 80-120 nm (Segura et al., 2006). Their surface envelope proteins determine the cells they can target, since a range of host viral cells can be used for the plasma membrane envelope, their therapeutic applications are also wide ranging. Pseudotyping can envelope these viral proteins onto LVs (Duvergé and Negroni, 2020). The VSV-G glycoprotein sourced from the vesicular stomatitis virus Indiana, is considered a gold standard due to its broad tropism and because it interacts with low density lipoprotein receptors. These receptors can be found on most cell types (Finkelshtein et al., 2013; Munis et al., 2020). A disadvantage of its use is that it displays cytotoxicity and when highly expressed it can result in LV cell lines that are prone to instability. This limits applications to ex vivo transfection (Perry and Rayat, 2021).

Overarching aims with recent research has been to facilitate the upstream production of sufficient titres and counter the low recoveries in downstream. Current limitations in scaling up lentiviral production have not hindered their adoption for research into cell and gene therapies, their ability to transfer transgenes into target cells. Target cells have included neurons, hematopoietic stem cells and lymphocytes (Hislop et al., 2014; Tomás et al., 2019; Takeuchi et al., 1994).

It has been reported that there being over 100 clinical trials worldwide from the US, European Union and Canada whether it be to demonstrate ex vivo cell modification or the efficacy of *in vivo* therapies (Milone and O'Doherty, 2018). With clinical trial successes, increasing clinical demands and the approval of other protein-based therapeutic products such as CAR-T, the market for LVs is predicted to keep growing and reach 800 million dollars by 2026 (Southey, 2018).

Some key physico-chemical challenges to lentiviral processing and storage revolve around. The issues with damaged/ absent envelope proteins and non-packed vectors can Immunogenic Bioprocess parameters such as salt concentration, pH, buffer osmolarity and the shear forces applied between and during processing stages, can all influence the final morphological integrity of the LV product (Segura et al., 2006; Higashikawa et al., 2001; Coroadinha et al., 2006).

If these factors are not optimised during the biomanufacturing line, not only will recovery rates and yields be lower, but the removal of impurity species would be less efficient. The purification of LVs typically involves a series of filtration and chromatography steps. The use of sterile filtration has been reported to lead to titre losses of between 30-50% with the use of 0.22 um filters, due to these poor recoveries this stage is placed at the start (Valkama et al., 2020;

Bandeira et al., 2012; Cornetta et al., 2005). This is followed by chromatography-based separation that operates using the chemical interactions of LVs with resins and beads (Perry and Rayat, 2021). Current methods of calculating recoveries involve time-consuming methods such as p24 ELISA and transduction assays.

For ex-vivo applications where the target is to produce transduced cells, quality assurance and quality control requirements are expectedly less stringent than those for in-vivo applications. Therefore, for ex-vivo where more vectors allow for more tests to be conducted using each batch, yield and vector quality would need to be assessed. For in-vivo implementation, CQAs are also expectedly centred on vector quality and the quality of transduction that can be achieved, but also the vector concentration particularly post-formulation to ensure they are within bioeffective ranges (Rodrigues et al., 2007; Perry and Rayat, 2021). The cellular targets of viral vectors can be designed through pseudotyping and the chemical efficiency of bioprocess operations can be assessed by virus recovery and functionality. Once fluorescence decay parameters are attributable to a particular protein sequence, they can be used to quantify that substance. Adding TRF spectroscopy to the analytical scope will allow users to characterise the effectiveness of certain pseudotypes and concentrations on chromatography column binding, filtration recovery, aggregation and degradation control (Tijani et al. 2018).

The size of lentiviruses are approximately 10 times larger than that of the mAbs investigated in Chapter 1. We have seen that in-line TRF spectroscopy can resolve the quantities of monomers, HCP, aggregate and fragment species despite their small hydrodynamic radii. By measuring the difference in the fluorescence decay intensity contributions of empty and full capsids, as well as other protein-based impurities there is potential for quantifying them in-line, without the need for time-consuming analytical assay/chromatographic techniques. It can also be used within a wide range of chemical environments and concentrations; strides are already being made in this area by Hales et al. 2019.

8.2. Scale-down and Automation

It has been observed that greater sensitivities can be achieved with a simple increase of the laser power rating and a re-alignment of the photodetector. Currently measurement repeats are carried out manually. Automated sampling at regular intervals will not only reduce the time required for sample preparation into HPLC-SEC injection vials but support the validity and reliability of results with more repeats possible in limited timeframes.

The decay parameter generation and decay fitting software were originally designed for an Origin 2015 execution platform. However, disabling system variable changes introduced for later versions of OriginLab allows one to run the scripts successfully via the Origin 2022 command line. Currently all decay parameter selection and exponential model fitting are performed separately for each test case. For easier industrial implementation these programs will need to be centralised to one control software platform. Ideally the process of mean decay parameter and quantity-describing decay associated chromatogram generation would be controlled from one window. An opportunity for AI implementation also exists here, artificial neural networks (samples>10000) or decision trees can be trained to identify regions where decay parameters converge to a threshold range of values. These convergence points are when single species are eluting, therefore, sample standards for species expected in the bioprocess can be used to obtain these decay parameters for the chemical environments (e.g. pH, ionic concentration, presence of other species) at particular bioprocess stages. Once obtained they can be used in the quantification of that species in the same chemical environment, bypassing the decay parameter characterisation stage. This would facilitate a streamlined approach to species quantification, eliminating the need to select species elution regions manually, generate decay parameters for each batch of tests and manually integrate each DAC peak.

Using a HPLC-SEC mobile phase with a sodium perchlorate component the facilitates high chromatogram resolution with reduced peak tailing. Any future tests can include this buffer component and would ensure consistency is maintained across my measurements.

Artificial methods of inducing controlled levels of aggregation in the samples can be applied to increase the species concentration and provide a comparative study angle. It may seem counterintuitive when the end goal is to demonstrate detection and quantification of residual levels. Nevertheless, increasing the concentration of the aggregate species would increase the fluorescence decay intensities of the aggregate species and reduce signal: noise post-fitting. Any decay characteristics for the dimer would be more easily distinguishable from noise or any signal arising from the monomer species. A degradation pathway itself, there are indeed difficulties with generating aggregates in a stable manner without forming large insoluble aggregates that are not representative of the bioprocess. Which is why several decay parameter values have been tested for each sample, new ways of identifying them have been tested such as through decay function simulation and averaging at species elution times.

After the initial cost of instrument purchase and bioprocess integration into an in-line configuration, the costs of analysis are steeply lower than current industrial standards. Most operational costs will stem from power consumption and maintenance. However, optical components have long lifetimes and are supplied with generous guarantees.

8.3. In-line Integration

The diagram in fig. 28 (6.1.) compares different analytical configurations and highlights the intended end use of TRF spectroscopy in-line.

The off-line nature of current analytical systems requires long sample preparation and analysis times, higher associated analytical running costs and reduced manufacturing efficiency due to the limited information available on the bioprocess. All of this contributes to high final product costs.

On-line analysis has been proposed which would eliminate the need send product to waste as it is returned back to the main production assembly, but depending on the connection fittings used there may still be contamination concerns over the volumes returning back to the main line. If analysed sample volumes are sufficiently small, returning them back to the production line will not present any impactful cost savings and can be considered unnecessary.

The validation of an in-line methodology has been the key goal of this research, and a target configuration for the final system. This would readily provide real-time, continuously, measurements, without product loss, with less risk of contamination, and with supreme flexibility in bioprocess stage positioning, therefore making it the most ideal system.

Quantification applications are not limited to mAb biomanufacture – we have seen cases where the differences in excitation and emission spectra due to different residue concentrations of cell metabolites have been capitalised upon with optical-fibre delivered changeable excitation wavelengths (Graf et al., 2019; Claßen et al., 2019). Rather than employing several photodetector modules, emission wavelengths and measured fluorescence decay intensity amplitudes can all be controlled by simply switching filters on a multiplexer. Excitation and emission wavelengths can be supplied and received via the same probe, albeit with separate optical fibre ports as illustrated in fig. 28b. Its flexible body would simplify the installation process and allow it to be retrofit to any upstream or downstream bioprocessing stage.

Outside of UV fluorescence spectroscopy, optical sensors with different wavelengths of operation (visible, near and mid-infrared) and also Raman-based methods have been in research for several decades (Claßen et al., 2017). The use of non-invasive, in-line spectroscopic sensors form a powerful PAT tool for the facilitation of real-time product analysis, early fault detection and minimisation of contamination risk. It has been used to provide deep insights into cell concentrations, metabolism, respiration and viability in cell culturing stages (Claßen et al., 2017; Claßen et al., 2019) and laboratory scale measurements have built upon proof-of-concept work by Hales et al. 2021, demonstrating the strong potential of in-line spectroscopic measurements to be performed in this manner upstream and downstream. Given that fluorescence spectra can be used to provide information on the concentrations and configurations of tryptophan, tyrosine, phenylalanine, which are present in cell and protein markers of viability, stability and integrity (Faassen and Hitzmann, 2015; Lakowicz, 2006; Hantelmann et al., 2006; Moon and Fleming, 2011), applications are not limited to measuring impurities or the final product, but also the CPPs involved with their production and purification.

9. Impact Statement: An Evaluation of the Academic, Economic and Societal Impact of this Project

9.1. Learning Outcomes

This project was born out of the challenges in resolving the biophysical differences between monomers and dimers during biomanufacture as their hydrodynamic radii can be within several nanometers of each other. In contrast to conventional analytical methods, the UCL assembly employs time-resolved fluorescence spectroscopy which has demonstrated capability in registering these minute differences even where dimer concentrations are very small. The business and bioprocess advantages through its use stem from the improved efficiencies of running quantification measurements.

A bench-top instrument was developed to demonstrate the potential of using the intrinsic fluorescence decay properties of species within a mixture in the quantitation of that species. This had already been demonstrated with ovalbumin and BSA The learning outcomes of this project revolved around demonstrating the quantification capabilities of an in-line TRF spectroscopy method established at UCL in benchtop format.

This was achieved by characterising the fluorescence decay intensities of samples from the mAb biomanufacturing line and directly comparing the decay contributions of constituent species to the proportions obtained using HPLC-SEC (aggregates and fragments) and ELISA (HCP). Limits of detection and the proportionality between TRF spectroscopy and standard techniques. By establishing the achievable dynamic range and resolutions of our method, the next objective was to identify a route for scaling down the current bench-top set up into portable format. Objectives have involved the selection of optical components that would support this scale down and allow bioprocess samples to be measured in-line in real-time without formulation constraints.

9.2. Practical Application in Industry

From Table 8 (7.), it can be seen that in-line TRF-spectroscopy offers a plethora of business benefits compared to off-line HPLC-SEC. For off-line HPLC-SEC one is typically looking at running 40 samples per use of the column. Results quality is dependent upon the separation efficiency of the sec column which reduces over time and with impurity-rich samples. Column replacement can set a company back by thousands of dollars. Constraints on the samples that can be injected into the column limit vital bioprocess-specific information from being gained such as the effect of pH on CQAs. Over 10 hours of column preparation and pooling time per analytical run and regular column replacement are to be expected. For in-line TRF spectroscopy, as there is no need to spend time preparing a HPLC-SEC column, the frequency of measurements are user controlled, which can be automated to offer live fluorescence decay intensities. As all the measurements are performed in-line without bifurcating the feedstream, the contamination concerns for an off-line or on-line method are eliminated.

Comparing the results output of the two types of technology, we can see that UCL time-resolved fluorescence spectroscopy on the right provides us with information on the fluorescence decay contributions of the species within a mixture through decay associated chromatograms or DAC plots. As you can see the process is not dependent on waiting for each specie to elute according to its molecular weight, with UCL TRF performing the analysis in-line on a sample in a matter of minutes. UCL TRF also eliminates all of the limitations associated with using an SEC column, namely protein concentration, flow rate, and mobile phase, allowing you to directly assess the effect of any bioprocess stages on your protein specie distribution.

9.3. Validation Summary of TRF Spectroscopy

The results of this work demonstrate that positive correlations can be achieved between our in-line method and the current industrial standards of assessing product and process impurities. Specifically, correlation coefficients above 0.9

satisfy USP reference standards which have been achieved for monomer species at concentrations below that which are used in the mAb biomanufactring line. This research has identified that mAb aggregate and fragment species share very similar decay behaviour which allows them to be quantified together. Decay associated mAb and HCP quantities are positively proportional to ELISA-derived HCP quantities which would be indicative of residual HCP concentration in mAb samples – however, further tests are required to demonstrate this is not due signal artefacts.

9.4. Health and Safety

A vast number of reagents used in the purification of mAbs and clean in place protocols involve the use of hazardous materials. Protein assays often employ hazardous chemicals, as do certain HPLC-SEC mobile phases and maintenance procedures. These range from the corrosive to the irritating. The mAb product itself together with the impurity HCP and aggregate species are classed as immunogenic. Depending on the scales of production, workers may also be required to handle pressure extremes between manufacturing stages. Whilst maintaining personnel safety would fall under the tenet of GMP together with ensuring their adherence to regulations, industries have a duty to reduce the risk exposure of their personnel. Where risks cannot be eliminated, they are required to provide extensive training to reduce them as much as possible. Implementing PAT-based measurement devices can eliminate the regulatory requirements for manual sampling. Manual sampling practices not only expose workers to the product, but can also expose the product to the workers - potentially introducing contamination into the production line. In-line measurements can reduce these risks and centralise CQA and CPP assessment to one screen. As no off-line measurements are made, TRF spectroscopy can also reduce the need for analytical techniques that increase risks to personnel. In situ fluorescence spectroscopy measurements can be used in the verification of protein species. Since intrinsic fluorescence is affected by biochemical environments, this technique can also be used in the evaluation of bioprocess conditions such as the effect of elution pH on product recovery and the chemical environments that give rise to certain protein conformations. This can support the identification of optimal mobile phase compositions and the CPPs that control them for high product yields.

9.5. Environmental Sustainability

Single-use bioprocess components have their advantages in complying with ICH guidelines and GMPs surrounding product contamination avoidance. They also eliminate the need to opt for expensive component sterilisation procedures – which have regulatory requirements of their own. With its established production lines, low unit costs, reasonable durability and versatility, the vast majority of single-use items are made of plastic compounds. In many cases these are recyclable, however, due to contact and proximity with cellular material their classification as clinical waste renders them incinerator fodder. This contributes to company carbon dioxide footprints and plastic waste generation. Cell preparation for regular analysis requires the use of a number of plastic tubes, ELISA test kits and specially packed SEC columns. TRF spectroscopy has demonstrated capability for accurate in-line measurements that are proportional to HPLC-SEC and can therefore reduce laboratory plastic usage in off-line analytics. Achieving sufficient sample excitation with lower power settings is another area that has been explored. The business and regulatory advantages of eliminating product removal for analysis are very clear – given that product vials-worth of mAb need to be removed for pre-optimised repeat HPLC-SEC analytical runs.

9.6. Projected Impact

9.6.1. Improving Accessibility to A Broader Range of Therapeutic Options

The underlying goal for this project was to shine light on a path to producing mAbs, biosimilars, and other protein-based therapeutics with greater manufacturing efficiency. Analytical bottlenecks were identified in off-line techniques which limited the body of information that could be extracted from batch samples that had to undergo significant formulation changes, and added to production costs through instrumentation, materials, run-times and personnel. Whilst protein assays, MS, gel electrophoresis and SEC-based analytical methods have been established as industrial standards in CQA and CPP evaluation, their robust implementation often requires samples to be diluted in non-bioprocess specific buffers and solvents. The exposure of mAbs to the high shear forces, the artificial potential differences and the dilution steps for these techniques can intensify degradation pathways leading to CQA quantification that is not entirely accurate or representative of a particular bioprocess stage. Where dilutions had been applied, results would need to be scaled to the concentrations used in the bioprocess line adding to any measurement errors already built up in the analysis. Financial concerns and inadequate financial management in the National Health Service (NHS) regularly occupy news headlines. Whereas the NHS is, figuratively and literally, the lifeblood of those who do not have access to private medical care. The potential for cheaper mAb-based treatments can reduce financial burdens on already stretched health systems.

10. References

Aboulaich, N., Chung, W. K., Thompson, J. H., Larkin, C., Robbins, D., & Zhu, M. (2014). A novel approach to monitor clearance of host cell proteins associated with monoclonal antibodies. Biotechnology progress, 30(5), 1114–1124. https://doi.org/10.1002/btpr.1948

Adams, G. P., and Weiner, L. M. (2005). Monoclonal antibody therapy of cancer. Nature biotechnology, 23(9), 1147–1157. https://doi.org/10.1038/nbt1137

Agostini, C., Canonica, G. W., & Maggi, E. (2015). European medicines agency guideline for biological medicinal products: a further step for a safe use of biosimilars. Clinical and molecular allergy : CMA, 13(1), 3. https://doi.org/10.1186/s12948-015-0010-3

Ahn, W. S., Jeon, J. J., Jeong, Y. R., Lee, S. J., and Yoon, S. K. (2008). Effect of culture temperature on erythropoietin production and glycosylation in a perfusion culture of recombinant CHO cells. Biotechnology and bioengineering, 101(6), 1234–1244. https://doi.org/10.1002/bit.22006

Albani J. R. (2014). Origin of tryptophan fluorescence lifetimes part 1. Fluorescence lifetimes origin of tryptophan free in solution. Journal of fluorescence, 24(1), 93–104. https://doi.org/10.1007/s10895-013-1277-8

Alcala, J. R., Gratton, E., and Prendergast, F. G.. (1987). Interpretation of Fluorescence Decays in Proteins Using Continuous Lifetime Distributions. Biophysical Journal, 51:925-936.

Aleem, A., and Slenker, A. K. (2022). Monoclonal Antibody Therapy For High-Risk Coronavirus (COVID 19) Patients With Mild To Moderate Disease Presentations. In StatPearls. StatPearls Publishing.

Anthis, N. J., and Clore, G. M. (2013). Sequence-specific determination of protein and peptide concentrations by absorbance at 205 nm. Protein science : a publication of the Protein Society, 22(6), 851–858. https://doi.org/10.1002/pro.2253

Antonini, P. S., Hillen, W., Ettner, N., Hinrichs, W., Fantucci, P., Doglia, S. M., Bousquet, J. A., and Chabbert, M.. (1997). Role of Trp-187 in the annexinV–membrane interaction: a molecular mechanics analysis. Biophys J 72:1800–1811

Apanasovich, V.V. and Novikov, E.G.. (1990). Deconvolution method for fluorescence decays, Optics Communications, 78 (3–4): 279-282. ISSN 0030-4018. https://doi.org/10.1016/0030-4018(90)90361-V. (https://www.sciencedirect.com/science/article/pii/003040189090361V)

Arakawa, T., Ejima, D., Li, T., and Philo, J. S. (2010). The critical role of mobile phase composition in size exclusion chromatography of protein pharmaceuticals. Journal of pharmaceutical sciences, 99(4), 1674–1692. https://doi.org/10.1002/jps.21974

Axelsen, P. H. and Prendergast, F. G.. (1989). Molecular dynamics of tryptophan in ribonuclease. Biophys J. Biophysical Society, 56: 43-66.

Backhouse, C. M., Ball, P. R., Booth, S., Kelshaw, M. A., Potter, S. R., and McCollum, C. N. (1987). Particulate contaminants of intravenous medications and infusions. The Journal of pharmacy and pharmacology, 39(4), 241–245. https://doi.org/10.1111/j.2042-7158.1987.tb06260.x

Baeshen, M. N., Al-Hejin, A. M., Bora, R. S., Ahmed, M. M., Ramadan, H. A., Saini, K. S., Baeshen, N. A., and Redwan, E. M. (2015). Production of Biopharmaceuticals in E. coli: Current Scenario and Future Perspectives. Journal of microbiology and biotechnology, 25(7), 953–962. https://doi.org/10.4014/jmb.1412.12079

Bakeev, K. A.. (2010). Process analytical technology: Spectroscopic tools and implementation strategies for the chemical and pharmaceutical industries. New York, Wiley.

Baldo B. A. (2013). Adverse events to monoclonal antibodies used for cancer therapy: Focus on hypersensitivity responses. Oncoimmunology, 2(10), e26333. doi:10.4161/onci.26333.

Bandeira, V., Peixoto, C., Rodrigues, A. F., Cruz, P. E., Alves, P. M., Coroadinha, A. S., and Carrondo, M. J. (2012). Downstream processing of lentiviral vectors: releasing bottlenecks. Human gene therapy methods, 23(4), 255–263. https://doi.org/10.1089/hgtb.2012.059

Bängtsson, P., Estrada, E., Lacki, K., and Skoglar, H.. (2010). A method in a chromatography system. (International Patent No. WO2010151214A1) World Intellectual Property Organization, International Bureau. https://patentimages.storage.googleapis.com/9d/c6/28/773443b9008d82/WO2010151214A1.pdf

Barth, H.G., Saunders, G.D., and Majors, R.E. (2012). The State of the Art and Future Trends of Size-Exclusion Chromatography Packings and Columns. Lc Gc North America, 30.

Bee, J. S., Stevenson, J. L., Mehta, B., Svitel, J., Pollastrini, J., Platz, R., Freund, E., Carpenter, J. F., & Randolph, T. W. (2009). Response of a concentrated monoclonal antibody formulation to high shear. Biotechnology and bioengineering, 103(5), 936–943. https://doi.org/10.1002/bit.22336

Beer, C., Meyer, A., Müller, K., and Wirth, M. (2003). The temperature stability of mouse retroviruses depends on the cholesterol levels of viral lipid shell and cellular plasma membrane. Virology, 308(1), 137–146. https://doi.org/10.1016/s0042-6822(02)00087-9

Beesley, T. E., Buglio, B., and Scott, R. P. W.. (2001). Quantitative Chromatographic Analysis. Chromatographic Science Series, Volume 85, Marcel Dekker, USA.

Behring, E. and Kitasato, S.. (1890). Ueber das Zustandekommen der Diphtherie-Immunitat und der Tetanus-Immunitat bei thieren. Deutsche medizinsche Wochenschrift 16, 1113-1114.

Berkowitz, S. A., Engen, J. R., Mazzeo, J. R., and Jones, G. B. (2012). Analytical tools for characterizing biopharmaceuticals and the implications for biosimilars. Nature reviews. Drug discovery, 11(7), 527–540. https://doi.org/10.1038/nrd3746

Bilhorn, R. B., Sweedler, J. V., Epperson, P. M., and Denton, M.B.. (1987). Charge-transfer device detectors for analytical optical spectroscopy—operation and characteristics. Appl Spectrosc 41:1114–1124.

Bisschops, M,. Frick, L., Fulton, S., and Ransohoff, T.. (2009). Single-use, continuous-countercurrent, multicolumn chromatography. BioProcess International Conference. June. 18–23.

Blakesley, J. C., See, P., Shields, A. J., Kardynał, B. E., Atkinson, P., Farrer, I., and Ritchie, D. A. (2005). Efficient single photon detection by quantum dot resonant tunneling diodes. Physical review letters, 94(6), 067401. https://doi.org/10.1103/PhysRevLett.94.067401

Bluma, A., Höpfner, T., Lindner, P., Rehbock, C., Beutel, S., Riechers, D., Hitzmann, B., and Scheper, T. (2010). In-situ imaging sensors for bioprocess monitoring: state of the art. Analytical and bioanalytical chemistry, 398(6), 2429–2438. https://doi.org/10.1007/s00216-010-4181-y

Bosch, F., and Rosich, L. (2008). The contributions of Paul Ehrlich to pharmacology: a tribute on the occasion of the centenary of his Nobel Prize. Pharmacology, 82(3), 171–179. https://doi.org/10.1159/000149583.

Boulanger, B., Rozet, E., Moonen, F., Rudaz, S., & Hubert, P. (2009). A risk-based analysis of the AAPS conference report on quantitative bioanalytical methods validation and implementation. Journal of chromatography. B, Analytical technologies in the biomedical and life sciences, 877(23), 2235–2243. https://doi.org/10.1016/j.jchromb.2009.06.019

Bracewell DG, Smith V, Delahaye M, Smales CM. Analytics of host cell proteins (HCPs): lessons from biopharmaceutical mAb analysis for Gene therapy products. Curr Opin Biotechnol. 2021 Oct;71:98-104. doi: 10.1016/j.copbio.2021.06.026. Epub 2021 Jul 24. PMID: 34311150.

Brannon-Pepas, L. (1993). Drug, device and diagnostic manufacturing, the ultimate resource handbook: Carol DeSain, Second Edn, 1993. Interpharm Press, Buffalo Grove, IL, 429 pages, $ 139.00. Journal of Controlled Release, 26, 240.

Brestrich, N., Briskot, T., Osberghaus, A., and Hubbuch, J.. (2014). A tool for selective inline quantification of co-eluting proteins in chromatography using spectral analysis and partial least squares regression. Biotechnology Bioengineering, 111:1365–1373.

Brestrich, N., Sanden, A., Kraft, A., McCann, K., Bertolini, J., and Hubbuch, J.. (2015). Advances in inline quantification of co-eluting proteins in chromatography: Process-data-based model calibration and application towards real-life separation issues. Biotechnology Bioengineering, 112:1406–1416.

Brestrich N., Rüedt M., Buechler D., and Hubbuch J.. (2018). Selective protein quantification for preparative chromatography using variable pathlength UV/VIS spectroscopy and partial least squares regression. Chem Eng Sci, 176:157–164. doi: 10.1016/j.ces.2017.10.030.

Bucciantini, M., Giannoni, E., Chiti, F., Baroni, F., Formigli, L., Zurdo, J., Taddei, N., Ramponi, G., Dobson, C. M., and Stefani, M. (2002). Inherent toxicity of aggregates implies a common mechanism for protein misfolding diseases. Nature, 416(6880), 507–511. https://doi.org/10.1038/416507a

Burnet, M. (1957). Cancer; a biological approach. I. The processes of control. British medical journal, 1(5022), 779–786. https://doi.org/10.1136/bmj.1.5022.779

Buss, N. A., Henderson, S. J., McFarlane, M., Shenton, J. M., and de Haan, L. (2012). Monoclonal antibody therapeutics: history and future. Current opinion in pharmacology, 12(5), 615–622. https://doi.org/10.1016/j.coph.2012.08.001

Busse, A., & Lüftner, D. (2019). What Does the Pipeline Promise about Upcoming Biosimilar Antibodies in Oncology?. Breast care (Basel, Switzerland), 14(1), 10–16. https://doi.org/10.1159/000496834

Carvalho, L. S. , Silva, O. B. d. , deAlmeida, G. C. , de Oliveira, J. D. , and Carmo, N. S. P. a. S. (2017). Production Processes for Monoclonal Antibodies. In (Ed.), Fermentation Processes. IntechOpen. https://doi.org/10.5772/64263

Champion, K., Nishihara, J. C., Joly, J. C., and Arnott, D.. (2001). Similarity of the Escherichia coli proteome upon completion of different biopharmaceutical fermentation process. Proteomics 1:1133–1148.

Chan, L. A., Phillips, M. L., Wims, L. A., Trinh, K. R., Denham, J., and Morrison, S. L. (2004). Variable region domain exchange in human IgGs promotes antibody complex formation with accompanying structural changes and altered effector functions. Molecular immunology, 41(5), 527–538. https://doi.org/10.1016/j.molimm.2004.03.034

Chang, M.C., Petrich, J.W., McDonald, D.B., & Fleming, G.R. (1983). Nonexponential Fluorescence Decay of Tryptophan, Tryptophylglycine, and Glycyltryptophan. Journal of the American Chemical Society, 105, 3819-3824.

Chartrain, M., and Chu, L. (2008). Development and production of commercial therapeutic monoclonal antibodies in Mammalian cell expression systems: an overview of the current upstream technologies. Current pharmaceutical biotechnology, 9(6), 447–467. https://doi.org/10.2174/138920108786786367

Chase, H.A. (1986). Rapid chromatographic monitoring of bioprocesses. Biosensors, 2 5, 269-86 .

Chen, B., Bautista, R., Yu, K., Zapata, G. A., Mulkerrin, M. G., and Chamow, S. M. (2003). Influence of histidine on the stability and physical properties of a fully human antibody in aqueous and solid forms. Pharmaceutical research, 20(12), 1952–1960. https://doi.org/10.1023/b:pham.0000008042.15988.c0

Chiang, G. G., and Sisk, W. P. (2005). Bcl-x(L) mediates increased production of humanized monoclonal antibodies in Chinese hamster ovary cells. Biotechnology and bioengineering, 91(7), 779–792. https://doi.org/10.1002/bit.20551

Claßen, J., Aupert, F., Reardon, K. F., Solle, D., and Scheper, T. (2017). Spectroscopic sensors for inline bioprocess monitoring in research and pharmaceutical industrial application. Analytical and bioanalytical chemistry, 409(3), 651–666. https://doi.org/10.1007/s00216-016-0068-x

Claßen, J., Graf, A., Aupert, F., Solle, D., Höhse, M., and Scheper, T. (2019). A novel LED-based 2D-fluorescence spectroscopy system for inline bioprocess monitoring of Chinese hamster ovary cell cultivations-Part II. Engineering in life sciences, 19(5), 341–351. https://doi.org/10.1002/elsc.201800146

Clegg, I.. (2020). Chapter 7 - Process analytical technology, Editor(s): Riley, C. M., Rosanske, T. W., and Reid, G.. Specification of Drug Substances and Products (Second Edition), Elsevier, pp. 149-173, ISBN 9780081028247, https://doi.org/10.1016/B978-0-08-102824-7.00007-5.

Cleland, J. L., Lam, X., Kendrick, B., Yang, J., Yang, T. H., Overcashier, D., Brooks, D., Hsu, C., and Carpenter, J. F. (2001). A specific molar ratio of stabilizer to protein is required for storage stability of a lyophilized monoclonal antibody. Journal of pharmaceutical sciences, 90(3), 310–321. https://doi.org/10.1002/1520-6017(200103)90:3<310::aid-jps6>3.0.co;2-r

Cohen, A. E., and Moerner, W. E. (2008). Controlling Brownian motion of single protein molecules and single fluorophores in aqueous buffer. Optics express, 16(10), 6941–6956. https://doi.org/10.1364/oe.16.006941

Córdoba-Rodríguez, R. V.. (2008). Aggregates in mAb and recombinant therapeutic proteins: A regulatory perspective FDA perspectives on speci-fications and effective control strategies. Biopharm Int 21(11):44–53.

Cornetta, K., Matheson, L., and Ballas, C. (2005). Retroviral vector production in the National Gene Vector Laboratory at Indiana University. Gene therapy, 12 Suppl 1, S28–S35. https://doi.org/10.1038/sj.gt.3302613

Coroadinha, A. S., Silva, A. C., Pires, E., Coelho, A., Alves, P. M., and Carrondo, M. J. (2006). Effect of osmotic pressure on the production of retroviral vectors: Enhancement in vector stability. Biotechnology and bioengineering, 94(2), 322–329. https://doi.org/10.1002/bit.20847

Davis, S. P., Abrams, M. C., and Brault, J. W.. (2001). Fourier Transform Spectrometry. Academic Press.

Debaene, F., Wagner-Rousset, E., Colas, O., Ayoub, D., Corvaïa, N., Van Dorsselaer, A., Beck, A., and Cianférani, S. (2013). Time-resolved native ion-mobility mass spectrometry to monitor dynamics of IgG4 Fab arm exchange and "bispecific" monoclonal antibody formation. Analytical chemistry, 85(20), 9785–9792. https://doi.org/10.1021/ac402237v

Demas, J.N. (1983). Excited State Lifetime Measurements.

den Engelsman, J., Garidel, P., Smulders, R., Koll, H., Smith, B., Bassarab, S., Seidl, A., Hainzl, O., & Jiskoot, W. (2011). Strategies for the assessment of protein aggregates in pharmaceutical biotech product development. Pharmaceutical research, 28(4), 920–933. https://doi.org/10.1007/s11095-010-0297-1

Diress, A., Lorbetskie, B., Larocque, L., Li, X., Alteen, M., Isbrucker, R., and Girard, M. (2010). Study of aggregation, denaturation and reduction of interferon alpha-2 products by size-exclusion high-performance liquid chromatography with fluorescence detection and biological assays. Journal of chromatography. A, 1217(19), 3297–3306. https://doi.org/10.1016/j.chroma.2009.10.081

Djikanović, D., Kalauzi, A., Jeremić, M., Mićić, M., and Radotić, K.. (2007). Deconvolution of fluorescence spectra: Contribution to the structural analysis of complex molecules, Colloids and Surfaces B: Biointerfaces, 54 (2): 188-192, ISSN 0927-7765. https://doi.org/10.1016/j.colsurfb.2006.10.015.(https://www.sciencedirect.com/science/article/pii/S0927776506003365)

Dorris, G. G., Bivins, B. A., Rapp, R. P., Weiss, D. L., DeLuca, P. P., and Ravin, M. B. (1977). Inflammatory potential of foreign particulates in parenteral drugs. Anesthesia and analgesia, 56(3), 422–428. https://doi.org/10.1213/00000539-197705000-00022

Duvergé, A., and Negroni, M. (2020). Pseudotyping Lentiviral Vectors: When the Clothes Make the Virus. Viruses, 12(11), 1311. https://doi.org/10.3390/v12111311

Ecker, D.M., Jones, S.D., and Levine, H.L.. (2015). The therapeutic monoclonal antibody market. MAbs 7, 9–14. https://doi.org/10.4161/19420862.2015.989042

Edelman, G. M., Benacerraf, B., Ovary, Z., and Poulik, M. D. (1961). Structural differences among antibodies of different specificities. Proceedings of the National Academy of Sciences of the United States of America, 47(11), 1751–1758. https://doi.org/10.1073/pnas.47.11.1751

Ehrenberg, M. and Rigler. R.. (1974). Rotational Brownian motion and fluorescence intensity fluctuation. Chem. Phys., 4: 390-401

Elson, E. L. and Magde, D.. (1974). Fluorescence correlation spectroscopy. I. Conceptual basis and theory. Biopolymers, 13: 1-27

Engelhardt, H., and Ahr, G.. (1983). Optimization of efficiency in size-exclusion chromatography, Journal of Chromatography A, 282: 385-397, ISSN 0021-9673. https://doi.org/10.1016/S0021-9673(00)91616-9. (https://www.sciencedirect.com/science/article/pii/S0021967300916169)

Engvall E. (2010). The ELISA, enzyme-linked immunosorbent assay. Clinical chemistry, 56(2), 319–320. https://doi.org/10.1373/clinchem.2009.127803

Engvall, E., and Perlmann, P.. (1971). Enzyme-linked immunosorbent assay (ELISA). Quantitative assay of immunoglobulin G. Immunochemistry, 8(9), 871–874. https://doi.org/10.1016/0019-2791(71)90454-x

Epperson PM, Denton MB. 1989. Binding spectral images in a charge-coupled device. Anal Chem 61:1513–1519.

Erickson, B. E.. (2010). Untangling biosimilars. Chem Eng News, 88:25–27.

Eriksson, L., Johansson, E., Kettaneh-Wold, N., Trygg, J., Wikström, C., and Wold, S.. (2006). Multi-and megavariate data analysis. Umeå: Umetrics Academy.

Faassen, S. M., and Hitzmann, B. (2015). Fluorescence spectroscopy and chemometric modeling for bioprocess monitoring. Sensors (Basel, Switzerland), 15(5), 10271–10291. https://doi.org/10.3390/s150510271

Fagraeus, A. (1948). Antibody Production in relation to the Development of Plasma Cells. In vivo and in vitro Experiments. Acta Medica Scandinavica, 130.

Fahrner, R. L. and Blank ,G. S.. (1999a). Real-time control of antibody loading during protein A affinity chromatography using an on-line assay. J Chromatogr A 849:191–196.

Fahrner, R. L. and Blank ,G. S.. (1999b). Real-time monitoring of recombinant antibody break-through during protein A affinity chromatography. Biotechnol Appl Biochem 29:109–112.

FDA. (1991). US FDA Office of Compliance. Guideline on the Preparation of Investigational New Drug Products (Human and Animal). FDA, Rockville, USA.

FDA. (2004). Guidance for industry, PAT-A framework for innovative pharmaceutical development, manufacturing and quality assurance. http://www.fda. gov/cder/guidance/published.html.

FDA. (2006a). US Food and Drug Administration. Guidance for industry: Q8 pharmaceutical development, US Department of Health and Human Service. Rockville, MD, May 2006.

FDA. (2006b). US Food and Drug Administration. Guidance for industry: Q9 quality risk management, US Department of Health and Human Service. Rockville, MD, June 2006.

FDA, Office of Biotechnology Products. (2008). Notice of pilot program for submission of quality information for biotechnology products in the Office of Biotechnology Products, Food and Drug Administration, docket number FDA-2008-N-03551 (FDA, Washington, DC, 2008) http://www.fda.gov/OHRMS/DOCKETS/98fr/FDA-2008-N-0355-n.pdf

FDA. (2009). Guidance for Industry: Q8(R2) Pharmaceutical Development, U.S. Department of Health and Human Services and Food and Drug Administration, Silver Spring, Maryland.

FDA. (2011). Advancing regulatory science at FDA – A strategic plan. August. Available from: http://www.fda.gov/regulatoryscience

FDA. (2016). Advanced Manufacturing: A Snapshot of Priority Technical Areas Across the Federal Government" by the National Science and Technology Council, US Government. Published online: https://www.whitehouse.gov/sites/whitehouse.gov/files/images/Blog/NSTC%20SAM%20technology%20areas%20snapshot.pdf (retrieved August 2019)

Fekete, S., Beck, A., Veuthey, J. L., and Guillarme, D. (2014). Theory and practice of size exclusion chromatography for the analysis of protein aggregates. Journal of pharmaceutical and biomedical analysis, 101, 161–173. https://doi.org/10.1016/j.jpba.2014.04.011

Fekete, S., Ganzler, K., and Guillarme, D. (2013). Critical evaluation of fast size exclusion chromatographic separations of protein aggregates, applying sub-2 μm particles. Journal of pharmaceutical and biomedical analysis, 78-79, 141–149. https://doi.org/10.1016/j.jpba.2013.02.013

Finkelshtein, D., Werman, A., Novick, D., Barak, S., and Rubinstein, M. (2013). LDL receptor and its family members serve as the cellular receptors for vesicular stomatitis virus. Proceedings of the National Academy of Sciences of the United States of America, 110(18), 7306–7311. https://doi.org/10.1073/pnas.1214441110

Fogolín, M. B., Wagner, R., Etcheverrigaray, M., and Kratje, R. (2004). Impact of temperature reduction and expression of yeast pyruvate carboxylase on hGM-CSF-producing CHO cells. Journal of biotechnology, 109(1-2), 179–191. https://doi.org/10.1016/j.jbiotec.2003.10.035

Foltz, I. N., Karow, M., and Wasserman, S. M.. (2013). Evolution and Emergence of Therapeutic Monoclonal Antibodies. Circulation. 127, 2222-2230

Fraunhofer, W., and Winter, G. (2004). The use of asymmetrical flow field-flow fractionation in pharmaceutics and biopharmaceutics. European journal of pharmaceutics and biopharmaceutics : official journal of Arbeitsgemeinschaft fur Pharmazeutische Verfahrenstechnik e.V, 58(2), 369–383. https://doi.org/10.1016/j.ejpb.2004.03.034

Fussenegger, M., Schlatter, S., Dätwyler, D., Mazur, X., and Bailey, J. E. (1998). Controlled proliferation by multigene metabolic engineering enhances the productivity of Chinese hamster ovary cells. Nature biotechnology, 16(5), 468–472. https://doi.org/10.1038/nbt0598-468

Gagnon P.. (2012). Technology trends in antibody purification. Journal of Chromatography A, 1221: 57–70. doi: 10.1016/j.chroma.2011.10.034

Galan, P.. (2022). PIS-correction-based control system implementation. Control Engineering. Online article April 12, 2022, available from: https://www.controleng.com/articles/pid-correction-based-control-system-implementation/

Gan, S. D., and Patel, K. R. (2013). Enzyme immunoassay and enzyme-linked immunosorbent assay. The Journal of investigative dermatology, 133(9), e12. https://doi.org/10.1038/jid.2013.287

Gao, S. X., Zhang, Y., Stansberry-Perkins, K., Buko, A., Bai, S., Nguyen, V. and Brader, M. L.. (2010). Fragmentation of a Highly Purified Monoclonal AntibodyAttributed to Residual CHO Cell Protease Activity. Communication to the editor.. Biotechnology and Bioengingeering. Vol. 108, No. 4, Wiley Periodicals Inc..

Georghiou, S., Nordlund, T. M. and Saim, A. M.. (1985). Picosecond fluorescence decay time measurements of nucleic acids at room temperature in aqueous solution. Photochem. Photobiol., 41: 209-212

Ghose, S., Tao, Y., Conley, L., & Cecchini, D. (2013). Purification of monoclonal antibodies by hydrophobic interaction chromatography under no-salt conditions. mAbs, 5(5), 795–800. https://doi.org/10.4161/mabs.25552

Ghosh Dastidar, M., Thekkooden, I., Nayak, P. K., and Praveen Bhallamudi, V. (2022). Quantum emitters and detectors based on 2D van der Waals materials. Nanoscale, 14(14), 5289–5313. https://doi.org/10.1039/d1nr08193d

Gibson, S. J., van Kasteren, B., Tekcan, B., Cui, Y., van Dam, D., Haverkort, J., Bakkers, E., and Reimer, M. E. (2019). Tapered InP nanowire arrays for efficient broadband high-speed single-photon detection. Nature nanotechnology, 14(5), 473–479. https://doi.org/10.1038/s41565-019-0393-2

Gillespie, C., Holstein, M., Mullin, L., Cotoni, K., Tuccelli, R., Caulmare, J., and Greenhalgh, P. (2019). Continuous Inline Virus Inactivation for Next Generation Bioprocessing. Biotechnology journal, 14(2), e1700718. https://doi.org/10.1002/biot.201700718

Golovchenko, N. P., Kataeva, I. A., and Akimenko, V. K. (1992). Analysis of pH-dependent protein interactions with gel filtration medium. Journal of chromatography, 591(1-2), 121–128. https://doi.org/10.1016/0021-9673(92)80229-n

Gomme, P. T., Hunt, B. M., Tatford, O. C., Johnston, A., and Bertolini, J. (2006a). Effect of lobe pumping on human albumin: investigating the underlying mechanisms of aggregate formation. Biotechnology and applied biochemistry, 43(Pt 2), 103–111. https://doi.org/10.1042/BA20050147

Gomme, P. T., Prakash, M., Hunt, B., Stokes, N., Cleary, P., Tatford, O. C., and Bertolini, J. (2006b). Effect of lobe pumping on human albumin: development of a lobe pump simulator using smoothed particle hydrodynamics. Biotechnology and applied biochemistry, 43(Pt 2), 113–120. https://doi.org/10.1042/BA20050188

Grabski, A., and Mierendorf, R.. (2009). Simulating moving bed chromatography: Semba's SMBC system attacks the bottlenecks created by upstream protein increase. Genet Eng Biotechnol News 29(18): http://www.genengnews.com/gen-articles/simulated-moving-bed-chromatography/3076/

Graf, A., Claßen, J., Solle, D., Hitzmann, B., Rebner, K., Hoehse, M.. (2019). A novel LED-based 2D-fluorescence spectroscopy system for inline monitoring of Chinese hamster ovary cell cultivations – Part I. Engineering Life Sciences, 19: 352– 362. https://doi.org/10.1002/elsc.201800149

Grav, L. M., la Cour Karottki, K. J., Lee, J. S., and Kildegaard, H. F. (2017). Application of CRISPR/Cas9 Genome Editing to Improve Recombinant Protein Production in CHO Cells. Methods in molecular biology (Clifton, N.J.), 1603, 101–118. https://doi.org/10.1007/978-1-4939-6972-2_7

Grebe M ., Rüssmann M., Leyh M., Franke M. R.. (2018). Digital maturity is paying off, Boston Consulting Group.

Grilo A. L. and Mantalaris A.. (2019). The increasingly human and profitable monoclonal antibody market. Trends Biotechnology, 37(1): 9–16. doi: 10.1016/j.tibtech.2018.05.014.

Grinvald, A., and Steinberg, I. Z. (1974). On the analysis of fluorescence decay kinetics by the method of least-squares. Analytical biochemistry, 59(2), 583–598. https://doi.org/10.1016/0003-2697(74)90312-1

Grinvald, A., and Steinberg, I. Z. (1976). The fluorescence decay of tryptophan residues in native and denatured proteins. Biochimica et biophysica acta, 427(2), 663–678. https://doi.org/10.1016/0005-2795(76)90210-5

Grossweiner, L. I., and Usui, Y. (1971). Flash photolysis and inactivation of aqueous lysozyme. Photochemistry and photobiology, 13(3), 195–214. https://doi.org/10.1111/j.1751-1097.1971.tb06106.x

Guiochon G, Beaver LA. 2011. Separation science is the key to successful biopharmaceuticals. J Chromatogr A 1218: 8836– 8858.

Gupta, M.. editor. (2002). Methods for affinity-based separations of enzymes and proteins. Basel, Switzerland: Birkhäuser Basel.

Hahn, R., Shimahara, K., Steindl, F., and Jungbauer, A.. (2006). Comparison of protein A affinity sorbents III. Life time study. J Chromatogr A 1102:224–231.

Hales, J. E., Matmon, G., Dalby, P. A., Ward, J. M., and Aeppli, G. (2019). Virus lasers for biological detection. Nature communications, 10(1), 3594. https://doi.org/10.1038/s41467-019-11604-z

Hales, J. E., Aoudjane, S., Aeppli, G., and Dalby, P. A. (2021). Proof-of-concept analytical instrument for label-free optical deconvolution of protein species in a mixture. Journal of chromatography. A, 1641, 461968. https://doi.org/10.1016/j.chroma.2021.461968

Hogwood, C. E., Bracewell, D. G., and Smales, C. M. (2014). Measurement and control of host cell proteins (HCPs) in CHO cell bioprocesses. Current opinion in biotechnology, 30, 153–160. https://doi.org/10.1016/j.copbio.2014.06.017

Hamamatsu. (2020). Photosensor amplifiers, Photodiode modules, Technical note. December 2020. Hamamatsu Photonics K. K., Solid State Division, Hamamatsu City, 435-8558 Japan.

Hamamatsu. (2022a). Si photodiodes, Lineup for near infrared to ultraviolet and ven to high-energy. May 2022 Selection guide, Hamamatsu Photonics K. K., Solid State Division, Hamamatsu City, 435-8558 Japan.

Hamamatsu. (2022b). Si photodiodes, Technical note. May 2022.

Hansen, S. K., Jamali, B., and Hubbuch, J. (2013). Selective high throughput protein quantification based on UV absorption spectra. Biotechnology and bioengineering, 110(2), 448–460. https://doi.org/10.1002/bit.24712

Hantelmann, K., Kollecker, M., Hüll, D., Hitzmann, B., and Scheper, T. (2006). Two-dimensional fluorescence spectroscopy: a novel approach for controlling fed-batch cultivations. Journal of biotechnology, 121(3), 410–417. https://doi.org/10.1016/j.jbiotec.2005.07.016

Han, Z. W., Song, K. F., Zhang, H. J., Yu, M., He, L. P., Guo, Q. F., Wang, X., Liu, Y., and Chen, B. (2020). Photon Counting Imaging with Low Noise and a Wide Dynamic Range for Aurora Observations. Sensors (Basel, Switzerland), 20(20), 5958. https://doi.org/10.3390/s20205958

Harrison, J. S., Gill, A., and Hoare, M. (1998). Stability of a single-chain Fv antibody fragment when exposed to a high shear environment combined with air-liquid interfaces. Biotechnology and bioengineering, 59(4), 517–519. https://doi.org/10.1002/(sici)1097-0290(19980820)59:4<517::aid-bit15>3.0.co;2-6

Harrison, Todd, P., Rudge, S. R., & Petrides, D. P. (2020). Bioseparations science and engineering / Roger G. Harrison, Paul W. Todd, Scott R. Rudge, and Demetri P. Petrides. (Second edition.). Oxford University Press.

Hart, R., Herring, A., Howell, G. P., McKeever-Abbas, B., Pedge, N., and Woodward, R.. (2015). Real-Time Monitoring and Control of Critical Process Impurities during the Manufacture of Fostamatinib Disodium. Org. Process Res. Dev., 19 (4), pp. 537-542, 10.1021/acs.oprd.5b00008

Hart S. J. and JiJi R. D.. (2002). Light emitting diode excitation emission matrix fluorescence spectroscopy. Analyst 127:1643–1699.

Hawe, A., Kasper, J. C., Friess, W., and Jiskoot, W. (2009). Structural properties of monoclonal antibody aggregates induced by freeze-thawing and thermal stress. European journal of pharmaceutical sciences : official journal of the European Federation for Pharmaceutical Sciences, 38(2), 79–87. https://doi.org/10.1016/j.ejps.2009.06.001

Hermeling, S., Crommelin, D. J., Schellekens, H., and Jiskoot, W. (2004). Structure-immunogenicity relationships of therapeutic proteins. Pharmaceutical research, 21(6), 897–903. https://doi.org/10.1023/b:pham.0000029275.41323.a6

Hersher R. (2012). Small biotechs raring to cash in on the orphan disease market. Nature medicine, 18(3), 330–331. https://doi.org/10.1038/nm0312-330

Higashikawa, F., and Chang, L. (2001). Kinetic analyses of stability of simple and complex retroviral vectors. Virology, 280(1), 124–131. https://doi.org/10.1006/viro.2000.0743

Hiraoka, Y., Sedat, J. W., Agard, D. A.. (1987). The use of a charge-coupled device for quantitative optical microscopy of biological structures. Science 238:36–41.

Hislop, J. N., Islam, T. A., Eleftheriadou, I., Carpentier, D. C., Trabalza, A., Parkinson, M., Schiavo, G., and Mazarakis, N. D. (2014). Rabies virus envelope glycoprotein targets lentiviral vectors to the axonal retrograde pathway in motor neurons. The Journal of biological chemistry, 289(23), 16148–16163. https://doi.org/10.1074/jbc.M114.549980

Hmiel, L., Brorson, K., and Boyne, M.. (2015). Post-translational structural modifications of immunoglobulin G and their effect on biological activity. Analytical and Bioanalytical Chemistry. 407, (1), 79-94.

Hong, M. S., Severson, K. A., Jiang, M., Lu, A. E., Love, J. C., and Braatz, R. D.. (2018). Challenges and opportunities in biopharmaceutical manufacturing control, Computers and Chemical Engineering, 110: 106-114. ISSN 0098-1354. https://doi.org/10.1016/j.compchemeng.2017.12.007. (https://www.sciencedirect.com/science/article/pii/S0098135417304374)

Hong, P., Koza, S., and Bouvier, E. S. (2012). Size-Exclusion Chromatography for the Analysis of Protein Biotherapeutics and their Aggregates. Journal of liquid chromatography and related technologies, 35(20), 2923–2950. https://doi.org/10.1080/10826076.2012.743724

Horowitz, B., Lazo, A., Grossberg, H., Page, G., Lippin, A., and Swan, G.. (1998). Virus inactivation by solvent/detergent treatment and the manufacture of SD-plasma. Vox Sang 74 (Suppl 1):203–206

Igne, B., Drennen III, J. K., and Anderson, C. A.. (2014). Improving near-infrared prediction model robustness with support vector machine regression: a pharmaceutical tablet assay example. Soc Appl Spectrosc, 68 (12): 1348-1356

Inbar, D., Hochman, J., and Givol, D. (1972). Localization of antibody-combining sites within the variable portions of heavy and light chains. Proceedings of the National Academy of Sciences of the United States of America, 69(9), 2659–2662. https://doi.org/10.1073/pnas.69.9.2659

Jagschies, G., and Lacki, K.. (2010). Manufacturing solutions with potential to unlock existing facilities for future production. ACS-BIOT National Meeting. San Francisco, CA, March.

Jawa, V., Joubert, M. K., Zhang, Q., Deshpande, M., Hapuarachchi, S., Hall, M. P., and Flynn, G. C.. (2016). Evaluating Immunogenicity Risk Due to Host Cell Protein Impurities in Antibody-Based Biotherapeutics. AAPS J; 18(6):1439-1452. doi: 10.1208/s12248-016-9948-4. PMID: 27450229.

Jiang, C., Liu, J., Rubacha, M., and Shukla, A. A.. (2009). A mechanistic study of protein A chro-matography resin lifetime. J Chromatogr A 1216:5849–5855.

Jones M, Palackal N, Wang F, Gaza-Bulseco G, Hurkmans K, Zhao Y, Chitikila C, Clavier S, Liu S, Menesale E, Schonenbach NS, Sharma S, Valax P, Waerner T, Zhang L, Connolly T. "High-risk" host cell proteins (HCPs): A multi-company collaborative view. Biotechnol Bioeng. 2021 Aug;118(8):2870-2885. doi: 10.1002/bit.27808. Epub 2021 May 31. PMID: 33930190.

Kaer, K., Mätlik, K., Metsis, M., and Speek, M. (2008). Combination of native and denaturing PAGE for the detection of protein binding regions in long fragments of genomic DNA. BMC genomics, 9, 272. https://doi.org/10.1186/1471-2164-9-272

Kelley B.. (2009). Industrialization of mAb production technology: the bioprocessing industry at a crossroad. MAbs, 1: 443-452

Khidir, A. L. and Decius, J. C.. (1962). Numerical methods for the correction of apparent band shapes due to finite slit width, Spectrochimica Acta, 18, 12:

1629-1639. ISSN 0371-1951, https://doi.org/10.1016/0371-1951(62)80027-7. (https://www.sciencedirect.com/science/article/pii/0371195162800277)

Khoo, H. T., and Leow, C. H. (2021). Advancements in the preparation and application of monolithic silica columns for efficient separation in liquid chromatography. Talanta, 224, 121777. https://doi.org/10.1016/j.talanta.2020.121777

Kiese, S., Pappenberger, A., Friess, W., and Mahler, H. C.. (2008). Shaken, not stirred: Mechanical stress testing of an IgG1 antibody. J Pharm Sci 97(10):4347–4366.

Kim, J. Y., Kim, Y. G., and Lee, G. M. (2012). CHO cells in biotechnology for production of recombinant proteins: current state and further potential. Applied microbiology and biotechnology, 93(3), 917–930. https://doi.org/10.1007/s00253-011-3758-5

Knight, A.W., and Selinger, B.K. (1971). The deconvolution of fluorescence decay curves: A non-method for real data. Spectrochimica Acta Part A: Molecular and Biomolecular Spectroscopy, 27, 1223-1234.

Köhler, G., and Milstein, C. (1975). Continuous cultures of fused cells secreting antibody of predefined specificity. Nature, 256(5517), 495–497. https://doi.org/10.1038/256495a0

Kolata, G. (2016). Gene Therapy Hits a Peculiar Roadblock: A Virus Shortage. The New York Times.

Kolouch, F. (1938). Origin of Bone Marrow Plasma Cell Associated with Allergic and Immune States in the Rabbit. Proceedings of the Society for Experimental Biology and Medicine, 39, 147 - 148.

Kondragunta, B., Drew, J. L., Brorson, K. A., Moreira, A. R., and Rao, G.. (2010). Advances in clone selection using high-throughput bioreactors. Biotechnology Progress. 26, (4), 1095-1103

Konstantinov, K. B. and Cooney, C. L.. (2015). White paper on continuous bioprocessing may 20-21, 2014 continuous manufacturing symposium. J. Pharm. Sci., 104: 813-820.

Konstantinov, K., Goudar, C., Ng, M., Meneses, R., Thrift, J., Chuppa, S., Matanguihan, C., Michaels, J., and Naveh, D. (2006). The "push-to-low" approach for optimization of high-density perfusion cultures of animal cells. Advances in biochemical engineering/biotechnology, 101, 75–98. https://doi.org/10.1007/10_016

Kopaciewicz, W., and Regnier, F. E. (1982). Nonideal size-exclusion chromatography of proteins: effects of pH at low ionic strength. Analytical biochemistry, 126(1), 8–16. https://doi.org/10.1016/0003-2697(82)90102-6

Kornecki, M., Mestmäcker, F., Zobel-Roos, S., Heikaus de Figueiredo, L., Schlüter, H., and Strube, J. (2017). Host Cell Proteins in Biologics Manufacturing: The Good, the Bad, and the Ugly. Antibodies (Basel, Switzerland), 6(3), 13. https://doi.org/10.3390/antib6030013

Kowolik, C. M., and Yee, J. K. (2002). Preferential transduction of human hepatocytes with lentiviral vectors pseudotyped by Sendai virus F protein. Molecular therapy : the journal of the American Society of Gene Therapy, 5(6), 762–769. https://doi.org/10.1006/mthe.2002.0603

Krawitz, D. C., Forrest, W., Moreno, G. T., Kittleson, J., and Champion, K. M. (2006). Proteomic studies support the use of multi-product immunoassays to monitor host cell protein impurities. Proteomics, 6(1), 94–110. https://doi.org/10.1002/pmic.200500225

Kroon, D. J., Baldwin-Ferro, A., and Lalan, P. (1992). Identification of sites of degradation in a therapeutic monoclonal antibody by peptide mapping. Pharmaceutical research, 9(11), 1386–1393. https://doi.org/10.1023/a:1015894409623

Kükrer, B., Filipe, V., van Duijn, E., Kasper, P. T., Vreeken, R. J., Heck, A. J., and Jiskoot, W. (2010). Mass spectrometric analysis of intact human monoclonal antibody aggregates fractionated by size-exclusion chromatography. Pharmaceutical research, 27(10), 2197–2204. https://doi.org/10.1007/s11095-010-0224-5

Kumru, O. S., Wang, Y., Gombotz, C., Kelley-Clarke, B., Cieplak, W., Kim, T., Joshi, S. B., and Volkin, D. B. (2018). Physical Characterization and Stabilization of a Lentiviral Vector Against Adsorption and Freeze-Thaw. Journal of pharmaceutical sciences, 107(11), 2764–2774. https://doi.org/10.1016/j.xphs.2018.07.010

Kunert, R., and Reinhart, D. (2016). Advances in recombinant antibody manufacturing. Applied microbiology and biotechnology, 100(8), 3451–3461. https://doi.org/10.1007/s00253-016-7388-9

Kuszaj, S., Kaszycki, P., and Wasylewski, Z. (1999). Fluorescence and phosphorescence study of Tet repressor-operator interaction. Journal of protein chemistry, 18(2), 147–156. https://doi.org/10.1023/a:1020615703727

Ladisch, M.R. (2001). Bioseparations Engineering: Principles, Practice, and Economics.

Lakowicz, J. R.. (2006). Principles of Fluorescence Spectroscopy (3rd ed.), Kluwer Academic, Baltimore.

Lanczsos, C.. (1956). Applied Analysis, p. 272, Prentiw-Hall, Enandwood Cliffs, NJ.

Landgraf, S.. (2004). Use of ultrabright LEDs for the determination of static and time-resolved fluorescence information of liquid and solid crude oil samples. J Biochem Biophys Methods 61:125–134.

Leavy O. (2010). Therapeutic antibodies: past, present and future. Nature reviews. Immunology, 10(5), 297. https://doi.org/10.1038/nri2763

Lee, H. J., Lee, C. M., Kim, K., Yoo, J. M., Kang, S-m., Ha, G-s., Park, M. K., Choi, M-A., Seong, B. L., and Lee, D. E.. (2018).Purification of antibody fragments for the reduction of charge variants using cation exchange chromatography, Journal of Chromatography B, 1080: 20-26, ISSN 1570-0232. https://doi.org/10.1016/j.jchromb.2018.01.030.

Lee, J., Kim, S. H., Se, T., and Kim, D. (2022). Characterization of Noise in a Single-Molecule Fluorescence Signal. The journal of physical chemistry. B, 126(6), 1160–1167. https://doi.org/10.1021/acs.jpcb.1c08621

Levy, N.E., Valente, K.N., Choe, L.H., Lee, K.H. and Lenhoff, A.M. (2014). Identification and characterization of host cell protein product-associated impurities in monoclonal antibody bioprocessing. Biotechnology and Bioengineering, 111: 904-912. https://doi.org/10.1002/bit.25158

Li, F., Vijayasankaran, N., Shen, A. Y., Kiss, R., and Amanullah, A. (2010). Cell culture processes for monoclonal antibody production. mAbs, 2(5), 466–479. https://doi.org/10.4161/mabs.2.5.12720

Liggins, I. I. M., Hall, D., and Llinas, J.. (2017). Handbook of multisensor data fusion: Theory and practice. Boca Raton: CRC Press.

Lim, Y., Wong, N. S., Lee, Y. Y., Ku, S. C., Wong, D. C., and Yap, M. G. (2010). Engineering mammalian cells in bioprocessing - current achievements and future perspectives. Biotechnology and applied biochemistry, 55(4), 175–189. https://doi.org/10.1042/BA20090363

Li, S. Q., Bomser, J. A., and Zhang, Q. H. (2005). Effects of pulsed electric fields and heat treatment on stability and secondary structure of bovine immunoglobulin G. Journal of agricultural and food chemistry, 53(3), 663–670. https://doi.org/10.1021/jf048923r

Li, T., Gao, T., Chen, H., Pekker, P., Menyhart, A., and Guttman, A. (2020). Rapid Determination of Full and Empty Adeno-Associated Virus Capsid Ratio by Capillary Isoelectric Focusing. Current molecular medicine, 20(10), 814–820. https://doi.org/10.2174/1566524020666200915105456

Liu, H., Gaza-Bulseco, G., and Lundell, E. (2008). Assessment of antibody fragmentation by reversed-phase liquid chromatography and mass spectrometry. Journal of chromatography. B, Analytical technologies in the biomedical and life sciences, 876(1), 13–23. https://doi.org/10.1016/j.jchromb.2008.10.015

Liu, J., Sun, Y., Qi, J., and Marcu, L. (2012). A novel method for fast and robust estimation of fluorescence decay dynamics using constrained least-squares deconvolution with Laguerre expansion. Physics in medicine and biology, 57(4), 843–865. https://doi.org/10.1088/0031-9155/57/4/843

Li, J. J., Lynch, M. and Cetlin, D.. (2019). Monoclonal Antibody Aggregates Polish and Viral Clearance Using Hydrophobic-Interaction Chromatography. BioProcess International, 17(11-12).

Li, Y., Ogunnaike, B. A., and Roberts, C. J. (2010). Multi-variate approach to global protein aggregation behavior and kinetics: effects of pH, NaCl, and temperature for alpha-chymotrypsinogen A. Journal of pharmaceutical sciences, 99(2), 645–662. https://doi.org/10.1002/jps.21869

Long, D. (1977). Photovoltaic and Photoconductive Infrared Detectors. In: Keyes, R.J. (eds) Optical and Infrared Detectors. Topics in Applied Physics, vol 19. Springer, Berlin, Heidelberg. https://doi.org/10.1007/978-3-540-37378-0_4

Li, Y., Polozova, A., Gruia, F., & Feng, J. (2014). Characterization of the degradation products of a color-changed monoclonal antibody: tryptophan-derived chromophores. Analytical chemistry, 86(14), 6850–6857. https://doi.org/10.1021/ac404218t

Liu, H. F., Ma, J., Winter, C., & Bayer, R. (2010). Recovery and purification process development for monoclonal antibody production. mAbs, 2(5), 480–499. https://doi.org/10.4161/mabs.2.5.12645

Lu, A. E., Paulson, J. A., Mozdzierz, N. J., Stockdale, A., Ford Versypt, A. N., Love, K. R., Love, J. C., Braatz, R. D.. (2015). Control systems technology in the advanced manufacturing of biologic drugs. Proceedings of the IEEE Conference on Control Applications, Sydney, Australia (2015), pp. 1505-1515.

Luo, W., Weng, Q., Long, M., Wang, P., Gong, F., Fang, H., Luo, M., Wang, W., Wang, Z., Zheng, D., Hu, W., Chen, X., and Lu, W. (2018). Room-Temperature Single-Photon Detector Based on Single Nanowire. Nano letters, 18(9), 5439–5445. https://doi.org/10.1021/acs.nanolett.8b01795

MacKerell, A. D., Jr, Rigler, R., Nilsson, L., Hahn, U., and Saenger, W. (1987). Protein dynamics. A time-resolved fluorescence, energetic and molecular dynamics study of ribonuclease T1. Biophysical chemistry, 26(2-3), 247–261. https://doi.org/10.1016/0301-4622(87)80027-3

Mahler, H. C., Friess, W., Grauschopf, U., and Kiese, S. (2009). Protein aggregation: pathways, induction factors and analysis. Journal of pharmaceutical sciences, 98(9), 2909–2934. https://doi.org/10.1002/jps.21566

Maruthamuthu, M. K., Rudge, S. R., Ardekani, A. M., Ladisch, M. R., and Verma, M. S. (2020). Process Analytical Technologies and Data Analytics for the Manufacture of Monoclonal Antibodies. Trends in biotechnology, 38(10), 1169–1186. https://doi.org/10.1016/j.tibtech.2020.07.004

Maus, M., Cotlet, M., Hofkens, J., Gensch, T., De Schryver, F. C., Schaffer, J., and Seidel, C. A. (2001). An experimental comparison of the maximum likelihood estimation and nonlinear least-squares fluorescence lifetime analysis of single molecules. Analytical chemistry, 73(9), 2078–2086. https://doi.org/10.1021/ac000877g

Maximow, Alexander A. Papers, [Box 1, Folder 3], Hanna Holborn Gray Special Collections Research Center, University of Chicago Library

Maximow, A. (1902). Experimentelle Untersuchungen über die entzündliche Neubildung von Bindegewebe.

Mazzer, A. R., Perraud, X., Halley, J., O'Hara, J., and Bracewell, D. G. (2015). Protein A chromatography increases monoclonal antibody aggregation rate during subsequent low pH virus inactivation hold. Journal of chromatography. A, 1415, 83–90. https://doi.org/10.1016/j.chroma.2015.08.068

McCue, J. T., Engel, P., Ng, A., Macniven, R., & Thömmes, J. (2008). Modeling of protein monomer/aggregate purification and separation using hydrophobic interaction chromatography. Bioprocess and biosystems engineering, 31(3), 261–275. https://doi.org/10.1007/s00449-008-0200-1

McCoustra, M. R. S.. (1995). Chapter: Methods, diagnostics and instrumentation. An Introduction to Laser Spectroscopy. Edited by Andrews, D. L. and Demidov, A. A.. Plenum Press, New York.

Meirovitch, L.. (1985). Introduction to dynamics and control. John Wiley and Sons, Inc..

Mendhe, R., Thukkaram, M., Patil, N. and Rathore, A.S. (2015), Comparison of PAT based approaches for making real-time pooling decisions for process chromatography – use of feed forward control. J. Chem. Technol. Biotechnol., 90: 341-348. https://doi.org/10.1002/jctb.4448

Mets, U. and Rigler, R. (1994) Submillisecond detection of single Rhodamine molecules in water. J. Fluorescence 4, 259-264.

Milone, M. C., and O'Doherty, U. (2018). Clinical use of lentiviral vectors. Leukemia, 32(7), 1529–1541. https://doi.org/10.1038/s41375-018-0106-0

Mohan, C., Park, S. H., Chung, J. Y., and Lee, G. M. (2007). Effect of doxycycline-regulated protein disulfide isomerase expression on the specific productivity of recombinant CHO cells: thrombopoietin and antibody. Biotechnology and bioengineering, 98(3), 611–615. https://doi.org/10.1002/bit.21453

Molden R, Hu M, Yen E S, Saggese D, Reilly J, Mattila J, Qiu H, Chen G, Bak H, Li N. Host cell protein profiling of commercial therapeutic protein drugs as a benchmark for monoclonal antibody-based therapeutic protein development. MAbs. 2021 Jan-Dec;13(1):1955811. doi: 10.1080/19420862.2021.1955811. PMID: 34365906; PMCID: PMC8354607

Molecular Probes. (2007). SYPRO® Ruby Protein Gel Stain, Product Information, Revised: 20th November 2007. Molecular Probes, Invitrogen detection technologies. United States of America.

Montgomery, D. C.. (2008). Introduction to Statistical Quality Control (6th ed.), Wiley, New York.

Moon, C. P., and Fleming, K. G. (2011). Using tryptophan fluorescence to measure the stability of membrane proteins folded in liposomes. Methods in enzymology, 492, 189–211. https://doi.org/10.1016/B978-0-12-381268-1.00018-5

Mulgrew, B., Grant, P.M., & Thompson, J.S. (1999). Digital Signal Processing: Concepts and Applications.

Munis, A. M., Bentley, E. M., and Takeuchi, Y. (2020). A tool with many applications: vesicular stomatitis virus in research and medicine. Expert opinion on biological therapy, 20(10), 1187–1201. https://doi.org/10.1080/14712598.2020.1787981

Nakazawa M, Mukumoto M, Miyatake K. Production and purification of monoclonal antibodies. Methods Mol Biol. 2010;657:75-91. doi: 10.1007/978-1-60761-783-9_6. PMID: 20602208..

Naldini, L., Blömer, U., Gallay, P., Ory, D., Mulligan, R., Gage, F. H., Verma, I. M., and Trono, D. (1996). In vivo gene delivery and stable transduction of nondividing cells by a lentiviral vector. Science (New York, N.Y.), 272(5259), 263–267. https://doi.org/10.1126/science.272.5259.263

National Institute of Diabetes and Digestive and Kidney Diseases (NIDDKD). (2022). Monoclonal Antibodies. (2022). In LiverTox: Clinical and Research Information on Drug-Induced Liver Injury.

National Research Council (US) Committee on Methods of Producing Monoclonal Antibodies. (1999). Monoclonal Antibody Production. Washington (DC): National Academies Press (US); 5, Large-Scale Production of Monoclonal Antibodies. Available from: https://www.ncbi.nlm.nih.gov/books/NBK100189/

Neckers D. C.. (1973). Photochemical reactions of natural macromolecules. Photoreactions of proteins. Journal of chemical education, 50(3), 164–168. https://doi.org/10.1021/ed050p164

Nelson, P. N., Reynolds, G. M., Waldron, E. E., Ward, E., Giannopoulos, K., and Murray, P. G. (2000). Monoclonal antibodies. Molecular pathology : MP, 53(3), 111–117. https://doi.org/10.1136/mp.53.3.111

Nicoud, L., Jagielski, J., Pfister, D., Lazzari, S., Massant, J., Lattuada, M., and Morbidelli, M. (2016). Kinetics of Monoclonal Antibody Aggregation from Dilute toward Concentrated Conditions. The journal of physical chemistry. B, 120(13), 3267–3280. https://doi.org/10.1021/acs.jpcb.5b11791

Obrezanova, O., Arnell, A., de la Cuesta, R. G., Berthelot, M. E., Gallagher, T. R., Zurdo, J., and Stallwood, Y. (2015). Aggregation risk prediction for antibodies and its application to biotherapeutic development. mAbs, 7(2), 352–363. https://doi.org/10.1080/19420862.2015.1007828

Oliva, A., Fariña, J. B., and Llabrés, M. (2016). Pre-study and in-study validation of a size-exclusion chromatography method with different detection modes for the analysis of monoclonal antibody aggregates. Journal of chromatography. B, Analytical technologies in the biomedical and life sciences, 1022, 206–212. https://doi.org/10.1016/j.jchromb.2016.04.022

Oliva, A., Llabrés, M., and Fariña, J. B. (2001). Comparative study of protein molecular weights by size-exclusion chromatography and laser-light scattering. Journal of pharmaceutical and biomedical analysis, 25(5-6), 833–841. https://doi.org/10.1016/s0731-7085(01)00359-4

Orellana, C. A., Marcellin, E., Schulz, B. L., Nouwens, A. S., Gray, P. P., and Nielsen, L. K. (2015). High-antibody-producing Chinese hamster ovary cells up-regulate intracellular protein transport and glutathione synthesis. Journal of proteome research, 14(2), 609–618. https://doi.org/10.1021/pr501027c

Ozturk, S. S., Thrift, J. C., Blackie, J. D., and Naveh, D.. (1995). Real-time monitoring of protein secretion in mammalian cell fermentation: Measurement of monoclonal antibodies using a computer-controlled hplc system (biocad/rpm). Biotechnol Bioeng 48:201–206.

Pabari, R. M., Ryan, B., McCarthy, C., & Ramtoola, Z. (2011). Effect of microencapsulation shear stress on the structural integrity and biological activity of a model monoclonal antibody, trastuzumab. Pharmaceutics, 3(3), 510–524. https://doi.org/10.3390/pharmaceutics3030510

Paliwal, S.K., Nadler, T., Wang, D.I., & Regnier, F.E. (1993). Automated process monitoring of monoclonal antibody production. Analytical chemistry, 65 23, 3363-7 .

Pauling, L.. (1940). "A Theory of the Structure and Process of Formation of Antibodies." Journal of the American Chemical Society 62, 2643-2657.

Perisamy, N.. (1988). Analysis of fluorescence decay by the nonlinear least squares method. Brief communication. Biophysical Journal. Biophysical Society, 54 (5): 961-967. doi: 10.1016/S0006-3495(88)83032-7

Perry, C., and Rayat, A. (2021). Lentiviral Vector Bioprocessing. Viruses, 13(2), 268. https://doi.org/10.3390/v13020268

Petrossian, A., and DeGiovanni, A.. (1989). Porton International. Perfusion airlift reactor. Patent no.: US4806484

Wyatt, P.J. (1993). Light scattering and the absolute characterization of macromolecules. Analytica Chimica Acta, 272, 1-40.

Philo, J. S. (2009). A critical review of methods for size characterization of non-particulate protein aggregates. Current pharmaceutical biotechnology, 10(4), 359–372. https://doi.org/10.2174/138920109788488815

Pindrus, M., Shire, S. J., Kelley, R. F., Demeule, B., Wong, R., Xu, Y., & Yadav, S. (2015). Solubility Challenges in High Concentration Monoclonal Antibody

Formulations: Relationship with Amino Acid Sequence and Intermolecular Interactions. Molecular pharmaceutics, 12(11), 3896–3907. https://doi.org/10.1021/acs.molpharmaceut.5b00336

Porter, R. R. (1959). The hydrolysis of rabbit y-globulin and antibodies with crystalline papain. The Biochemical journal, 73(1), 119–126. https://doi.org/10.1042/bj0730119

Puntis, J. W., Wilkins, K. M., Ball, P. A., Rushton, D. I., and Booth, I. W. (1992). Hazards of parenteral treatment: do particles count?. Archives of disease in childhood, 67(12), 1475–1477. https://doi.org/10.1136/adc.67.12.1475

Radzicka, A., and Wolfenden, R.. (1996). Rates of uncatalyzed peptide bond hydrolysis in neutral solution and the transition state affinities of proteases. J Am Chem Soc. 118: 6105–6109.

Ramos-de-la-Peña, A. M., González-Valdez, J., and Aguilar, O. (2019). Protein A chromatography: Challenges and progress in the purification of monoclonal antibodies. Journal of separation science, 42(9), 1816–1827. https://doi.org/10.1002/jssc.201800963

Rathore, A. S., Yu, M., Yeboah, S., and Sharma, A. (2008). Case study and application of process analytical technology (PAT) towards bioprocessing: use of on-line high-performance liquid chromatography (HPLC) for making real-time pooling decisions for process chromatography. Biotechnology and bioengineering, 100(2), 306–316. https://doi.org/10.1002/bit.21759

Rathore A. S. (2009). Roadmap for implementation of quality by design (QbD) for biotechnology products. Trends in biotechnology, 27(9), 546–553. https://doi.org/10.1016/j.tibtech.2009.06.006

Rathore, A. S., and Winkle, H. (2009). Quality by design for biopharmaceuticals. Nature biotechnology, 27(1), 26–34. https://doi.org/10.1038/nbt0109-26

Read, E. K., Park, J. T., Shah, R. B., Riley, B. S., Brorson, K. A., and Rathore, A. S.. (2010). Process analytical technology (PAT) for biopharmaceutical products: Part I. concepts and applications. Biotechnology and bioengineering, 105(2), 276–284. https://doi.org/10.1002/bit.22528

Reichert, J. M., Rosensweig, C. J., Faden, L. B., and Dewitz, M. C. (2005). Monoclonal antibody successes in the clinic. Nature biotechnology, 23(9), 1073–1078. https://doi.org/10.1038/nbt0905-1073

Reichert, J. M.. (2010). Metrics for antibody therapeutics development. MAbs, 2: 695–700. doi:10.4161/mabs.2.6.13603.

Rigler, R. and Mets, U. (1992) Diffusion of single molecules through a Gaussian laser beam. SPIE. Laser Spectroscopy of Biomolecules 1921, 239-248

Reubsaet, J. L., Beijnen, J. H., Bult, A., van Maanen, R. J., Marchal, J. A., & Underberg, W. J. (1998). Analytical techniques used to study the degradation of proteins and peptides: physical instability. Journal of pharmaceutical and biomedical analysis, 17(6-7), 979–984. https://doi.org/10.1016/s0731-7085(98)00064-8

Rigler, R.. (1995). Fluorescence correlations, single molecule detection and large number screening Applications in biotechnology, Journal of Biotechnology, 41 (2–3): 177-186, ISSN 0168-1656, https://doi.org/10.1016/0168-1656(95)00054-T. (https://www.sciencedirect.com/science/article/pii/016816569500054T)

Ring, J., Stephan, W., and Brendel, W. (1979). Anaphylactoid reactions to infusions of plasma protein and human serum albumin. Role of aggregated proteins and of stabilizers added during production. Clinical allergy, 9(1), 89–97. https://doi.org/10.1111/j.1365-2222.1979.tb01527.x

Rodrigo, G., Gruvegård, M. and Van Alstine, J.. (2015). Antibody Fragments and Their Purification by Protein L Affinity Chromatography. Antibodies, 4(3), pp.259–277. Available at: http://dx.doi.org/10.3390/antib4030259.

Rodrigues, T., Carrondo, M. J., Alves, P. M., and Cruz, P. E. (2007). Purification of retroviral vectors for clinical application: biological implications and technological challenges. Journal of biotechnology, 127(3), 520–541. https://doi.org/10.1016/j.jbiotec.2006.07.028

Segura, M. M., Garnier, A., and Kamen, A. (2006). Purification and characterization of retrovirus vector particles by rate zonal ultracentrifugation. Journal of virological methods, 133(1), 82–91. https://doi.org/10.1016/j.jviromet.2005.10.030

Roberts C. J. (2014). Therapeutic protein aggregation: mechanisms, design, and control. Trends in biotechnology, 32(7), 372–380. https://doi.org/10.1016/j.tibtech.2014.05.005

Rolinger, L., Rüdt, M., and Hubbuch, J.. (2020). A critical review of recent trends, and a future perspective of optical spectroscopy as PAT in biopharmaceutical downstream processing. Analytical and bioanalytical chemistry, 412(9), 2047–2064. https://doi.org/10.1007/s00216-020-02407-z

Rosenberg A. S. (2006). Effects of protein aggregates: an immunologic perspective. The AAPS journal, 8(3), E501–E507. https://doi.org/10.1208/aapsj080359

Rüdt, M., Brestrich, N., Rolinger, L., and Hubbuch, J. (2017). Real-time monitoring and control of the load phase of a protein A capture step. Biotechnology and bioengineering, 114(2), 368–373. https://doi.org/10.1002/bit.26078

Sandberg, H., Lutkemeyer, D., Kuprin, S., Wrangel, M., Almstedt, A., Persson, P,Ek V., and Milkaelsson, M.. (2006). Mapping and partial characterization ofproteases expressed by a CHO production cell line. Biotechnology and Bioengineering. 95(5): 961–971.

Schellekens H. (2002). Immunogenicity of therapeutic proteins: clinical implications and future prospects. Clinical therapeutics, 24(11), 1720–1719. https://doi.org/10.1016/s0149-2918(02)80075-3

Schweitzer, M., Pohl, M., Hanna-Brown, M., Nethercote, P., Borman, P., Hansen, G., Smith, K., and Larew, J.. (2010). Implications and opportunities of applying QbD principles to analytical measurements. Pharm Technol 34(2):52–59

Sharma, A. and Schulman, S. G.. (1999). Introduction to Fluorescence Spectroscopy. Techniques in Analytical Chemistry Series. John Wiley and Sons.

Shepard, H. M., Phillips, G. L., D Thanos, C., and Feldmann, M. (2017). Developments in therapy with monoclonal antibodies and related proteins. Clinical medicine (London, England), 17(3), 220–232. https://doi.org/10.7861/clinmedicine.17-3-220

Shire, S. J., Shahrokh, Z., and Liu, J. (2004). Challenges in the development of high protein concentration formulations. Journal of pharmaceutical sciences, 93(6), 1390–1402. https://doi.org/10.1002/jps.20079

Shukla, A. A. and Thömmes, J.. (2010). Recent advances in large-scale production of monoclonal antibodies and related proteins. Trends in Biotechnology. 28: 253-261.

Shukla, A. A., Hubbard, B., Tressel, T., Guhan, S., and Low, D.. (2007). Downstream processing of monoclonal antibodies–Application of platform approaches. J Chromatogr B 848:28–39.

Singla, A., Bansal, R., Joshi, V., and Rathore, A. S. (2016). Aggregation Kinetics for IgG1-Based Monoclonal Antibody Therapeutics. The AAPS journal, 18(3), 689–702. https://doi.org/10.1208/s12248-016-9887-0

Simat, T. J., & Steinhart, H. (1998). Oxidation of Free Tryptophan and Tryptophan Residues in Peptides and Proteins. Journal of agricultural and food chemistry, 46(2), 490–498. https://doi.org/10.1021/jf970818c

Singh S. K. (2011). Impact of product-related factors on immunogenicity of biotherapeutics. Journal of pharmaceutical sciences, 100(2), 354–387. https://doi.org/10.1002/jps.22276

Smith, R. M. and Hansen, D. E.. (1998). The pH-Rate Profile for the Hydrolysis of a Peptide Bond. J Am Chem Soc., 120: 8910–8913.

Smith S. L. (1996). Ten years of Orthoclone OKT3 (muromonab-CD3): a review. Journal of transplant coordination: official publication of the North American Transplant Coordinators Organization (NATCO), 6(3), 109–121. https://doi.org/10.7182/prtr.1.6.3.8145l3u185493182

Sofer, G.K., & Hagel, L. (1997). Handbook of Process Chromatography: A Guide to Optimization, Scale Up, and Validation.

Song, H-N., Jang, J-H., Kim, Y-W., Kim, D-H., Park, S-G., Lee, MK., Paek, S-H., and Woo, E-J.. (2014). Refolded scFv Antibody Fragment against Myoglobin Shows Rapid Reaction Kinetics. International Journal of Molecular Sciences; 15(12):23658-23671. https://doi.org/10.3390/ijms151223658

Southey, F.. (2018). Oxford BioMedica to capture 25–30% of lentiviral vector market by 2026. Predicts CTO.

Sørensen, D. H., Christensen, N. P. A., Skibsted, E., Rantanen, J., & Rinnan, Å. (2022). In-line Fluorescence Spectroscopy for Quantification of Low

Amount of Active Pharmaceutical Ingredient. Journal of pharmaceutical sciences, 111(9), 2406–2410. https://doi.org/10.1016/j.xphs.2022.06.008

Steinman L. (1990). The use of monoclonal antibodies for treatment of autoimmune disease. Journal of clinical immunology, 10(6 Suppl), 30S–39S. https://doi.org/10.1007/BF00918689

Steinwandter V., Borchert D., and Herwig C.. (2019). Data science tools and applications on the way to pharma 4.0, Drug Discovery Today.
Strebhardt, K. and Ullrich, A. Paul Ehrlich's magic bullet concept: 100 years of progress. Nat Rev Cancer 8, 473–480 (2008). https://doi.org/10.1038/nrc2394

Takeuchi, Y., Cosset, F. L., Lachmann, P. J., Okada, H., Weiss, R. A., and Collins, M. K. (1994). Type C retrovirus inactivation by human complement is determined by both the viral genome and the producer cell. Journal of virology, 68(12), 8001–8007. https://doi.org/10.1128/JVI.68.12.8001-8007.1994

TALMAGE D. W. (1957). Allergy and immunology. Annual review of medicine, 8, 239–256.
https://doi.org/10.1146/annurev.me.08.020157.001323

Taschner, N., Müller, S. A., Alumella, V. R., Goldie, K. N., Drake, A. F., Aebi, U., and Arvinte, T. (2001). Modulation of antigenicity related to changes in antibody flexibility upon lyophilization. Journal of molecular biology, 310(1), 169–179. https://doi.org/10.1006/jmbi.2001.4736

<USP 1225>. Pharmacopeial Forum: Volume No. 34(3): 794.

<USP 857>. (2018). Ultraviolet-Visible Spectroscopy. US Pharmacopeia.

Thorlabs, 2022: https://www.thorlabs.com/newgrouppage9.cfm?objectgroup_id=4354; last accessed 23/09/2022.

Tijani, M., Munis, A. M., Perry, C., Sanber, K., Ferraresso, M., Mukhopadhyay, T., Themis, M., Nisoli, I., Mattiuzzo, G., Collins, M. K., and Takeuchi, Y. (2018). Lentivector Producer Cell Lines with Stably Expressed Vesiculovirus Envelopes. Molecular therapy. Methods and clinical development, 10, 303–312. https://doi.org/10.1016/j.omtm.2018.07.013

Turton, D. A., Reid, G. D., and Beddard, G. S. (2003). Accurate analysis of fluorescence decays from single molecules in photon counting experiments. Analytical chemistry, 75(16), 4182–4187. https://doi.org/10.1021/ac034325k

Tomás, H. A., Mestre, D. A., Rodrigues, A. F., Guerreiro, M. R., Carrondo, M., and Coroadinha, A. S. (2019). Improved GaLV-TR Glycoproteins to Pseudotype Lentiviral Vectors: Impact of Viral Protease Activity in the Production of LV Pseudotypes. Molecular therapy. Methods and clinical development, 15, 1–8. https://doi.org/10.1016/j.omtm.2019.08.001

Tomita, M., & Tsumoto, K. (2011). Hybridoma technologies for antibody production. Immunotherapy, 3(3), 371–380. https://doi.org/10.2217/imt.11.4

Tshiani Mbaya, O., Mukumbayi, P., & Mulangu, S. (2021). Review: Insights on Current FDA-Approved Monoclonal Antibodies Against Ebola Virus Infection. Frontiers in immunology, 12, 721328. https://doi.org/10.3389/fimmu.2021.721328

Vajda, J., Conze, W., & Müller, E. (2015). Kinetic plots in aqueous size exclusion chromatography of monoclonal antibodies and virus particles. Journal of chromatography. A, 1426, 118–125. https://doi.org/10.1016/j.chroma.2015.11.057

Valkama, A. J., Oruetxebarria, I., Lipponen, E. M., Leinonen, H. M., Käyhty, P., Hynynen, H., Turkki, V., Malinen, J., Miinalainen, T., Heikura, T., Parker, N. R., Ylä-Herttuala, S., and Lesch, H. P. (2020). Development of Large-Scale Downstream Processing for Lentiviral Vectors. Molecular therapy. Methods and clinical development, 17, 717–730. https://doi.org/10.1016/j.omtm.2020.03.025

Van Manen-Brush, K., Zeitler, J., White, J. R., Younge, P., Willis, S., and Jones, M. (2020). Improving Chinese hamster ovary host cell protein ELISA using Ella®: an automated microfluidic platform. BioTechniques, 69(3), 186–192. https://doi.org/10.2144/btn-2020-0074

Vázquez-Rey, M., and Lang, D. A. (2011). Aggregates in monoclonal antibody manufacturing processes. Biotechnology and bioengineering, 108(7), 1494–1508. https://doi.org/10.1002/bit.23155

Velugula-Yellela, S. R., Powers, D. N., Angart, P., Faustino, A., Faison, T., Kohnhorst, C., Fratz-Berilla, E. J., and Agarabi, C. D. (2019). Purification and Analytics of a Monoclonal Antibody from Chinese Hamster Ovary Cells Using an Automated Microbioreactor System. Journal of visualized experiments : JoVE, (147), 10.3791/58947. https://doi.org/10.3791/58947

Vlasak, J. and Ionescu, R.. (2011). Fragmentation of monoclonal antibodies. MAbs; 3(3):253-63. doi: 10.4161/mabs.3.3.15608. PMID: 21487244; PMCID: PMC3149706

Volkin, D. B. Klibanov, A. M.. (1989) Creighton, T. E. Protein Function: A Practical Approach Oxford Information Press 1–24.

Wälchli, R., Vermeire, P. J., Massant, J., & Arosio, P. (2020). Accelerated Aggregation Studies of Monoclonal Antibodies: Considerations for Storage Stability. Journal of pharmaceutical sciences, 109(1), 595–602. https://doi.org/10.1016/j.xphs.2019.10.048

Walsh, G.. (2010). Biopharmaceutical benchmarks 2010. Nature biotechnology, 28(9), 917–924. https://doi.org/10.1038/nbt0910-917

Waltz, E.. (2005). GlaxoSmithKline cancer drug threatens Herceptin market Nat. Biotechnol., 23 (12): 1453– 1454.

Wang, W., & Roberts, C. J. (2018). Protein aggregation - Mechanisms, detection, and control. International journal of pharmaceutics, 550(1-2), 251–268. https://doi.org/10.1016/j.ijpharm.2018.08.043

Wang, H., Guo, J., Miao, J., Luo, W., Gu, Y., Xie, R., Wang, F., Zhang, L., Wang, P., and Hu, W. (2022). Emerging Single-Photon Detectors Based on Low-Dimensional Materials. Small (Weinheim an der Bergstrasse, Germany), 18(5), e2103963. https://doi.org/10.1002/smll.202103963

Wang, H., Levi, M. S., Del Grosso, A. V., McCormick, W. M., and Bhattacharyya, L. (2017). An improved size exclusion-HPLC method for molecular size distribution analysis of immunoglobulin G using sodium perchlorate in the eluent. Journal of pharmaceutical and biomedical analysis, 138, 330–343. https://doi.org/10.1016/j.jpba.2017.02.025

Wang W. (1999). Instability, stabilization, and formulation of liquid protein pharmaceuticals. International journal of pharmaceutics, 185(2), 129–188. https://doi.org/10.1016/s0378-5173(99)00152-0

Wang, W., Singh, S., Zeng, D. L., King, K., and Nema, S. (2007). Antibody structure, instability, and formulation. Journal of pharmaceutical sciences, 96(1), 1–26. https://doi.org/10.1002/jps.20727

Wang, X., Hunter, A. K., and Mozier, N. M. (2009). Host cell proteins in biologics development: Identification, quantitation and risk assessment. Biotechnology and bioengineering, 103(3), 446–458. https://doi.org/10.1002/bit.22304

Warikoo, V., Godawat, R., Brower, K., Jain, S., Cummings, D., Simons, E., Johnson, T., Walther, J., Yu, M., Wright, B., McLarty, J., Karey, K. P., Hwang, C., Zhou, W., Riske, F., and Konstantinov, K. (2012). Integrated continuous production of recombinant therapeutic proteins. Biotechnology and bioengineering, 109(12), 3018–3029. https://doi.org/10.1002/bit.24584

Warnock, J. N., Daigre, C., and Al-Rubeai, M. (2011). Introduction to viral vectors. Methods in molecular biology (Clifton, N.J.), 737, 1–25. https://doi.org/10.1007/978-1-61779-095-9_1

Wechselberger, P., Seifert, A., and Herwig, C.. (2010). PAT method to gather bioprocess parameters in real-time using simple input variables and first principle relationships. Chem. Eng. Sci., 65 (21): 5734-5746

Weiner G. J. (2007). Monoclonal antibody mechanisms of action in cancer. Immunologic research, 39(1-3), 271–278. https://doi.org/10.1007/s12026-007-0073-4

Welfle, K., Misselwitz, R., Hausdorf, G., Höhne, W., and Welfle, H. (1999). Conformation, pH-induced conformational changes, and thermal unfolding of anti-p24 (HIV-1) monoclonal antibody CB4-1 and its Fab and Fc fragments. Biochimica et biophysica acta, 1431(1), 120–131. https://doi.org/10.1016/s0167-4838(99)00046-1

Wen, J., Arakawa, T., and Philo, J. S. (1996). Size-exclusion chromatography with on-line light-scattering, absorbance, and refractive index detectors for studying proteins and their interactions. Analytical biochemistry, 240(2), 155–166. https://doi.org/10.1006/abio.1996.0345

Woldeyes, M. A., Qi, W., Razinkov, V. I., Furst, E. M., & Roberts, C. J. (2019). How Well Do Low- and High-Concentration Protein Interactions Predict Solution Viscosities of Monoclonal Antibodies?. Journal of pharmaceutical sciences, 108(1), 142–154. https://doi.org/10.1016/j.xphs.2018.07.007

Woodcock, J., Griffin, J., Behrman, R., Cherney, B., Crescenzi, T., Fraser, B., Hixon, D., Joneckis, C., Kozlowski, S., Rosenberg, A., Schrager, L., Shacter, E., Temple, R., Webber, K., & Winkle, H. (2007). The FDA's assessment of follow-on protein products: a historical perspective. Nature reviews. Drug discovery, 6(6), 437–442. https://doi.org/10.1038/nrd2307

Wuest, D. M., Harcum, S. W., and Lee, K. H. (2012). Genomics in mammalian cell culture bioprocessing. Biotechnology advances, 30(3), 629–638. https://doi.org/10.1016/j.biotechadv.2011.10.010

Wurm, F. M.. (2004). Production of recombinant protein therapeutics in cultivated mammalian cells Nat. Biotechnol., 22 (11): 1393– 1398.

Xiang, T., Lundell, E., Sun, Z., and Liu, H.. (2007). Structural effect of a recombinant monoclonal antibody on hinge region peptide bond hydrolysis. Journal of Chromatography B. Analytical Technologies in the biomedical and life sciences. Biomed Life Sciences; 858(1-2): 254-62. doi: 10.1016/j.jchromb.2007.08.043. PMID: 17901002.

Yamada T. (2011). Therapeutic monoclonal antibodies. The Keio journal of medicine, 60(2), 37–46. https://doi.org/10.2302/kjm.60.37

Zahavi, D., and Weiner, L. (2020). Monoclonal Antibodies in Cancer Therapy. Antibodies (Basel, Switzerland), 9(3), 34. https://doi.org/10.3390/antib9030034

Zhang, Z. and Liu, Y.. (2017). Recent progresses of understanding the viscosity of concentrated protein solutions, Current Opinion in Chemical Engineering, 16, 48-55, https://doi.org/10.1016/j.coche.2017.04.001.

Zheng, J. Y., and Janis, L. J. (2006). Influence of pH, buffer species, and storage temperature on physicochemical stability of a humanized monoclonal antibody LA298. International journal of pharmaceutics, 308(1-2), 46–51. https://doi.org/10.1016/j.ijpharm.2005.10.024

Zurdo J.. (2013). Developability assessment as an early de-risking tool for biopharmaceutical development. Pharmaceutical Bioprocessing, 1:29-50; http://dx.doi.org/ 10.4155/pbp.13.3

Appendix

A. Product-related Impurity Analysis

A.1. Decay Parameter Selection

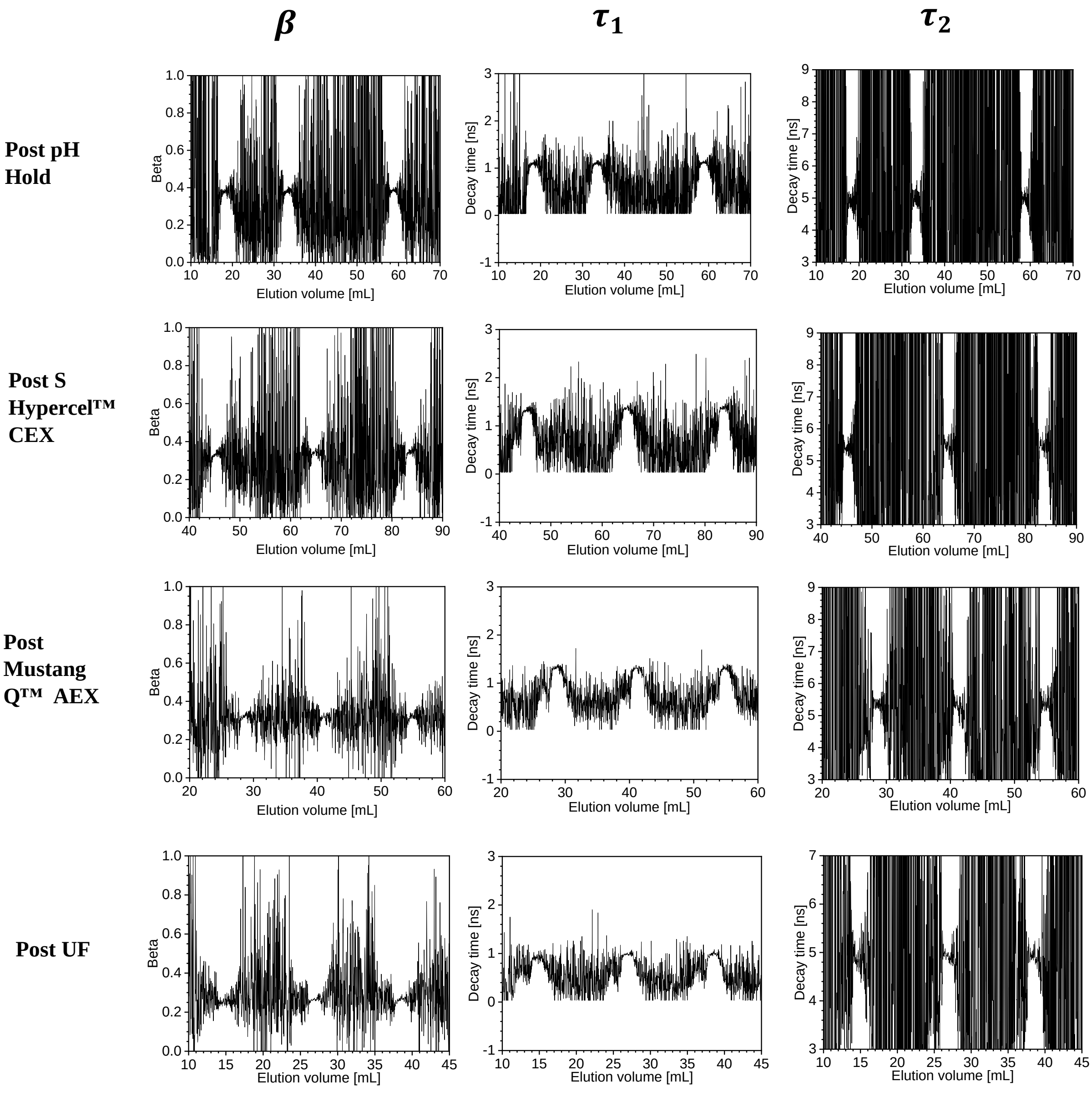

Figure 1: Decay chromatogram traces of the decay parameters for the mAb samples, obtained from FPLC-SEC-TRF. Decay parameters for the monomer and aggregate-fragment species were extracted from points of signal convergence.

A.2. Decay Parameter Evaluation on FPLC-SEC

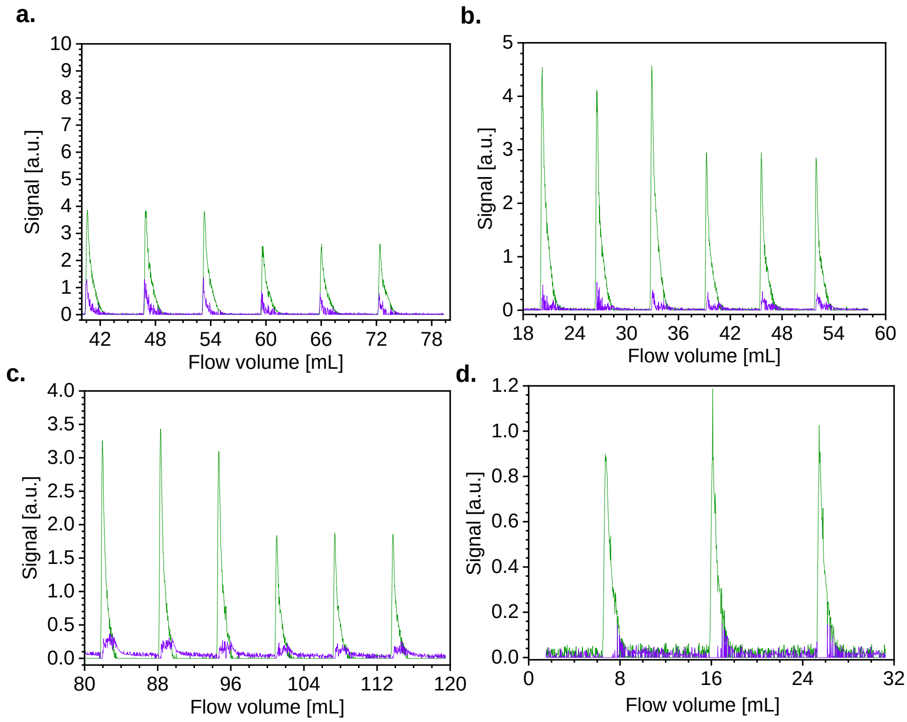

Figure 2: Column-free decay contributions of the aggregate-fragment and monomer species for a) pH Hold, b) S Hypercel™ , c) Mustang Q™ and d) Ultrafiltration eluates.

A.3.1. Post-Protein A Capture and Viral Inactivation

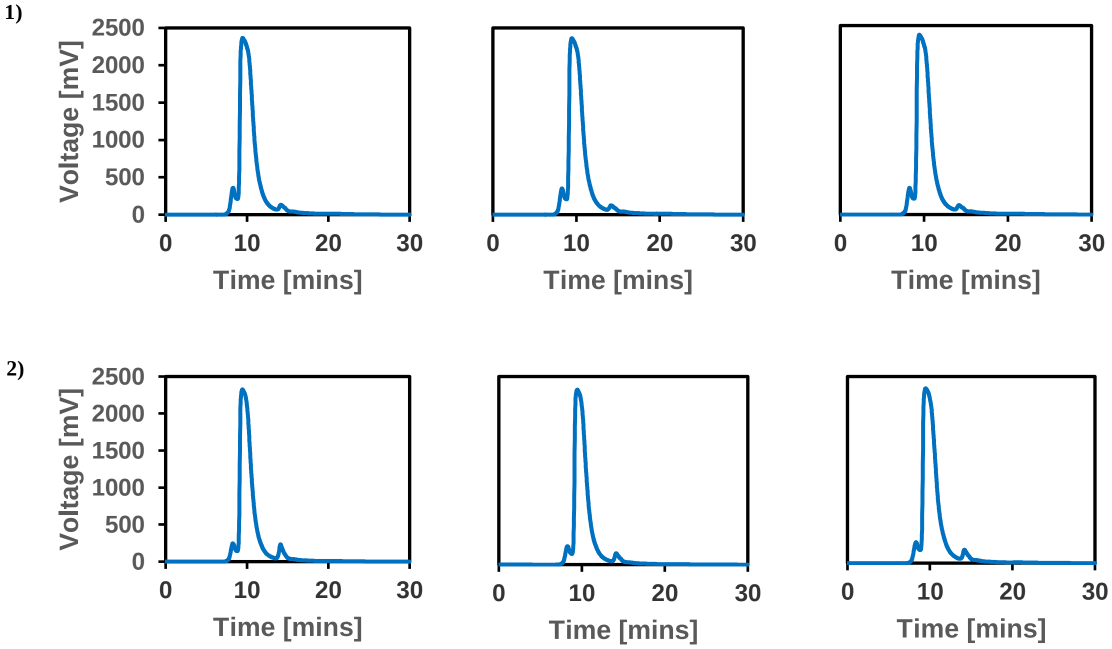

Figure 3: Protein A eluates were used to prepare dilutions of (1) 1:2 and (2) 1:3, mAb sample stock: buffer. Each row corresponds to a separate sample, the repeats of that sample are included in the same row.

A.3.2. S Hypercel™ Cation Exchange Eluates

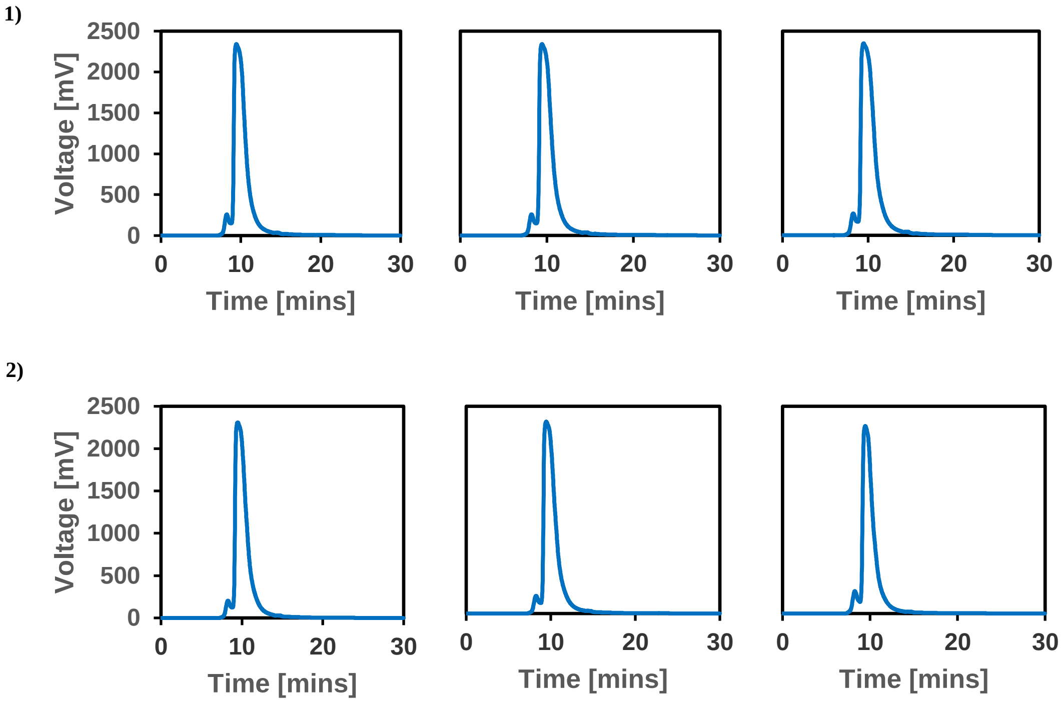

Figure 4: S Hypercel™ eluates were diluted by a factor of (1) 3 and a (2) factor of 4.

A.3.3. Mustang Q™ Anion Exchange Eluates

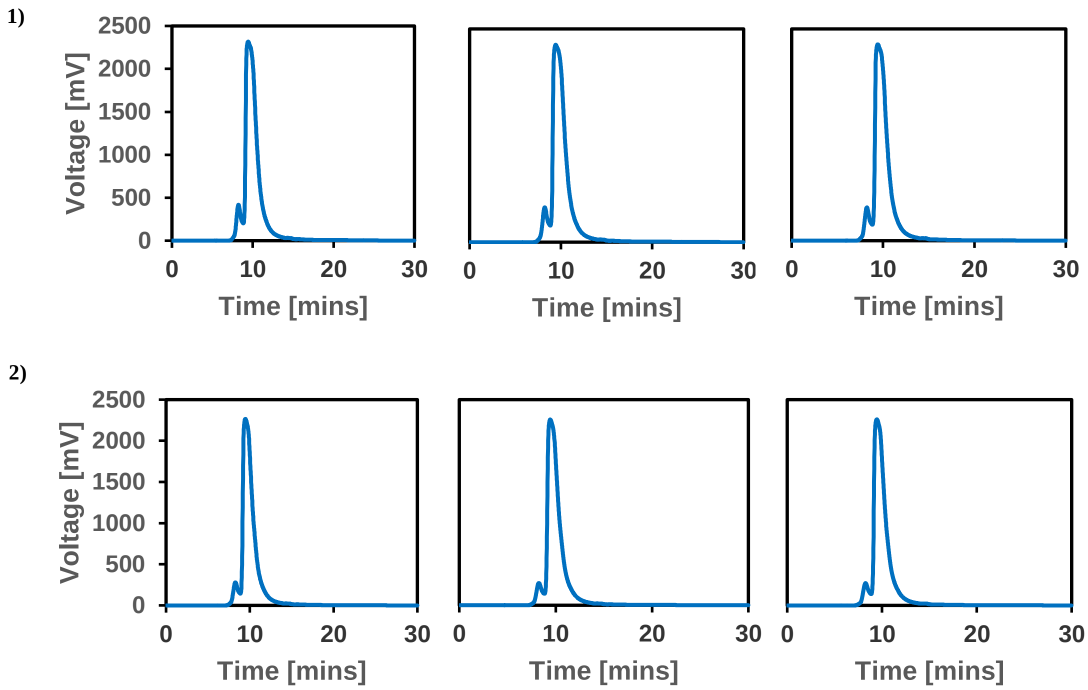

Figure 5: Mustang Q™ eluates were diluted to ratios of: (1) 1:2 and (2) 1:3, mAb stock to buffer.

A.3.4. UF Eluates

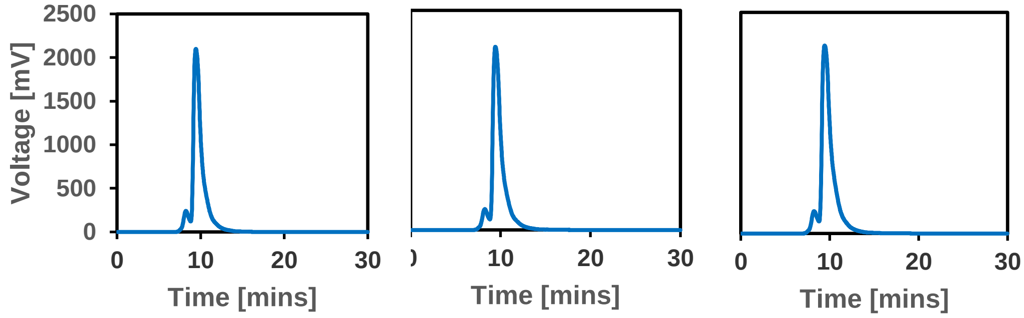

Figure 6: Ultrafiltration eluates, *high* concentration sample cases.

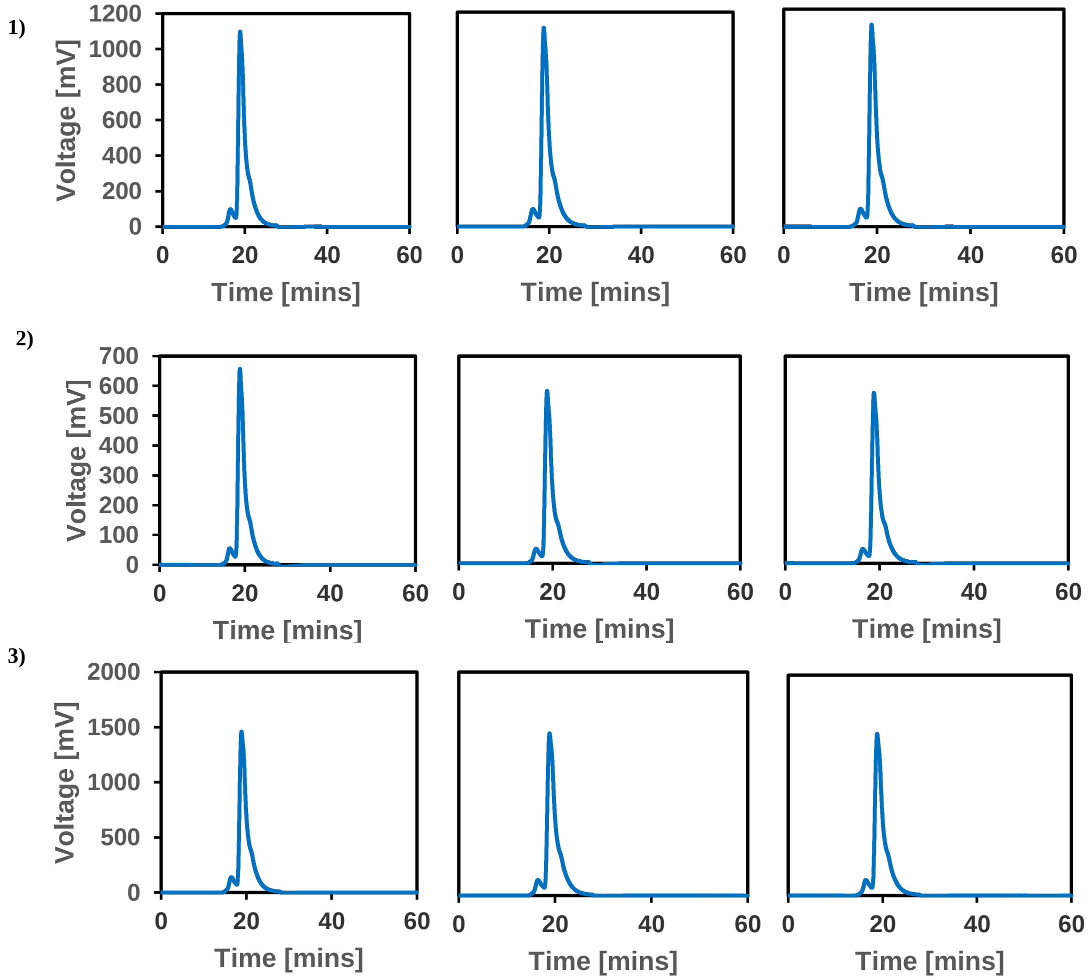

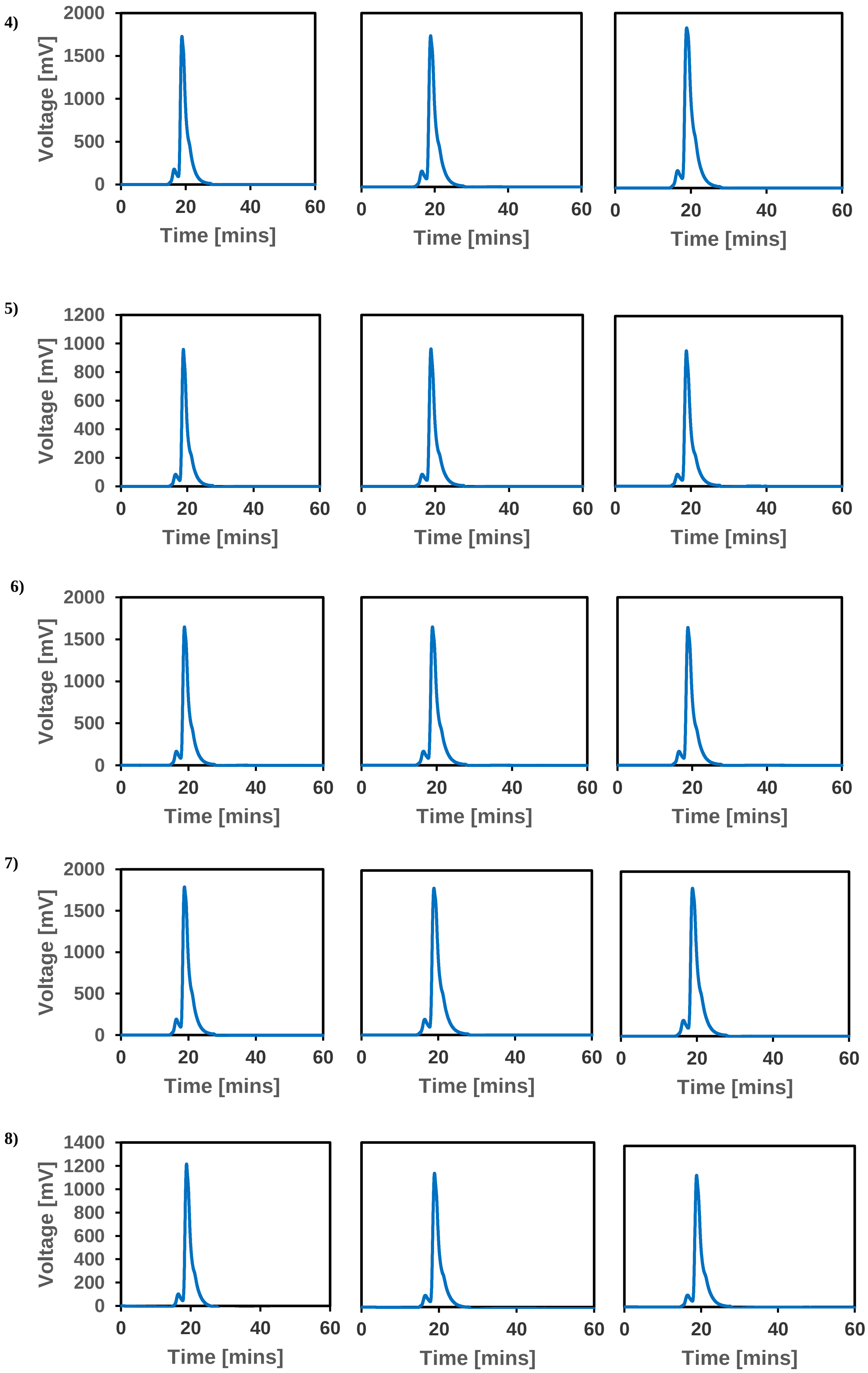

Figure 7: HPLC-SEC UV absorbance chromatograms for the low concentration

low sensitivity cases.

A.4. HPLC-SEC Chromatograms for Mustang Q™ Eluates (high sensitivity measurements)

1)

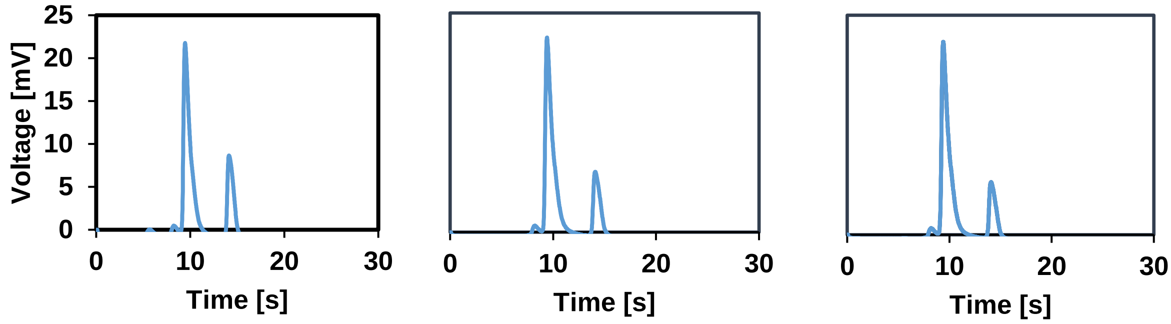

2)

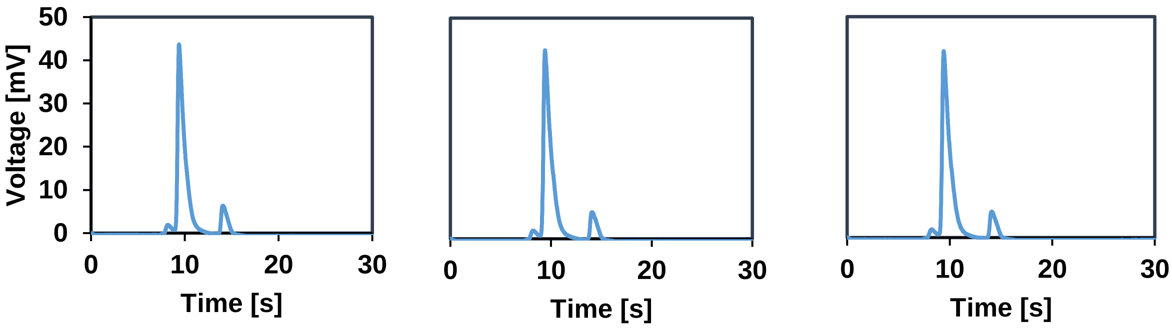

3)

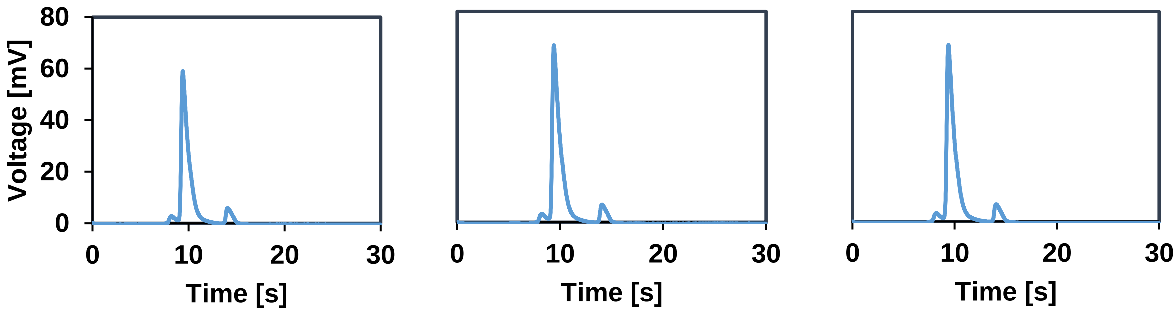

4)

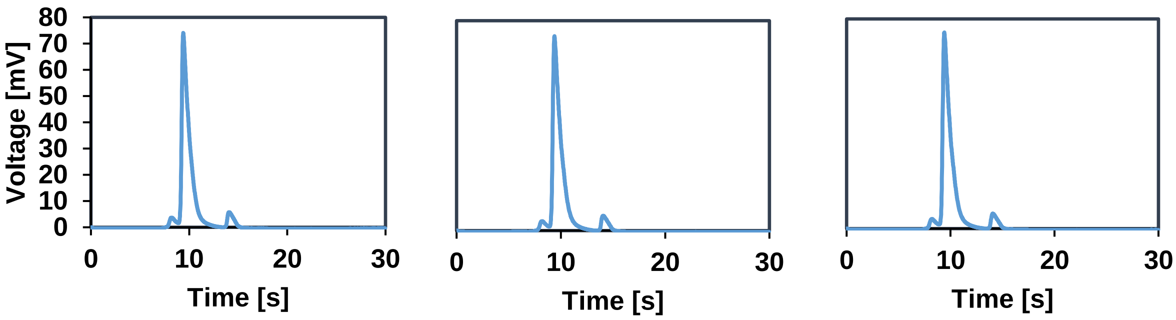

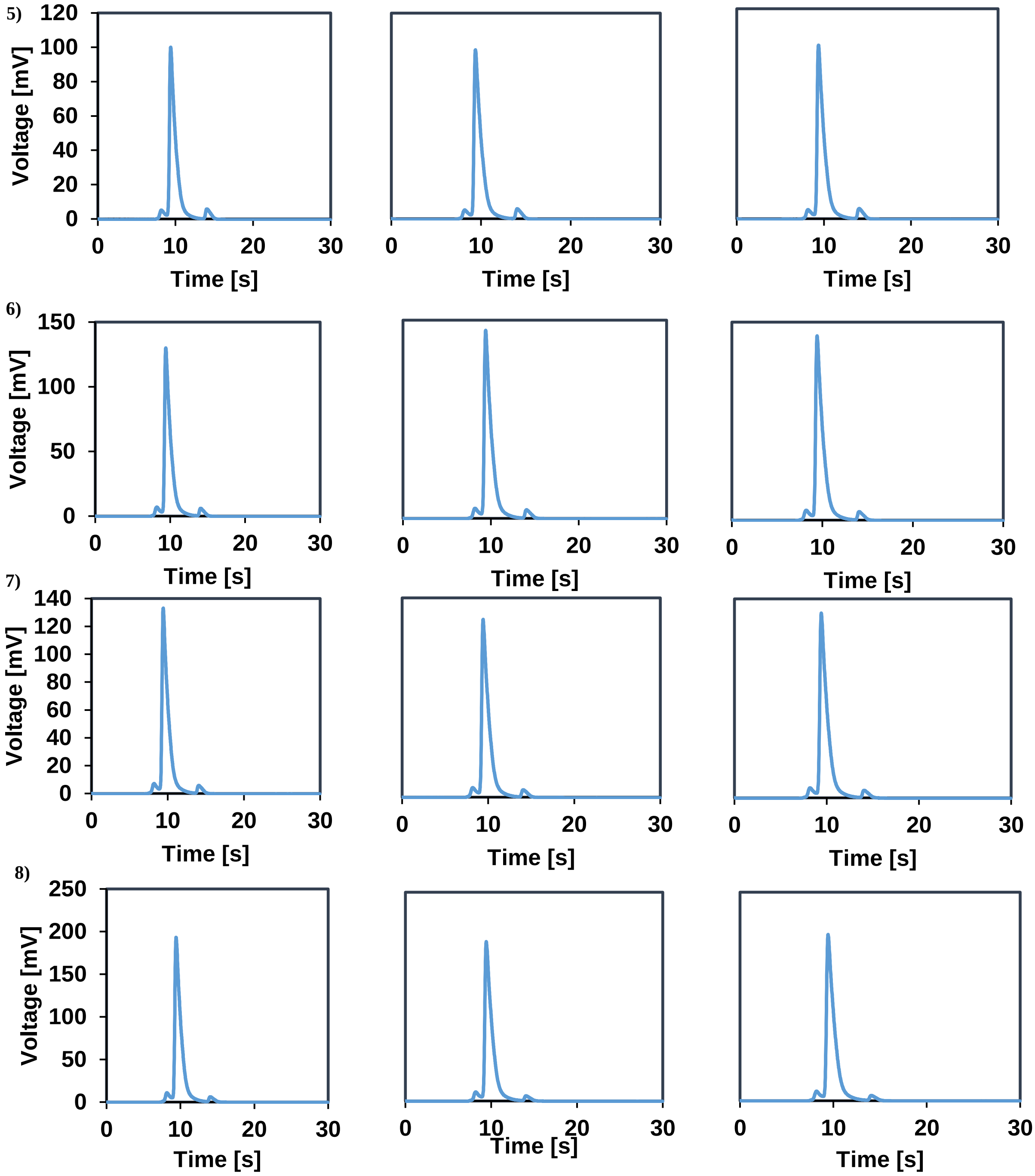

Figure 8: ***Low*** **concentration samples measured against high-sensitivity TRF spectroscopy. Concentrations of samples in ascending order of magnitude.**

B. Process-related Impurity Analysis

B.1. Total Fluorescence Intensity

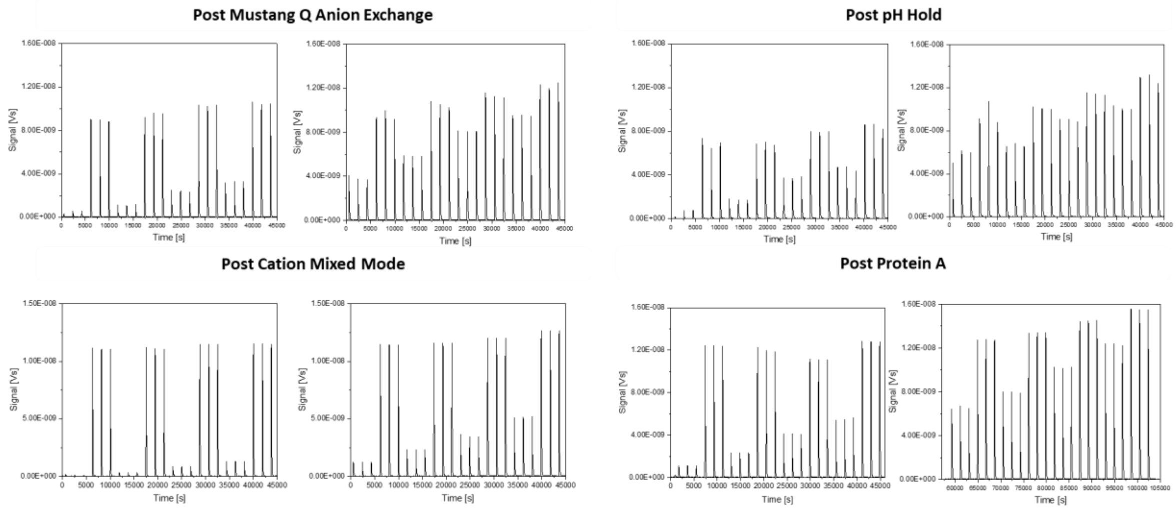

Figure 9: Total fluorescence intensities for unspiked (odd triplicates) and HCP-spiked (even triplicates) mAb eluates from different purification stages.

B2. DAC Peak Areas and ELISA HCP Concentrations

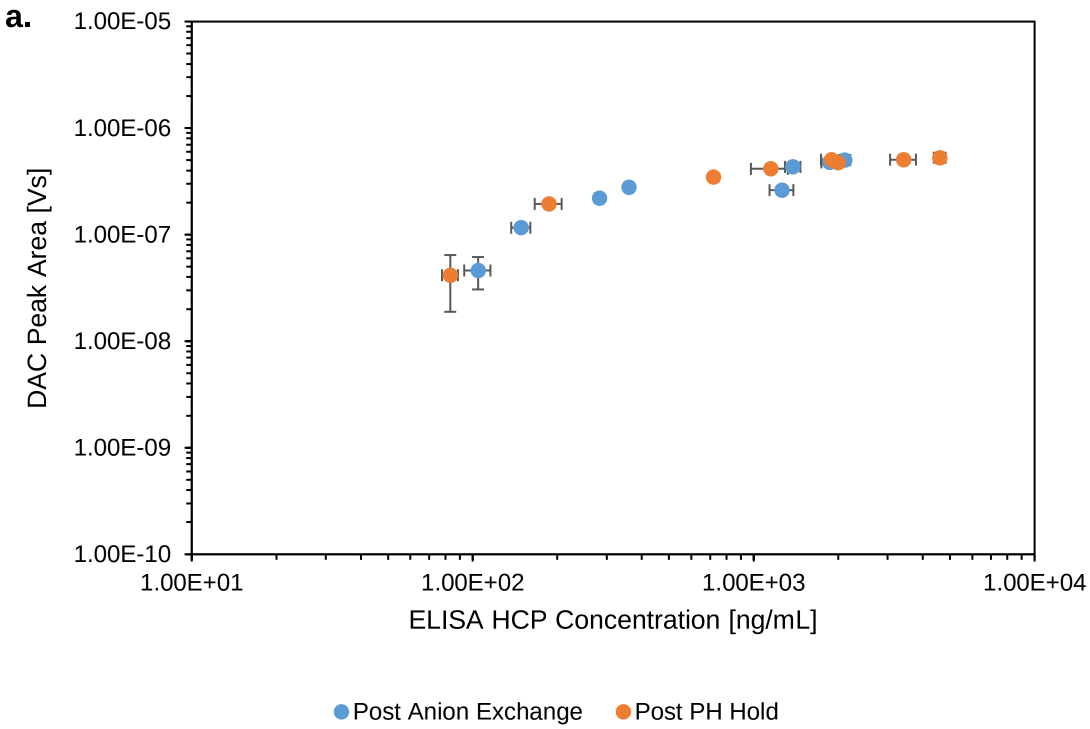

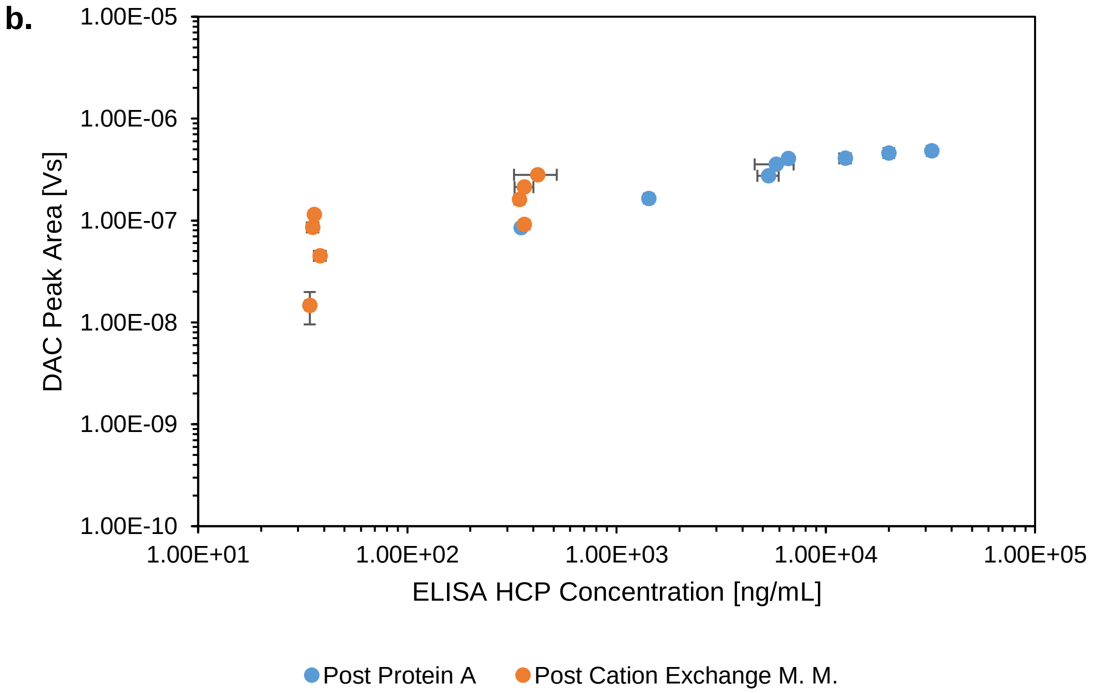

Figure 10: MAb DAC peak areas plotted against ELISA-derived HCP concentrations for 8 mAb concentrations from 4 different bioprocess stages. Samples from Pall BIotech a) Portsmouth and b) Westborough manufacturing lines.

B.3. ELISA Concentration Calibration Curves

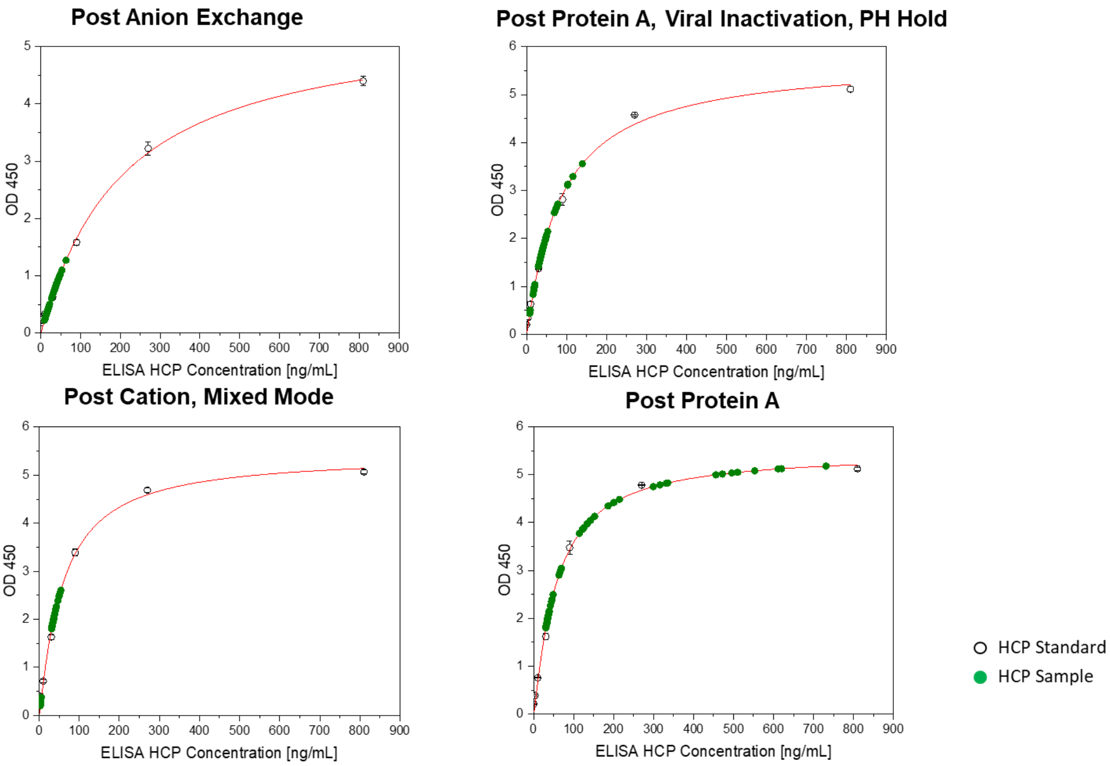

Figure 11: HCP concentrations calculated for each sample according to measured optical density (OD) values within standard ranges.

Table 9: Ultrafiltration (UF), post pH hold (PPH), S Hypercel cation exchange (SC) and Mustang Q anion exchange (MQ) mAb eluate concentrations measured on the Thermo Scientific™ NanoDrop™ 2000c Spectrophotometer (Thermo Fisher Scientific, US), with the extinction coefficient of 1.4 being used for mAbs.

Sample		"Low concentration" samples								"High concentration" samples						
		UF 1	UF 2	UF 3	UF 4	UF 5	UF 6	UF 7	UF 8	UF	PPH D1	PPH D2	SC D1	SC D2	MQ D1	MQ D2
Test	1	0.787	0.436	1.114	1.454	0.661	1.313	1.532	0.899	1.994	6.565	4.3	4.602	3.54	4.075	2.634
	2	0.743	0.433	1.087	1.426	0.664	1.319	1.533	0.878	1.957	6.575	4.269	4.58	3.581	4.106	2.616
	3	0.797	0.434	1.115	1.435	0.663	1.299	1.535	0.896	1.971	6.602	4.803	4.637	3.614	4.067	2.614
Average		0.776	0.434	1.105	1.438	0.663	1.310	1.533	0.891	1.974	6.581	4.457	4.606	3.578	4.083	2.621
Final Expected Concentration (mg/mL)		**0.554**	**0.310**	**0.790**	**1.027**	**0.473**	**0.936**	**1.095**	**0.636**	**1.410**	**4.700**	**3.184**	**3.290**	**2.556**	**2.916**	**1.872**

Table 10: Mustang Q anion exchange eluate concentrations measured on the Thermo Scientific™ NanoDrop™ Microvolume UV-Vis Spectrophotometer (Thermo Fisher Scientific, US). and tested on the sensitivity improved TRF spectroscopy system, concentrations calculated using an extinction coefficient of 1.4 for mAbs.

Sample		MQ sample concentrations							
		1	2	3	4	5	6	7	8
Test	1	0.375	0.847	1.174	1.525	1.986	2.474	2.863	3.967
	2	0.389	0.831	1.17	1.532	1.976	2.667	2.926	3.976
	3	0.409	0.854	1.115	1.497	2.008	2.631	2.892	3.91
Average		0.391	0.844	1.153	1.518	1.990	2.591	2.894	3.951
Final Expected Concentration (mg/mL)		**0.279**	**0.603**	**0.824**	**1.084**	**1.421**	**1.850**	**2.067**	**2.822**